Progress Report

Georgia Tech Project A-5858

Information-Based Multisensor Detection

Sponsored by:

Office of Naval Research
ONR Grant Number N00014-99-1-0084

Attention: **Dr. Rabinder N. Madan**
Program Officer
ONR 313
800 North Quincy Street
Arlington, Virginia 22217-5660

Period covered by Progress Report : October 1, 1999 through September 30, 2000

1 OVERVIEW OF PROGRAM

This program addresses the Navy need for extended firm track range for low altitude cruise missiles through the integration of multiple sensors. Track-Before-Declare (TBD) techniques that utilize signal features are proposed for the synergistic integration of an Electronically Scanned Array (ESA) radar with other sensors for the detection of weak targets. A comparison of the performances of a notional multisensor system with that of a federated system of sensors is planned. More specifically, the integration of an ESA radar and Infrared Search and Track (IRST) sensor for a shipboard combat system was proposed. The computer simulation models of the radars and IRST sensor will include the effects of many issues such as finite sensor resolution, limitations on the sensor resources, atmospheric refraction, sensor pointing errors, sea-surface induced multipath, nonhomogeneous clutter, sea clutter, etc. that are omitted in most of the legacy simulations. The computer simulation models will be utilized to develop tracking benchmark problems for broad distribution. These benchmark problems will serve to educate the research community on many of the "real-world" problems that are faced in actual tracking systems and the integration of multiple sensors.

The technical objectives of the project include the following:

- Development and demonstration through computer simulation of algorithms that provide enhanced detection of weak targets through the integration of multiple sensors. More specifically, Track-Before-Declare (TBD) techniques that utilize signal features are

proposed for the synergistic integration of an Electronically Scanned Array (ESA) radar with others sensors for the detection of weak targets. The integration of the ESA radar with the Infrared (IR) sensor are to be considered. The detection performance of a notional multisensor system will be compared with that of the federated system of sensors.

- Development and demonstration through computer simulation of efficient radar resource allocation techniques that maximizes the information procured by the multisensor suite, while accommodating remote cues and/or warnings and adapting to changes in the characteristics of the targets of interest, weather conditions, etc. The waveforms and revisit times of the ESA will be selected to maximize the information procured by the multisensor system. The detection performance of a notional multisensor system with the new resource allocation techniques will be compared to that of the multisensor system with conventional resource allocation and that of the federated system of sensors.

This report summaries the progress and accomplishments made during October 1, 1999 and September 30, 2000, which is the second year of a three year program. Since only a small amount of funding was provided for this program, the progress toward the goals of this program include a few publications and other related activities. Section 2 lists the papers that have been published or submitted for publication, and Section 3 summarizes related activities that were supported as part of this project.

2 PUBLICATIONS

The following four papers have been accomplished through funding from this grant. Copies of the papers are included in Enclosures 1 though 5.

1. W. D. Blair and M. Brandt-Pearce, "Monopulse DOA Estimation for Two Unresolved Rayleigh Targets," *IEEE Trans. on Aerospace and Electronic Systems,* to appear in 2001.

2. G.C. Brown, W.D. Blair, and D.A. Diaz "Track Management Technique for Electronically Scanned Radars," *in Signal and Data Processing for Small Targets 2000,* Oliver Drummond, Editor, Proceedings of SPIE Vol. 4048, pp. 203-210 (2000)

3. W. D. Blair and M. Brandt-Pearce, "Effects of Diffuse Multipath on the Statistics of Monopulse Measurements," accepted for the 2001 IEEE Radar Conference, Atlanta GA, May 2001.

4. W. Wong and W. D. Blair, "Steady-State Tracking With LFM Waveforms," *IEEE Transactions on Aerospace and Electronic Systems*, Vol. 36, No. 2, April 2000, pp. 701-709.

5. W. Wong and W. D. Blair, "Steady-State Tracking With LFM Waveforms," *Proceedings of 32nd Southeastern Symposium on Systems Theory*, Tallahassee, FL, March 2000, pp. 69-73.

3 RELATED ACTIVITIES

The follow related activities have been supported at the request of the Office of Naval Research.

1. Hosted the 3rd ONR/GTRI Workshop on Target Tracking and Sensor Fusion, May 17-18, 2000 at the Cobb Research Facility of the Georgia Tech Research Institute. The workshop included approximately 50 attendees and 20 technical presentations. A proceedings of the presentations were produced as a bound copy and on CD ROM.

2. Participated as Technical Expert in Plenary Panel Discussion entitled "Fusion: Vision and Challenges," Fusion 2000: 3rd International Conference on Information Fusion, Paris France, July 10-13 (see Enclosure 6 for slides of presentation).

3. Participated in several meetings with personnel from the United Kingdom on a Cooperative R&D Program on Data Fusion.

   - February 21-22, 2000 in NAVAIR in Lexington Park, MD: Participated in discussions on clutter modeling, data fusion, and naval weapons systems in UK and USA that utilize data fusion. A presentation on the JCTN Benchmark was given.

   - September 14-15, 2000, DERA in Portsmouth, UK: Participated in discussions with UK's DERA personnel on the UK's R&D programs that involve data fusion. A brief entitled "Multiplatform/Multisensor Tracking" was given (see Enclosure 7).

Respectfully,

William D. Blair

William Dale Blair, Senior Research Engineer
Project Director

Monopulse DOA Estimation of Two Unresolved Rayleigh Targets

W.D. Blair
Georgia Tech Research Institute
Georgia Institute of Technology
Atlanta, Georgia 30332-0857
dale.blair@gtri.gatech.edu

M. Brandt-Pearce
Dept. of Electrical Engineering
University of Virginia
Charlottesville, Virginia 22903
mb-p@virginia.edu

ABSTRACT

This paper provides for new approaches to the processing of unresolved measurements as two DOA measurements for tracking closely-spaced targets rather than the conventional single DOA measurement of the centroid. The measurements of the two closely-spaced targets are merged when the target echoes are not resolved in angle, range, or radial velocity (*i.e.*, Doppler processing). The conditional Cramer Rao lower bound (CRLB) is developed for the Direction-Of-Arrival (DOA) estimation of two unresolved Rayleigh targets using a standard monopulse radar. Then the modified CRLB is used to give insight into the boresight pointing for monopulse DOA estimation of two unresolved targets. Monopulse processing is considered for DOA estimation of two unresolved Rayleigh targets with known or estimated relative Radar Cross Section (RCS). The performance of the DOA estimator is studied via Monte Carlo simulations and compared to the modified CRLB.

Keywords: Radar Signal Processing, Target Tracking, Sensor Resolution

1. INTRODUCTION

While the problem of tracking multiple targets has been studied extensively in recent years, the issue of finite sensor resolution has been completely ignored in almost all studies [1]. Typically, the targets are assumed to be detected with a given probability of detection in the presence of false alarms and clutter, and the target measurements are modeled as the true values plus independent Gaussian errors [2]. However, when two targets are closely spaced with regard to the resolution of the sensor, the measurements from the two targets can be merged into a single measurement. The Joint Probabilistic Data Association (JPDA) algorithm [2] was extended in [3] to develop the JPDAM algorithm, which includes possibly merged measurements (*i.e.*, unresolved targets). Multiple Hypothesis Tracking (MHT) [4] was extended in [5] to include possibly unresolved measurements. In the JPDAM algorithm or MHT, merged measurements are modeled as a "power" weighted centroid of the two targets. While the application of the results of this paper can be used to enhance the JPDAM and MHT algorithms, the focus of this paper is the generation of two Direction-Of-Arrival (DOA) estimates for tracking two unresolved targets rather than the use of a centroid for the two targets.

Monopulse is a simultaneous lobing technique for determining the angular location of a source of radiation or of a "target" that reflects part of the energy incident upon it [6]. In an amplitude comparison monopulse radar system, a pulse of energy is transmitted directly at the predicted position of the target, and the target echo is received with two beams that are squinted relative to the predicted position of the target. (Note that two beams are required for each angular coordinate.) Traditionally, the DOA of a target is estimated with the in-phase part (*i.e.*, the real part) of the monopulse ratio, which is formed by dividing the difference of the two received signals by their sum. When target echoes interfere (*i.e.*, the echoes are not resolved in the frequency or time domains), the DOA estimate indicated by the in-phase monopulse ratio can wander far beyond the angular separation of the targets [6]. In [7], Daum studied the angular estimation accuracies of a standard monopulse radar system for two unresolved targets and showed that the estimation accuracies decline significantly as the variance of the target amplitude fluctuations increases. A generalized maximum likelihood ratio test is developed in [8] for detecting the presence of unresolved Rayleigh targets. While the problem of DOA estimation of unresolved targets has been addressed in several studies involving array signal processing [9,10] and multiple-beam monopulse (*i.e.*, more than two beams per angular coordinate) [11], the work of Sherman in [6,12] is the only technique that utilizes a standard monopulse system in the DOA estimation of two unresolved targets.

Since the hardware of many existing systems provides output signals for standard monopulse,

techniques which directly use this output can be implemented in timely and cost-efficient manner without the development of new hardware. Sherman proposed in [6,12] the use of complex monopulse ratios from two pulses separated sufficiently in time so that the relative phase of the two targets changes, but sufficiently close in time so that the amplitudes of the two targets remain fixed. Sherman then used the five measured quantities (*i.e.*, the in-phase and quadrature components of the two complex monopulse ratios and the ratio of the measured amplitudes of the sum signal) to compute the DOAs of the two targets, the two relative phases, and the ratio of the target amplitudes. In [12], the in-phase and quadrature monopulse ratios and the Method of Moments (MM) were used to develop estimators of the DOAs for tracking two unresolved, fixed-amplitude targets with known relative Radar Cross Section (RCS). Berkowitz and Sherman showed in [13] that under similar assumptions the in-phase monopulse ratios from the two angular coordinates and the ratio of the measured amplitudes from two pulses can be used to estimate the centroid of the two targets and the slope of the line connecting them. However, achieving two pulses with echoes that satisfy the requirements of Sherman's technique is questionable. Furthermore, Sherman utilized a deterministic formulation of the problem to develop his approach. Thus, to date, the results of Sherman have not been further developed and reported in the literature, and no algorithm is available for estimating the DOAs of two unresolved Rayleigh targets.

In this paper, the results on monopulse statistics derived in [8] are used to develop estimators that generate two DOA estimates to be used in tracking rather than relying on the centroid measurement conventionally used in tracking. The use of two DOA estimates will be critical for the tracking of two aircraft flying in formation or separating ballistic missiles, where the flight paths result in the targets being unresolved for more than a couple of measurements. The two DOA estimates are computed under the assumption of a known or estimated relative RCS of the two Rayleigh targets, which can be obtained through various methods. For example, *a priori* information about the targets such as type and flight pattern could be used to estimate the relative RCS. If RCS estimates of the individual resolved targets were obtained while tracking, they can also be used. Beam or spatial agility could be exploited to estimate the relative RCS. However, for this paper, the relative RCS is treated as a known or estimated quantity.

Some background material and notation are given in Section 2, while the probability distribution of the monopulse measurements for two unresolved Rayleigh targets is given in Section 3. In Section 4, the conditional Cramer Rao Lower Bounds (CRLBs) are developed for the DOA estimation of two unresolved Rayleigh targets using a standard monopulse radar. The modified CRLBs (MCRLB) [14], which are needed to remove the dependence on the received amplitudes, are calculated and then used to study the effects of antenna boresight pointing on the DOA

estimation. The DOA estimation for the case of two unresolved targets with known relative RCS is treated in Section 5, where the mean of the in-phase monopulse ratio and the variance of the in-phase and quadrature monopulse ratios are utilized to estimate the DOAs of the two targets. Simulation results that illustrate the performance of the DOA estimators and compares it to the MCRLB are also given in Section 5. Concluding remarks are given in Section 6.

2. DEFINITIONS AND BACKGROUND

The in-phase and quadrature parts of the sum and difference signals for two independent, unresolved Rayleigh targets can be written as

$$s_I = \alpha_1 \cos \phi_1 + \alpha_2 \cos \phi_2 + n_{SI} \tag{1}$$

$$s_Q = \alpha_1 \sin \phi_1 + \alpha_2 \sin \phi_2 + n_{SQ} \tag{2}$$

$$d_I = \alpha_1 \eta_1 \cos \phi_1 + \alpha_2 \eta_2 \cos \phi_2 + n_{dI} \tag{3}$$

$$d_Q = \alpha_1 \eta_1 \sin \phi_1 + \alpha_2 \eta_2 \sin \phi_2 + n_{dQ} \tag{4}$$

where α_i is the Rayleigh distributed amplitude of the received signal from target i, ϕ_i is phase of the received signal from target i, η_i is the unitless (volt/volt) DOA for target i, and

$$n_{SI} \sim N(0, \sigma_S^2) \qquad n_{SQ} \sim N(0, \sigma_S^2)$$
$$n_{dI} \sim N(0, \sigma_d^2) \qquad n_{dQ} \sim N(0, \sigma_d^2)$$

The notation $N(\bar{x}, \sigma^2)$ denotes a Gaussian distribution with mean $\bar{x}$ and variance σ^2. For this paper, the noise terms n_{SI}, n_{SQ}, n_{dI}, and n_{dQ}, are assumed to be independent.

Letting Λ and ψ denote the measured amplitude and phase of the sum signal gives

$$s_I = \Lambda \cos \psi \qquad s_Q = \Lambda \sin \psi \tag{5}$$

Then the observed SNR will be defined as

$$\Re_o = \frac{\Lambda^2}{2\sigma_S^2} \tag{6}$$

Since α_1 and α_2 are Rayleigh distributed and ϕ_1 and ϕ_2 are uniformly distributed on $(-\pi, \pi]$, s_I and s_Q are Gaussian random variables. Applying the transformation of random variables in (5) to the PDF of s_I and s_Q gives the PDF of the observed SNR as

$$f(\Re_o|\Re_R) = \frac{1}{\Re_R + 1} \exp\Big[- \frac{\Re_o}{\Re_R + 1} \Big], \qquad \Re_o \geq 0 \tag{7}$$

where $\Re_R$ is the SNR parameter of the Rayleigh signal given by

$$\Re_R = \frac{E[\alpha_1^2]}{2\sigma_S^2} + \frac{E[\alpha_2^2]}{2\sigma_S^2} = \Re_{R1} + \Re_{R2} \tag{8}$$

where $E[\cdot]$ denotes the expected value. Since the relative RCS of the targets is assumed to be known, let $\Re_{R2} = \lambda \Re_{R1}$, $\lambda > 0$. Then $\Re_R = (1+\lambda)\Re_{R1}$. For N subpulses at distinct frequencies (*i.e.*, independent), the Maximum Likelihood (ML) estimate of $\Re_R$ is given by

$$\widehat{\Re}_R = Y_N - 1, \qquad Y_N = \frac{1}{N}\sum_{k=1}^{N} \Re_{ok} \tag{9}$$

where $\Re_{ok}$ denotes the observed SNR for subpulse k. Then $\widehat{\Re}_R$ is an unbiased, efficient estimator of $\Re$ with variance given by $\mathrm{VAR}[\widehat{\Re}_R|\Re_R] = N^{-1}(\Re_R + 1)^2$.

Denoting $s = s_I + js_Q$ and $d = d_I + jd_Q$, the in-phase and quadrature parts of the monopulse ratio are given by

$$y_I = \mathrm{Re}\Big(\frac{d}{s}\Big) = \frac{s_I d_I + s_Q d_Q}{s_I^2 + s_Q^2} \tag{10}$$

$$y_Q = \mathrm{Im}\Big(\frac{d}{s}\Big) = \frac{s_I d_Q - s_Q d_I}{s_I^2 + s_Q^2} \tag{11}$$

3. STATISTICS OF THE MONOPULSE RATIOS

The PDF of the monopulse ratios, y_I and y_Q, for a single pulse can be obtained by application of the transformation of random variables in (5), (10) and (11) as in [8] to $f(s_I, s_Q, d_I, d_Q|\Phi)$, where Φ denotes the parameter set $\{\Re_{R1}, \Re_{R2}, \eta_1, \eta_2, \sigma_S, \sigma_d\}$. Integrating the result with respect to ψ and conditioning the density on Λ in the form of $\Re_o$ gives [8]

$$f(y_I, y_Q|\Re_o, \Phi) = f(y_I|\Re_o, \Phi) f(y_Q|\Re_o, \Phi) \tag{12}$$

where

$$f(y_I|\Re_o, \Phi) = N\Big(\bar{y}_I, \frac{q}{2\Re_o}\Big) \tag{13}$$

$$f(y_Q|\Re_o, \Phi) = N\Big(0, \frac{q}{2\Re_o}\Big) \tag{14}$$

$$\bar{y}_I = \frac{\Re_{R1}\eta_1 + \Re_{R2}\eta_2}{\Re_{R1} + \Re_{R2} + 1} \tag{15}$$

$$q = \Big[\frac{\sigma_d^2}{\sigma_S^2} + \frac{\Re_{R1}\eta_1^2 + \Re_{R2}\eta_2^2 + \Re_{R1}\Re_{R2}(\eta_1 - \eta_2)^2}{\Re_{R1} + \Re_{R2} + 1}\Big] \tag{16}$$

Thus, y_I and y_Q are conditionally independent, Gaussian random variables with a common variance. The mean of y_I is a "power" weighted average of the DOAs of the two targets and independent on $\Re_o$, while the mean of y_Q is zero.

Using N subpulses at distinct frequencies to ensure that the targets' amplitudes are independent for each subpulse, the conditional ML estimate of $\bar{y}_I$ given $\Re_o$ for each pulse is

$$\hat{y}_I = \Big[\sum_{n=1}^{N} \Re_{on}\Big]^{-1} \sum_{k=1}^{N} \Re_{ok} y_{Ik} = \frac{1}{NY_N} \sum_{k=1}^{N} \Re_{ok} y_{Ik} \tag{17}$$

where $\Re_{ok}$ and y_{Ik} denote the observed SNR and in-phase monopulse ratio for subpulse k and Y_N is given by (9). Note that while the ML estimate of $\bar{y}_I$ is conditional, $\bar{y}_I$ is independent of $\Re_{ok}$ by (15). Since the y_{Ik} are Gaussian random variables, $\hat{y}_I$ is the minimum variance estimate of $\bar{y}_I$ and a Gaussian random variable with variance given by

$$\sigma^2_{\hat{y}_I} = q\left[\sum_{k=1}^{N} 2\Re_{ok}\right]^{-1} = \frac{q}{2NY_N} \tag{18}$$

Then $\sigma^2_{\hat{y}_I}$ is the conditional CRLB for any unbiased estimator of $\bar{y}_I$ given $\{\Re_{ok}\}_{k=1}^{N}$. The term conditional here is used to denote the fact that the Fisher information and CRLB are developed with the amplitude-conditioned PDF. While $\sigma^2_{\hat{y}_I}$ provides the variance of $\hat{y}_I$ for real-time or actual tracking, $\sigma^2_{\hat{y}_I}$ cannot be used for performance prediction because it is a function of $\{\Re_{ok}\}_{k=1}^{N}$, which are measured quantities. The MCRLB [14] is obtained by averaging the conditional Fisher information with respect to the measured amplitudes of the received pulses. While the MCRLB is a somewhat looser bound than the CRLB, it can be used for performance prediction. Since $f(y_I|\Re_o, \Phi)$ satisfies the regularity conditions with respect to $\bar{y}_I$ [14], the MCRLB is a lower bound on the variance of any unbiased estimator of $\bar{y}_I$, which is given by

$$\tilde{J}_{y_I}(\hat{\bar{y}}_I|N,\Phi) = E\big[\sigma^{-2}_{\hat{y}_I}\big|N,\Phi\big]^{-1} = \frac{q}{2N(\Re_{R1}+\Re_{R2}+1)} \tag{19}$$

where $\hat{\bar{y}}_I$ is any unbiased estimator of $\bar{y}_I$.

Figure 1 gives a comparison of the MCRLBs of variance of $\hat{\bar{y}}_I$ for a single target and two unresolved, equal-amplitude targets versus the total SNR in a single frequency (*i.e.*, $N = 1$). The MCRLB of the variance of $\hat{\bar{y}}_I$ for a single target is obtained by setting $\Re_{R2} = 0$ in (19). For the two-target case, the total SNR is given by $\Re_{R1} + \Re_{R2} = 2\Re_{R1}$. In order to obtain $\bar{y}_I = 0$ in both cases, the single target was set at the boresight, and the two targets were situated symmetrically about the boresight (*i.e.*, $\eta_1 = -\eta_2$) and separated by one-half of a beamwidth with $\eta_1 = 0.4$.

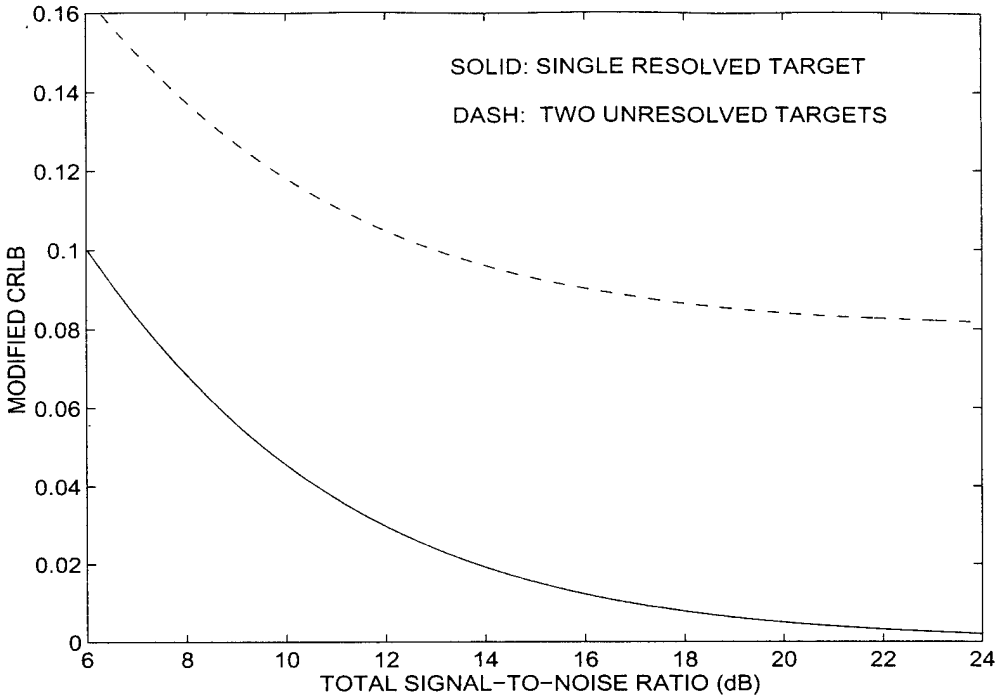

Figure 1. MCRLB of the variance of $\hat{\tilde{y}}_I$ for a single pulse and single target at the boresight and two targets separated by one-half beamwidth and symmetric about the boresight

Figure 1 shows that a total SNR of 14 dB gives a MCRLB of 0.02 for the single-target case and 0.095 for the two-target case. Figure 1 also shows that doubling the energy in a single-frequency waveform to obtain a total SNR of 17 dB gives a MCRLB of 0.01 for the single-target case and 0.09 for the two-target case. Thus, doubling the energy in a single-frequency pulse gives only a small reduction in the MCRLB for the two-target case. However, if the energy in the pulse was doubled by adding a second frequency so that two independent observations of the unresolved targets is obtained, the variance would be reduced by 50 percent because the errors are Gaussian (not shown in figure). Therefore, frequency agility is critical to improving the monopulse angle estimation when two unresolved targets are present.

4. CONDITIONAL AND MODIFIED CRLBS FOR DOA ESTIMATION

The conditional and modified CRLBs associated with $\hat{\eta}_1$ and $\hat{\eta}_2$ are developed in this section. The MCRLB is used here to study the effects of antenna pointing on the DOA estimation and it is used in Section 5 to assess the performance of the DOA estimators.

The conditional Fisher Information Matrix (FIM) [15, p. 79] associated with $\hat{\eta}_1$ and $\hat{\eta}_2$ based

on N observations of y_I and y_Q is given by

$$I_{y_I,y_Q}(\hat{\eta}_1,\hat{\eta}_2|N,\{\Re_{ok}\}_{k=1}^N,\Phi) = \tag{20}$$
$$-\sum_{k=1}^{N}\begin{bmatrix} E\Big[\dfrac{\partial^2 \ln f(y_{Ik},y_{Qk}|\Re_{ok},\Phi)}{\partial\eta_1^2}\Big|\Re_{ok},\Phi\Big] & E\Big[\dfrac{\partial^2 \ln f(y_{Ik},y_{Qk}|\Re_{ok},\Phi)}{\partial\eta_1\partial\eta_2}\Big|\Re_{ok},\Phi\Big] \\ E\Big[\dfrac{\partial^2 \ln f(y_{Ik},y_{Qk}|\Re_{ok},\Phi)}{\partial\eta_1\partial\eta_2}\Big|\Re_{ok},\Phi\Big] & E\Big[\dfrac{\partial^2 \ln f(y_{Ik},y_{Qk}|\Re_{ok},\Phi)}{\partial\eta_2^2}\Big|\Re_{ok},\Phi\Big] \end{bmatrix}$$

where $f(y_{Ik},y_{Qk}|\Re_{ok},\Phi)$ is the conditional PDF of the monopulse ratios for pulse k. Using (12) through (15) in (20) gives

$$I_{y_I,y_Q}(\hat{\eta}_1,\hat{\eta}_2|N,\{\Re_{ok}\}_{k=1}^N,\Phi) = \frac{2N\Re_{R1}\Re_{R2}}{q(\Re_{R1}+\Re_{R2}+1)^2} \tag{21}$$
$$\times\begin{bmatrix} \dfrac{\Re_{R1}}{\Re_{R2}}\Big[Y_N+\dfrac{2}{q}\Big(\eta_1+\Re_{R2}\Delta\eta\Big)^2\Big] & Y_N+\dfrac{2}{q}\Big(\eta_1+\Re_{R2}\Delta\eta\Big)\Big(\eta_2-\Re_{R1}\Delta\eta\Big) \\ Y_N+\dfrac{2}{q}\Big(\eta_1+\Re_{R2}\Delta\eta\Big)\Big(\eta_2-\Re_{R1}\Delta\eta\Big) & \dfrac{\Re_{R2}}{\Re_{R1}}\Big[Y_N+\dfrac{2}{q}\Big(\eta_2-\Re_{R1}\Delta\eta\Big)^2\Big] \end{bmatrix}$$

where $\Delta\eta = \eta_1 - \eta_2 > 0$. The dependence of $I_{y_I,y_Q}(\hat{\eta}_1,\hat{\eta}_2|N,\{\Re_{ok}\}_{k=1}^N,\Phi)$ on Y_N can removed by averaging over the observed SNR, $\{\Re_{ok}\}_{k=1}^N$, thereby deriving the modified FIM,

$$\tilde{I}_{y_I,y_Q}(\hat{\eta}_1,\hat{\eta}_2|N,\Phi) = E[I_{y_I,y_Q}(\hat{\eta}_1,\hat{\eta}_2|N,\{\Re_{ok}\}_{k=1}^N,\Phi)|N,\Phi)] \tag{22}$$

which is equivalent to setting $Y_N = E[Y_N|\Phi] = \Re_{R1}+\Re_{R2}+1$ in (21) since Y_N appears only linearly.

A bound on the covariance of any unbiased estimator of η_1 and η_2 [15, p. 79] is given by the conditional CRLB,

$$COV\begin{bmatrix}\hat{\eta}_1\\ \hat{\eta}_2\end{bmatrix} \geq J_{y_I,y_Q}(\hat{\eta}_1,\hat{\eta}_2|N,\{\Re_{ok}\}_{k=1}^N,\Phi) = \Big[I_{y_I,y_Q}\hat{\eta}_1,\hat{\eta}_2|N,\{\Re_{ok}\}_{k=1}^N,\Phi)\Big]^{-1} \tag{23}$$

where

$$J_{y_I,y_Q}(\hat{\eta}_1,\hat{\eta}_2|N,\{\Re_{ok}\}_{k=1}^N,\Phi) = \frac{q^2}{4N\Re_{R1}\Re_{R2}\Delta\eta^2} \tag{24}$$
$$\times\begin{bmatrix} \dfrac{\Re_{R2}}{\Re_{R1}}\Big[1+\dfrac{2}{qY_N}\Big(\eta_2-\Re_{R1}\Delta\eta\Big)^2\Big] & -1-\dfrac{2}{qY_N}\Big(\eta_1+\Re_{R2}\Delta\eta\Big)\Big(\eta_2-\Re_{R1}\Delta\eta\Big) \\ -1-\dfrac{2}{qY_N}\Big(\eta_1+\Re_{R2}\Delta\eta\Big)\Big(\eta_2-\Re_{R1}\Delta\eta\Big) & \dfrac{\Re_{R1}}{\Re_{R2}}\Big[1+\dfrac{2}{qY_N}\Big(\eta_1+\Re_{R2}\Delta\eta\Big)^2\Big] \end{bmatrix}$$

In (23), the matrix inequality for matrices A and B with $A \geq B$ is defined as $A-B$ is nonnegative definite. Since $f(y_I,y_Q|\Re_o,\Phi)$ satisfies the regularity conditions with respect to η_1 and η_2 [14],

the MCRLB is a lower bound on the covariance of any unbiased estimator of η_1 and η_2 [14]. The MCRLB, $\tilde{J}_{y_I,y_Q}(\hat{\eta}_1,\hat{\eta}_2|N,\Phi)$, is derived by using the modified FIM of (22) instead of the conditional FIM of (21) in (23). Thus, the MCRLB, $\tilde{J}_{y_I,y_Q}(\hat{\eta}_1,\hat{\eta}_2|N,\Phi)$, is obtained by setting $Y_N = E[Y_N|\Phi] = \Re_{R1} + \Re_{R2} + 1$ in (24) and given by

$$\tilde{J}_{y_I,y_Q}(\hat{\eta}_1,\hat{\eta}_2|N,\Phi) = \frac{q^2}{4N\Re_{R1}\Re_{R2}\Delta\eta^2} \times \begin{bmatrix} \frac{\Re_{R2}}{\Re_{R1}}\left[1+\frac{2(\eta_2-\Re_{R1}\Delta\eta)^2}{q(\Re_{R1}+\Re_{R2}+1)}\right] & -1-\frac{2(\eta_1+\Re_{R2}\Delta\eta)(\eta_2-\Re_{R1}\Delta\eta)}{q(\Re_{R1}+\Re_{R2}+1)} \\ -1-\frac{2(\eta_1+\Re_{R2}\Delta\eta)(\eta_2-\Re_{R1}\Delta\eta)}{q(\Re_{R1}+\Re_{R2}+1)} & \frac{\Re_{R1}}{\Re_{R2}}\left[1+\frac{2(\eta_1+\Re_{R2}\Delta\eta)^2}{q(\Re_{R1}+\Re_{R2}+1)}\right] \end{bmatrix} \tag{25}$$

Although the MCRLB is known to be a somewhat looser bound than the CRLB, it is needed to remove the dependence on the received amplitudes so that performance prediction can be accomplished. The diagonal elements of $\tilde{J}_{y_I,y_Q}(\hat{\eta}_1,\hat{\eta}_2|N,\Phi)$ give the MCRLBs for the variances of $\hat{\eta}_1$ and $\hat{\eta}_2$ and are used to assess the efficiency [15, p. 71] of the DOA estimators in the next section.

The MCRLB of (25) can be used to study the effects of sensor pointing on the DOA estimation. For this study, the effects of the antenna gain pattern are not assumed to be included in λ, the relative RCS of the two targets. The effects of the antenna gain pattern can instead be included in the anaylsis of the MCRLB by using

$$\widetilde{\Re}_{R1} = \Re_{R1}\cos^4\left(\frac{\eta_1\pi}{4\eta_{bw}}\right) \tag{26}$$

$$\widetilde{\Re}_{R2} = \Re_{R2}\cos^4\left(\frac{\eta_2\pi}{4\eta_{bw}}\right) \tag{27}$$

in (25) for $\Re_{R1}$ and $\Re_{R2}$, respectively. The η_{bw} denotes the DOA value at the one-way, half-power point on the antenna gain pattern of the sum channel. Thus, at $\eta_1 = \eta_{bw}$, $\widetilde{\Re}_{R1} = \Re_{R1} - 6$ dB. For a monopulse error slope k_m in beamwidths, $2\eta_{bw} \approx k_m$. For all of the examples in this paper, $\eta_{bw} = 0.8$.

Figure 2(a) shows the average MCRLB for two 19 dB targets (*i.e.*, $\Re_{R1} = \Re_{R2} = 19$ dB in (26) and (27) for $N = 1$) separated by one-half beamwidth (*i.e.*, $\Delta\eta = \eta_{bw} = 0.8$) versus the DOA of target 1, η_1, for $N = 1,\ 2,\ 4,\ 8$ and 16 subpulses. The average MCRLB is the average of the two diagonal elements of (25). For each case in Figure 2(a), the energy in the transmitted pulse is fixed and it is divided into N subpulses at different frequencies. Thus, for $N = 8$ subpulses, $\Re_{R1} = \Re_{R2} = 10$ dB in (26) and (27). The DOA for target 2 is given by $\eta_2 = \eta_1 - \Delta\eta$. Thus, $\eta_1 = 0$ in Figure 2(a) corresponds to target 1 on the antenna boresight, while $\eta_1 = 0.8$ corresponds to target 2 on the antenna boresight. Also, $\eta_1 = -0.2$ and $\eta_2 = -1.0$ in Figure 2(a)

corresponds to pointing the antenna boresight on the outside of the two targets. The average of the two MCRLBs in Figure 2(a) shows that pointing the antenna boresight exactly between the two targets (*i.e.*, $\eta_1 = 0.4$) gives the smallest average MCRLB for $N = 4$, 8, and 16 and the largest bound for pointing between the targets when $N = 1$. For $N = 1$, the minimum average MCRLB is achieved by pointing the antenna boresight just to the outside of one of the two targets. Figure 2(a) also shows that the average MCRLB is rather insensitive to the antenna boresight when it is positioned between the two targets. For $N = 16$, the rapid increases in the average MCRLB near the edges of the plot are due to the rapid increase of the MCRLB for the weaker target. To illustrate this point, Figure 2(b) gives the individual MCRLBs of the two targets for $N = 4$ and 8. Figure 2(b) shows that pointing the antenna boresight closer to target 1 gives a smaller MCRLB for the variance of $\hat{\eta}_1$ and a larger MCRLB for the variance of $\hat{\eta}_2$. Note the rapid increase in the MCRLB of the weaker target when the antenna is pointed to the outside of one of the two targets. Also, note that the reduction in the MCRLB gained through frequency agility (*i.e.*, $N = 8$ rather than $N = 4$) is lost due to the low subpulse SNR at $\eta_1 = -0.15$ for η_2 and $\eta_1 = 0.95$ for η_1.

If the DOA estimate for a single target is desired, Figure 2(b) shows that pointing the antenna closer to or beyond the target of interest (but away from the interfering target) minimizes the MCRLB for that target. The minimum MCRLB for the variance of $\hat{\eta}_1$ with $N = 4$ is 0.015 at $\eta_1 = -0.3$ and with $N = 8$ is 0.012 at $\eta_1 = -0.2$. For $N = 1$ (not shown in Figure 2(b)), the minimum MCLRB for the variance of $\hat{\eta}_1$ is 0.012 at $\eta_1 = -0.5$. For the single target DOA estimation, an optimal pointing angle always exists, which moves towards the target of interest as N increases for the given separation of the two targets and target amplitudes. For $N > 1$, note that pointing the antenna boresight away from the intefering target is optimal for single DOA estimation, whereas pointing between the targets is optimal when estimating both DOAs.

Figure 2(c) gives further insight into the pointing of the antenna boresight for the DOA estimation of two unresolved targets. Using eight frequencies (*i.e.*, $N = 8$) to simultaneously estimate both DOAs gives a minimum MCRLBs for the individual targets of 0.028 with the antenna boresight pointed exactly between the two targets, as seen also in Figure 2(a). If the eight subpulses are used in two dwells of four subpulses each, the two DOAs can be sequentially estimated by using the first dwell to estimate the nearer target DOA, and using the second to estimate the other target DOA. This method also gives a minimum MCRLB of 0.028 obtained by pointing to the outside of the targets. Further analysis showed that if the separation between the targets is larger than one half of the beamwidth (*i.e.*, $\Delta\eta > \eta_{bw}$), sequential estimation yields a lower MCRLB, whereas if the separation is less than one half the beamwidth, simultaneous estimation provides the best performance bound (not shown). Therefore, for equal amplitude

targets, the case $\Delta\eta = \eta_{bw}$ shown in Figure 2(c) denotes a boundary in the decision process for the optimal pointing strategy.

Figure 3(a) shows the average MCRLB for two 19 dB targets (*i.e.*, $\Re_{R1} = \Re_{R2} = 19$ dB in (26) and (27) for $N = 1$) separated by one-fourth beamwidth (*i.e.*, $\Delta\eta = 0.5\eta_{bw} = 0.4$) versus η_1 for $N = 1,\ 2,\ 4,\ 8$, and 16 subpulses. Thus, $\eta_1 = 0$ in Figure 3(a) corresponds to target 1 on the antenna boresight, while $\eta_1 = 0.4$ corresponds to target 2 on the antenna boresight. The average of the two MCRLBs in Figure 3(a) shows that pointing the antenna boresight exactly between the two targets (*i.e.*, $\eta_1 = 0.2$) gives the smallest average MCRLB for all values of N. Figure 3(a) also shows that increasing the number of frequencies from $N = 8$ to $N = 16$ actually results in an increase in the average MCRLB. Note that this result differs from that shown in Figure 2(a), and it is thought to be the result of a low subpulse SNR at $N = 16$ and a lower average MCRLB in 3(a) compared to that in 2(a).

Figure 3(b) gives insight into the pointing of the antenna boresight for the DOA estimation of a single target in the presence of another target for one-fourth beamwidth separation. It is interesting to note the minimum MCRLB for single DOA estimation corresponds to pointing between the two equal amplitude targets for $N = 8$, in contrast to the results of Figure 2(b). A comparision of the sequential and the simultaneous estimation algorithms for this case in a manner similar to that of Figure 2(c) indicates that it is always advantageous to use simultaneous estimation.

Figure 4(a) shows the average MCRLB for a 19 dB target and a 16 dB target (*i.e.*, $\Re_{R1} = 2\Re_{R2} = 19$ dB) separated by one-fourth beamwidth versus η_1 for $N = 1,\ 2,\ 4$ and 8 subpulses. For the $N = 1$ and 2 cases, the optimal pointing strategy is to steer the antenna boresight slightly towards the stronger target, while for the other cases, steering should lean toward the weaker target. It appears that the simultaneous DOA estimator favors pointing towards the lower power target when subpulse powers are too low ($N = 4$ or 8), perhaps to avoid very low SNR observations. Note also that the advantages of frequency agility have been achieved by $N = 4$ and the degradation in performance due to low subpulse SNR can be seen by the steepening of the graph at extreme values of η_1 for $N = 8$. The MCRLB for the single target DOA estimator shown in Figure 4(b) agrees with the results for the equal energy case of Figure 3(b) that for a small number of subpulses the antenna should be pointed at or outside the position of the targets and for a larger number of subpulses it should point on the inside. For the case of two unequal amplitude targets, the pointing strategy for sequential estimation is less clear. Figure 4(b) suggests a potential iterative approach. The pointing of the first dwell is in the neighborhood of the stronger target in order to minimize the interference from the weaker

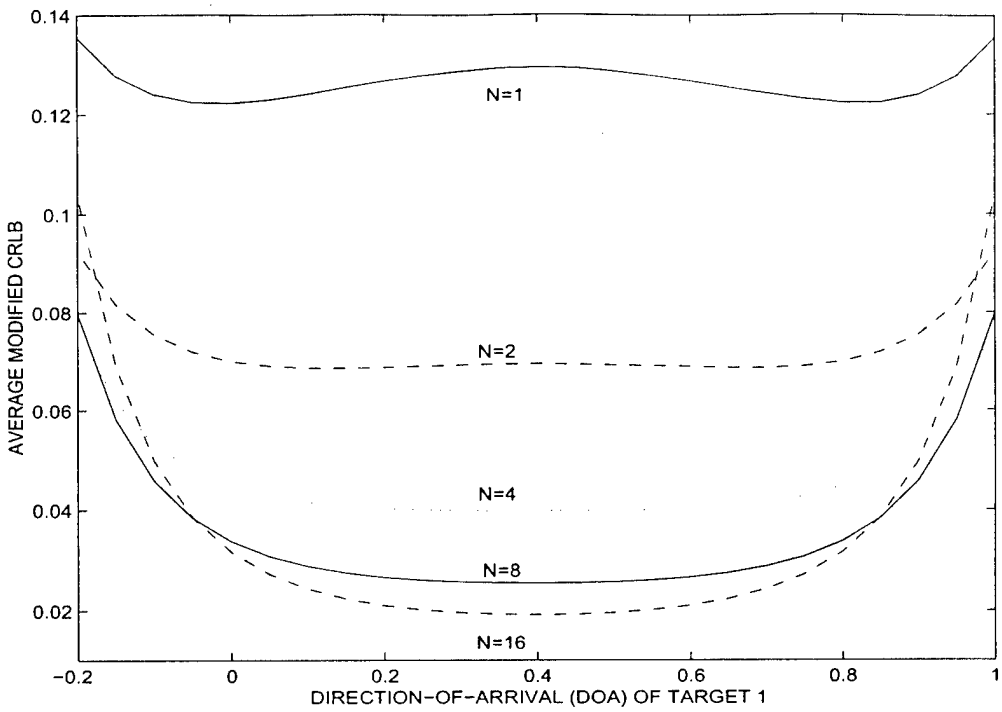

Figure 2(a) Average MCRLB for the variances of $\hat{\eta}_1$ and $\hat{\eta}_2$ with $\Delta\eta = \eta_{bw}$ and two 19 dB targets

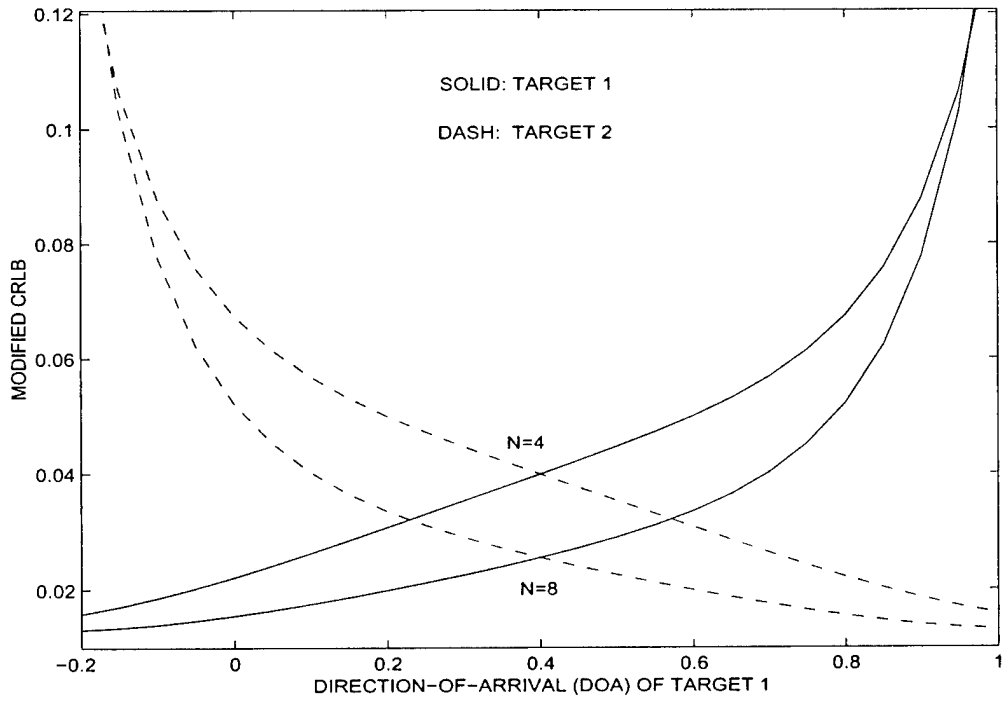

Figure 2(b) MCRLBs for variances of $\hat{\eta}_1$ and $\hat{\eta}_2$ with $\Delta\eta = \eta_{bw}$ and two 19 dB targets

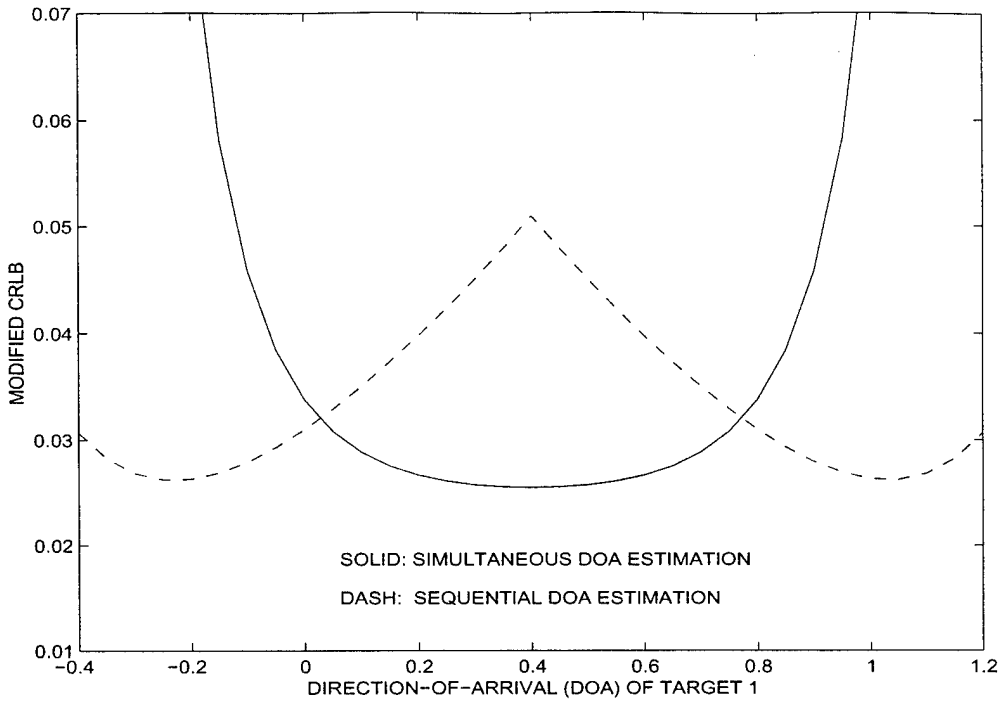

Figure 2(c) MCRLBs for sequential and simultaneous estimation of η_1 and η_2 with $\Delta\eta = \eta_{bw}$, two 19 dB targets, and eight subpulses of equal energy (Sequential: $N = 4$ in two consecutive dwells; simultaneous: $N = 8$ in one dwell)

target. The pointing of the second dwell is then chosen to minimize the bound in estimating the DOA of the second, weaker, target using the information in the first dwell.

5. DOA ESTIMATION FOR TWO UNRESOLVED TARGETS

As seen in the previous section, the pointing of the antenna boresight affects the information obtained during a radar dwell. Based on the results of Section 4, two sensor pointing strategies are set forth. The simultaneous pointing strategy that was found to be optimal for targets separated by less than one-half beamwidth involves pointing between the targets and estimating both DOAs from data gathered in one dwell. This case is referred to as the fully unresolved case. The second strategy proposed, applicable to targets which are separated by more than one-half of a beamwidth, is the sequential strategy in which the DOAs are estimated from data gathered from two consecutive dwells, each pointing in the general direction of one target. This case can be thought of as a partially resolved target scenario since estimation of each parameter can be performed individually. In this section, a DOA estimation algorithm based on the Method of Moments (MM) for the fully unresolved two-target case is proposed. The partially resolved

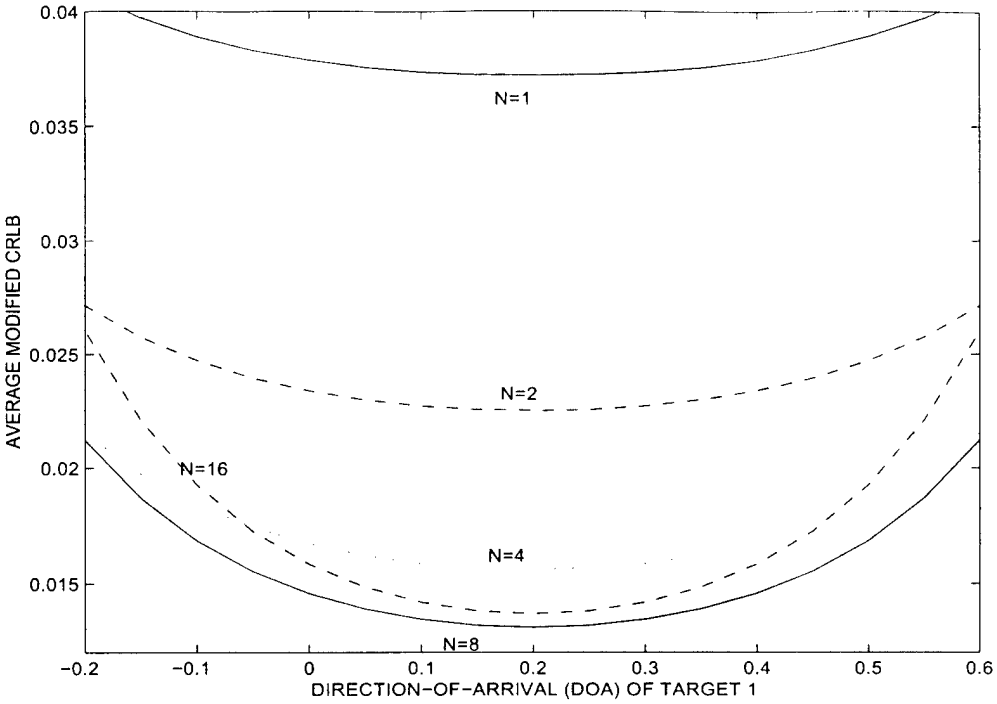

Figure 3(a) Average MCRLB for the variances of $\hat{\eta}_1$ and $\hat{\eta}_2$ with $\Delta\eta = 0.5\eta_{bw}$ and two 19 dB targets

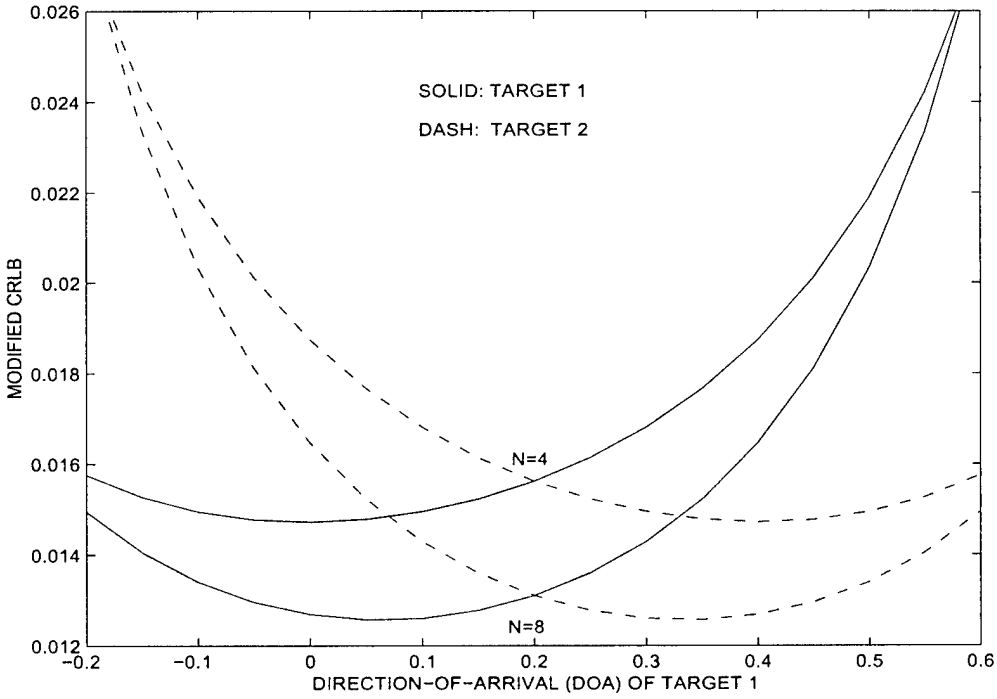

Figure 3(b) MCRLBs for variances of $\hat{\eta}_1$ and $\hat{\eta}_2$ with $\Delta\eta = 0.5\eta_{bw}$ and two 19 dB targets

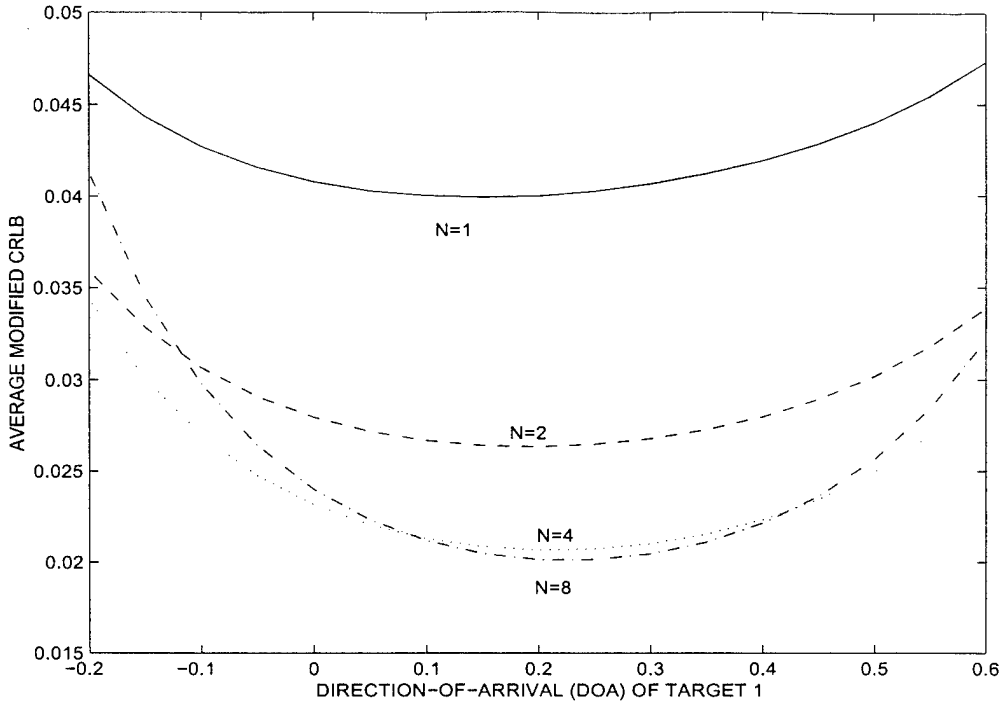

Figure 4(a) Average MCRLB for the variances of $\hat{\eta}_1$ and $\hat{\eta}_2$ with $\Delta\eta = 0.5\eta_{bw}$ and 19 dB and 16 dB targets, respectively

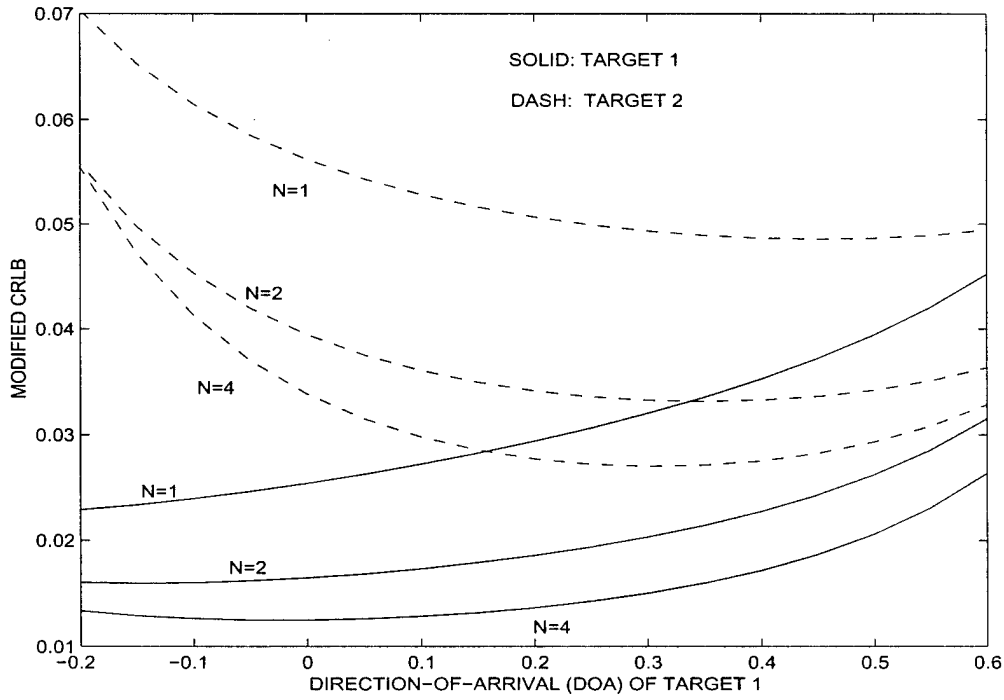

Figure 4(b) MCRLB for the variances of $\hat{\eta}_1$ and $\hat{\eta}_2$ with $\Delta\eta = 0.5\eta_{bw}$ and 19 dB and 16 dB targets, respectively

target case is briefly discussed in [17].

For the case of two fully unresolved Rayleigh targets, the antenna boresight is pointed between the targets and the DOA estimation of both targets is accomplished simultaneously via MM. For the MM, two sample moments are required for the estimation of two DOAs. Since the observations y_{Ik} are conditionally nonstationary (*i.e.*, the variance of y_{Ik} given $\Re_{ok}$ changes with $\Re_{ok}$ - see (13)) sample moments cannot be used directly. Thus, $\hat{y}_I$ from (17) will be used to obtain the first expression as

$$\hat{y}_I \approx \frac{\Re_{R1}\eta_1 + \Re_{R2}\eta_2}{\Re_{R1} + \Re_{R2} + 1} = \bar{y}_I \tag{28}$$

Let $\Delta\eta = \eta_1 - \eta_2 > 0$, so that $\eta_1 > \eta_2$. Then, for $\Re_{R1} \gg 1$, since $\Re_{R2} = \lambda\Re_{R1}$, where $\lambda > 0$,

$$\eta_1 \approx \hat{y}_I + \frac{\lambda}{1+\lambda}\Delta\eta \tag{29}$$

$$\eta_2 \approx \hat{y}_I - \frac{1}{1+\lambda}\Delta\eta \tag{30}$$

Since the y_{Ik} are conditionally nonstationary, Gaussian random variables, the second expression for DOA estimation will be obtained by forming a Chi-squared random variable with $2N-1$ degrees of freedom from y_{Ik}, $\Re_{ok}$, and $\hat{y}_I$ and setting the random variable equal to its mean. Thus, for $N > 1$, let

$$X_N = [\, y_{I1} - \hat{y}_I \quad \cdots \quad y_{IN} - \hat{y}_I \quad y_{Q1} \quad \cdots \quad y_{QN} \,] \tag{31}$$

$$R_N = 2\ \mathrm{diag}\,[\, \Re_{o1} \quad \cdots \quad \Re_{oN} \quad \Re_{o1} \quad \cdots \quad \Re_{oN} \,] \tag{32}$$

Since for $N = 1$, $\hat{y}_I = y_{I1}$, let $X_1 = y_{Q1}$ and $R_1 = 2\Re_{o1}$. Also let

$$v_N = X_N^T R_N X_N q^{-1} \tag{33}$$

where q is given by (16). Since the conditional PDF of the in-phase and quadrature monopulse ratios are Gaussian with variance given by (13) through (16), v_N is a Chi-squared random variable with $2N - 1$ degrees of freedom as one degree of freedom has been lost due to the estimation of $\bar{y}_I$ [16]. Then

$$E[v_N|\Phi, \{\Re_{ok}\}_{k=1}^N] = 2N - 1 \tag{34}$$

$$\mathrm{VAR}[v_N|\Phi, \{\Re_{ok}\}_{k=1}^N] = 2(2N - 1) \tag{35}$$

Setting v_N equal to its mean gives

$$\hat{q} = \frac{X_N^T R_N X_N}{2N - 1}, \qquad N \geq 1 \tag{36}$$

Since for $\Delta\eta > 1.0$ the targets would be processed as partially unresolved targets, assume that $\Delta\eta < 1.0$. Thus, pointing the antenna boresight between the targets gives $|\eta_1| < 1$ and $|\eta_2| < 1$, which allows the approximation of q by

$$q \approx \frac{\sigma_d^2}{\sigma_S^2} + \frac{\lambda \Re_{R1}}{1+\lambda}\Delta\eta^2 \tag{37}$$

because $\Re_{R1}\eta_1^2 + \Re_{R2}\eta_2^2 << \Re_{R1}\Re_{R2}(\eta_1 - \eta_2)^2$ in (16). Note that (37) implies that any estimate of q must be greater than σ_d^2/σ_S^2 and less than $\sigma_d^2/\sigma_S^2 + \lambda(1+\lambda)^{-1}\Re_{R1}\max(\Delta\eta^2)$. Inserting $\hat{q}$ from (36) for q, using (37) in (29) and (30), and applying the restrictions on an estimate of q gives DOA estimates as

$$\hat{\eta}_1 = \hat{y}_I + \sqrt{\frac{\lambda\tilde{q}}{\widehat{\Re}_R}} \tag{38}$$

$$\hat{\eta}_2 = \hat{y}_I - \sqrt{\frac{\tilde{q}}{\lambda\widehat{\Re}_R}} \tag{39}$$

where

$$\tilde{q} = \begin{cases} 0, & \hat{q} \le \sigma_d^2\sigma_S^{-2} \\ \dfrac{4\eta_{bw}^2\lambda}{(1+\lambda)^2}\widehat{\Re}_R, & \hat{q} \ge \dfrac{4\eta_{bw}^2\lambda}{(1+\lambda)^2}\widehat{\Re}_R + \sigma_d^2\sigma_S^{-2} \\ \hat{q} - \sigma_d^2\sigma_S^{-2}, & \text{otherwise} \end{cases} \tag{40}$$

η_{bw} is defined in conjunction with (26) and (27), $\Re_R$ and $\widehat{\Re}_R$ are given by (8) and (9). The first case of (40) is introduced to ensure that the DOA estimates are real numbers, while the second is introduced to prevent the difference of the two DOA estimates from being larger than $2\eta_{bw}$. Limiting the difference of the two DOA estimates was found to be critical when correcting the known relative RCS λ for the effects of the antenna gain pattern of the sum channel.

In order to use the DOA estimates for tracking, estimates of the variances of $\hat{\eta}_1$ and $\hat{\eta}_2$ are needed. As detailed in the Appendix, the variances of the DOA estimates for $q \gg \sigma_d^2\sigma_S^{-2}$ can be approximated as

$$\mathrm{VAR}[\hat{\eta}_1|\Phi, \{\Re_{ok}\}_{k=1}^N] \approx q\left[\frac{1}{2NY_N} + \frac{\lambda q}{2\widehat{\Re}_R(2N-1)(q-\sigma_d^2\sigma_S^{-2})}\right] \tag{41}$$

$$\mathrm{VAR}[\hat{\eta}_2|\Phi, \{\Re_{ok}\}_{k=1}^N] \approx q\left[\frac{1}{2NY_N} + \frac{q}{2\lambda\widehat{\Re}_R(2N-1)(q-\sigma_d^2\sigma_S^{-2})}\right] \tag{42}$$

Setting $q = \hat{q}$ in (41) and (42) and by analysis of simulation results $q(q-\sigma_d^2\sigma_S^{-2})^{-1} = 3.0$ was found to provide relatively good estimates of the variances for the DOA estimates, which are

given by

$$\hat{\sigma}^2_{\hat{\eta}_1} = \hat{q}\left[\frac{1}{2NY_N} + \frac{1.5\lambda}{\widehat{\Re}_R(2N-1)}\right] \tag{43}$$

$$\hat{\sigma}^2_{\hat{\eta}_2} = \hat{q}\left[\frac{1}{2NY_N} + \frac{1.5}{\lambda\widehat{\Re}_R(2N-1)}\right] \tag{44}$$

Note that these estimates of the variances are functions of the measured data and cannot be used for performance prediction of the estimators.

Monte Carlo simulations with 40000 experiments were conducted to study the performance of the DOA estimators for various values of N, $\Delta\eta$, and λ. While the relative RCS of the two targets is assumed to be known, the effect of the antenna gain pattern is not assumed to be included in λ. The effects of the antenna gain pattern were included in the simulation of (1)-(4) by using

$$\tilde{\alpha}_1 = \alpha_1 \cos\left(\frac{\eta_1\pi}{4\eta_{bw}}\right) \tag{45}$$

$$\tilde{\alpha}_2 = \alpha_2 \cos\left(\frac{\eta_2\pi}{4\eta_{bw}}\right) \tag{46}$$

for α_1 and α_2, respectively. The effects of the antenna gain pattern were addressed in the DOA estimation by using a modified λ in (38) through (40), which is given by

$$\tilde{\lambda} = \lambda \frac{\cos^4\left(\frac{\tilde{\eta}_2\pi}{4\eta_{bw}}\right)}{\cos^4\left(\frac{\tilde{\eta}_1\pi}{4\eta_{bw}}\right)} \tag{47}$$

where $\tilde{\eta}_1$ and $\tilde{\eta}_2$ are the DOA estimates that result from ignoring the effects of the antenna gain pattern. The multiplier modification to λ was restricted to greater than 0.25 and less than 4. Also, during the simulations, only measurements with $NY_N > 20$ dB were utilized in the DOA estimation and $\eta_{bw} = 0.8$, the same value as that used in Section 4. Analysis of the simulation results showed that the use of measurements with a total SNR less than 20 dB can cause the estimation errors to deviate significantly from the MCRLB and the estimator to be unreliable. This requirement for a rather large SNR is most likely due to the lack of tracking information such as predicted antenna gains for the targets. While an SNR of 20 dB is a rather strict requirement, previous methods such as super resolution may require as much as 40 dB [18].

The effect of N on the DOA estimation was studied using $\Delta\eta = 0.4$ and setting $N\Re_{R1} = N\Re_{R2} = 22$ dB (*i.e.*, without the effects of the antenna pattern). The sample averages of the

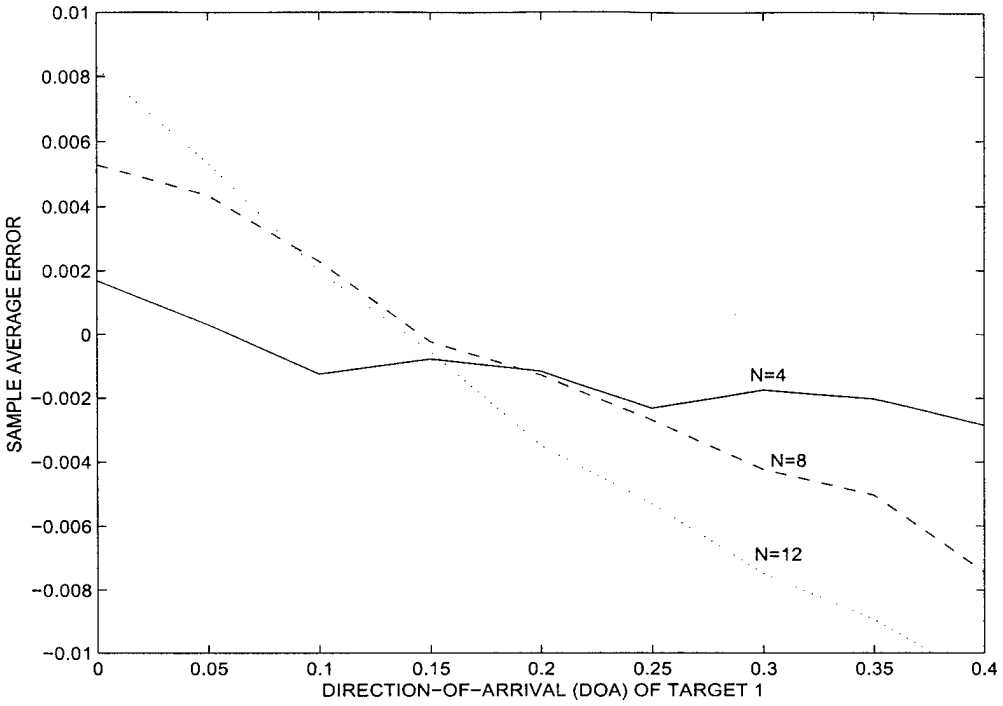

Figure 5(a) Averages of Errors in DOA Estimates of Target 1 for $\Delta\eta = 0.5\eta_{bw}$ and $\lambda = 1$

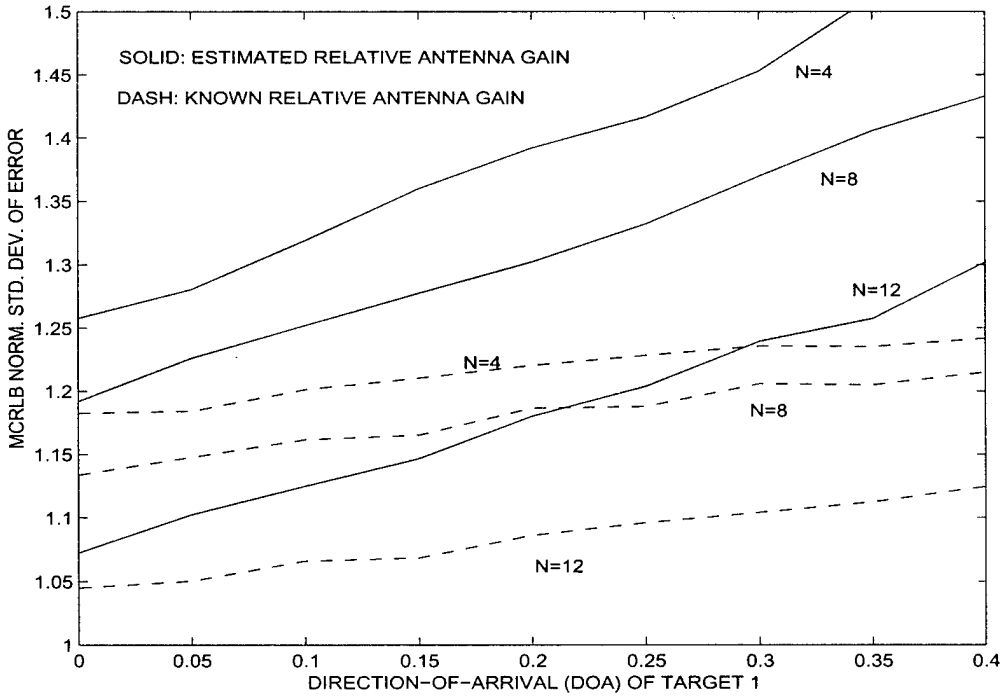

Figure 5(b) Modified CRLB of Target 1 for $\Delta\eta = 0.5\eta_{bw}$ and $\lambda = 1$

errors in the DOA estimates for target 1 are shown versus the DOA of target 1 in Figure 5(a). The DOA for target 2 is given by $\eta_2 = \eta_1 - \Delta\eta$. Thus, $\eta_1 = 0$ in Figure 5(a) corresponds to target 1 on the antenna boresight, while $\eta_1 = 0.4$ corresponds to target 2 on the antenna boresight. Figure 5(a) shows that the sample average errors are rather small for each case of N and have the smaller magnitudes when the antenna boresight is pointed between the two targets (*i.e.*, $\eta_1 \approx 0.2$). The sample standard deviations of the errors in the DOA estimates for target 1 normalized by the square root of the MCRLB are shown versus the DOA of target 1 in Figure 5(b) by the solid lines. Figure 5(b) shows that the efficiency of the MM estimator improves (*i.e.*, sample variance approaches the MCRLB) as N increases from 4 to 12 and is best when the antenna boresight is pointed at target 1 (*i.e.*, $\eta_1 = 0$). However, the MM estimators are shown to be rather inefficient in Figure 5(b). In order to assess the effects of the estimation of the antenna gain pattern effects on the relative RCS on the efficiency of the MM estimators, the simulation studies were conducted with $\tilde{\lambda}$ as a known quantity rather than an estimated quantity (*i.e.*, the true values of η_1 and η_2 were used in (47)). For $\tilde{\lambda}$ known, the sample standard deviations of the errors in the DOA estimates for target 1 normalized by the MCRLB are shown versus the DOA of target 1 in Figure 5(b) by the dashed lines. Figure 5(b) shows that the efficiency of the MM estimators are degraded rather significantly by the estimation of $\tilde{\lambda}$. Thus, if the two targets are under track, the target state estimates should be used to predict the effects of the antenna gain pattern. Figure 5(b) in conjunction with Figure 3(a) also shows that increasing the number of subpulses at distinct frequencies in a radar pulse improves the accuracy and efficiency of the DOA estimation.

The effect of $\Delta\eta$ on DOA estimation was studied using $N = 8$ and setting $\Re_{R1} = \Re_{R2} = 13$ dB. The averages and standard deviations of the errors in the DOA estimates for target 1 are shown in Figures 6(a) and 6(b) for various DOAs of target 1 and $\Delta\eta = 0.2,\ 0.4,\ 0.6$, and 0.8. The DOA estimation for $\Delta\eta = 0.8$ is significantly degraded when compared to that for $\Delta\eta = 0.2$ or 0.4. Thus, when two targets are separated by about one-half of the one-way beamwidth, sequential DOA estimation with two consecutive dwells at the individual targets will be better than the simultaneous DOA estimation with a single dwell. This observation agrees with those of Section 4.

The effect of λ on DOA estimation was studied using $N = 8$, $\Delta\eta = 0.4$, and $\Re_{R1} = 16$ dB. The sample averages and standard deviations of the errors in the DOA estimates for targets 1 and 2 are shown in Figures 7(a) and 7(b) for the positive DOAs of target 1, the corresponding negative DOAs of target 2, and $\lambda = 1,\ 0.5$, and 0.25 (*i.e.*, $\Re_{R2} = 16,\ 13$, and 10 dB). The $\eta_1 = 0$ in Figures 7(a) and 7(b) corresponds to target 1 on the antenna boresight and $\eta_2 = -0.4$, while $\eta_2 = 0$ corresponds to target 2 on the antenna boresight and $\eta_1 = 0.4$. The accuracy of the DOA

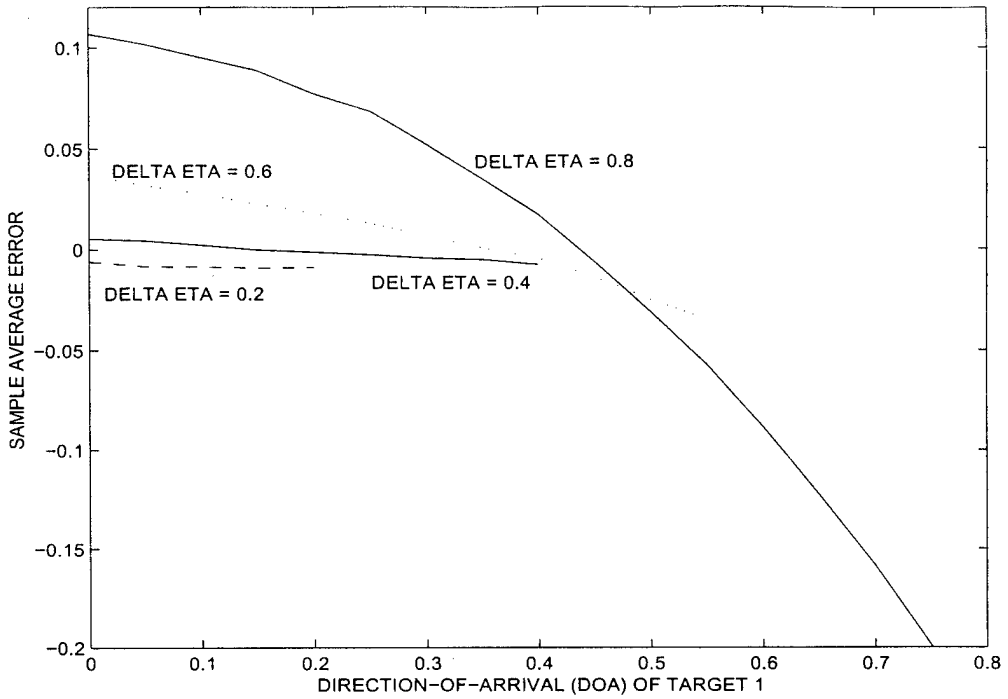

Figure 6(a) Averages of Errors in DOA Estimates of Target 1 for $N = 8$ and $\lambda = 1$

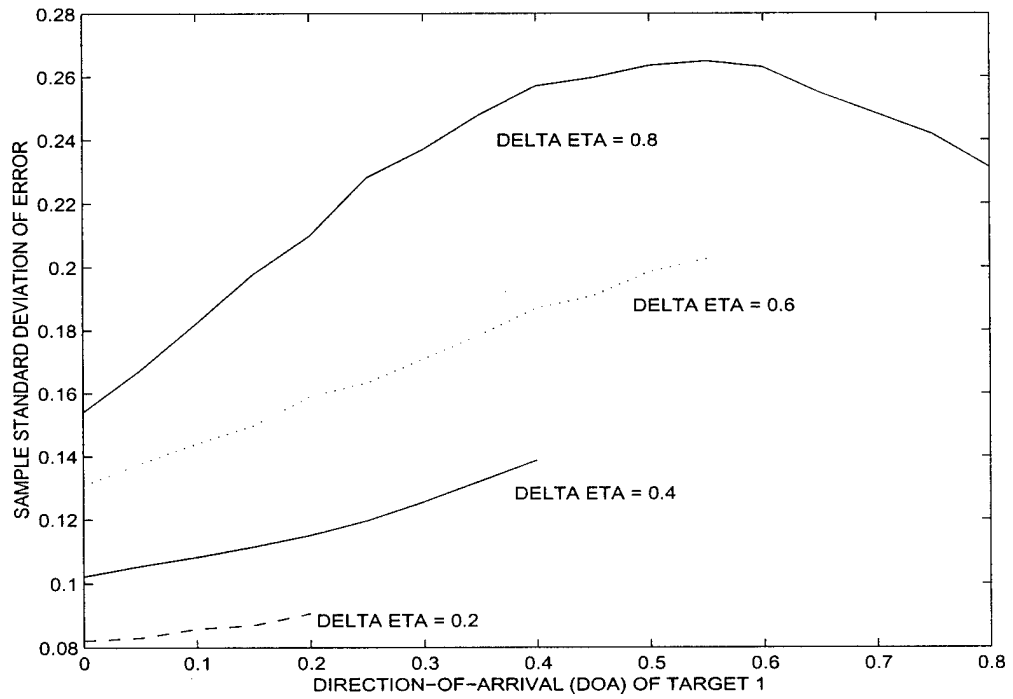

Figure 6(b) Sample Standard Deviations of Errors in DOA Estimates of Target 1 for $N = 8$ and $\lambda = 1$

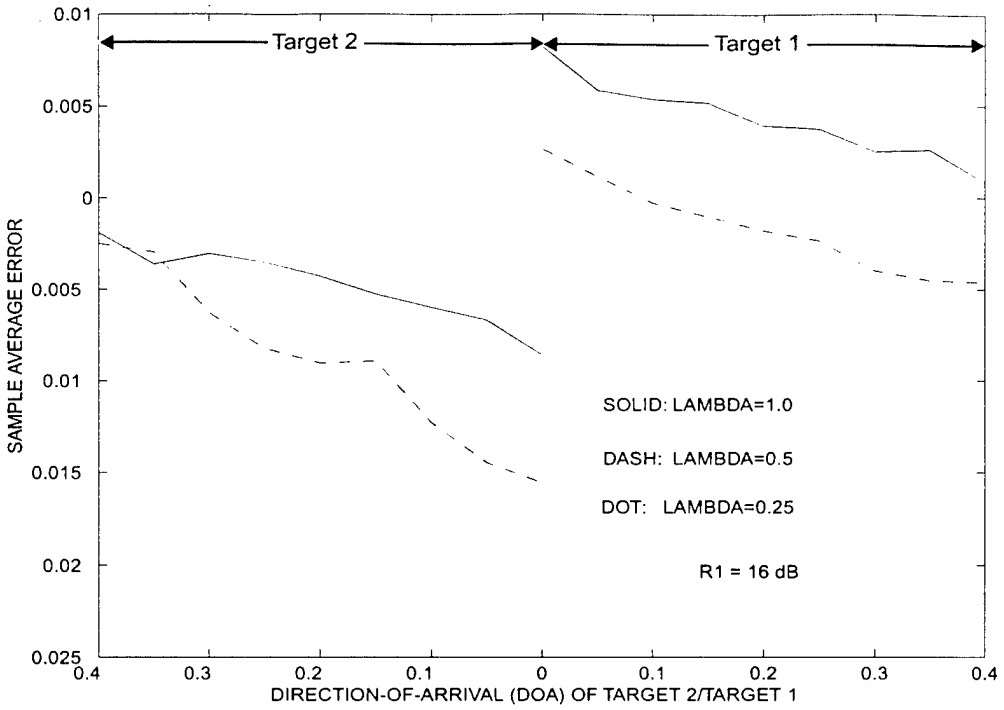

Figure 7(a) Averages of Errors in DOA Estimates for $N = 8$ and $\Delta\eta = 0.5\eta_{bw}$

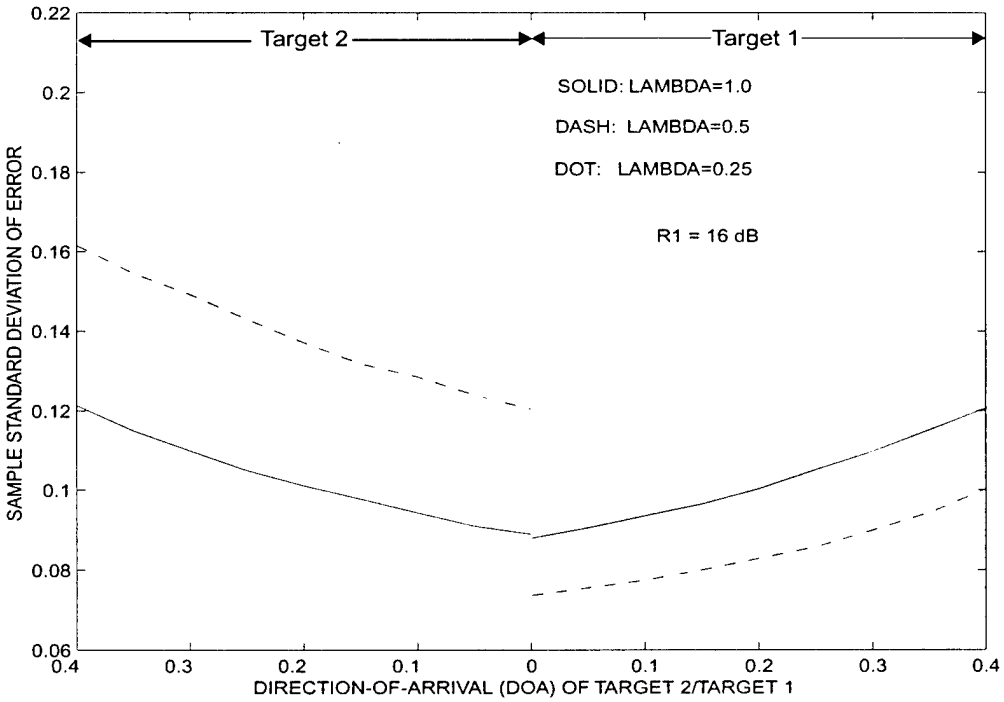

Figure 7(b) Standard Deviations of Errors in DOA Estimates for $N = 8$ and $\Delta\eta = 0.5\eta_{bw}$

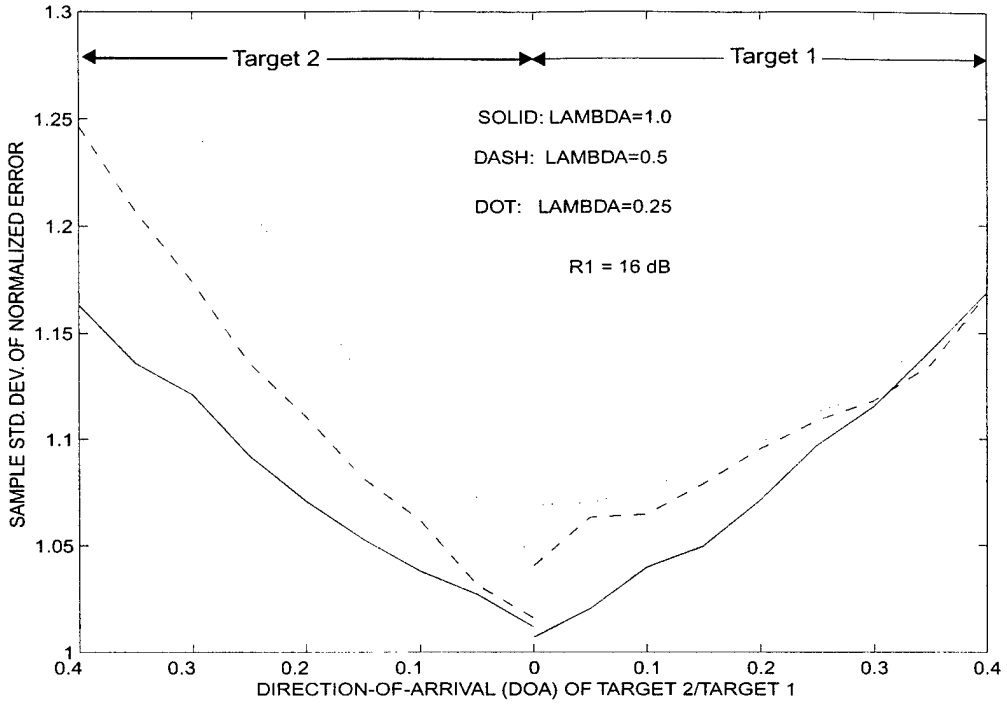

Figure 7(c) Sample Standard Deviations of Errors in DOA Estimates Normalized by the Estimates of Standard Deviations for $N = 8$ and $\Delta\eta = 0.5\eta_{bw}$

estimation for target 1 improves as $\Re_{R2}$ decreases, while accuracy of the DOA estimation for target 2 degrades as $\Re_{R2}$ decreases. The errors were also normalized by the standard deviation estimates of (43) and (44) and the sample standard deviations of these errors are given in Figure 7(c), which indicates that the variances estimates of (43) and (44) are reasonably good. Figure 7(c) also shows that the variance estimates are best for a target at the antenna boresight.

To assess the impacts on the DOA estimation of uncertainty in λ, Monte Carlo experiments were conducted using incorrect values for the relative RCS, $\tilde{\lambda}$. The percent error in λ is define as $(\tilde{\lambda} - \lambda)\lambda^{-1}$. The simulations were conducted for two 16 dB targets separated by one-fourth beamwidth and situated symmetrically about the antenna boresight. The results are shown in Figure 8. For this case of equal RCSs (*i.e.*, $\lambda = 1.0$), negative values of the percent error indicate that $\Re_1$ is thought to be greater than $\Re_2$, while positive values of the percent error indicate that $\Re_2$ is thought to be greater than $\Re_1$. The average errors in Figure 8(a) show that the bias in the DOA estimate is of the same sign as the percent error. The biases in the DOA estimates are due to the DOA estimator shifting the estimates toward the target that is thought to be weaker, which is the result of matching the data to the assumed parameters. For less than 25% error in λ, the biases in the DOA estimates is less than 10% for this case. Figure 8(b) shows that the

effects of errors in λ on the standard deviations of the DOA estimates are very small. Note that the standard deviations of the errors are smaller for the target that is thought to be stronger. The results of Figure 8 suggest that the DOA estimator is rather robust to uncertainty in λ.

6. CONCLUDING REMARKS

The conditional CRLB and modified CRLB were developed for monopulse DOA estimation of two unresolved Rayleigh targets. The MCRLB was used to investigate the effects of frequency diversity and antenna boresight steering on the DOA estimation. For a given waveform energy, the accuracy of the DOA estimation was found to improve as the number of distinct frequencies increases and as long as the expected subpulse energy remains above a few dB. The study revealed two sensor pointing strategies for the DOA estimation: simultaneous and sequential. The simultaneous pointing strategy involves pointing between the targets and estimating both DOAs from data gathered in one dwell, while the sequential pointing strategy involves estimating the DOAs with data gathered from two consecutive dwells, each pointing in the general direction of one target. While the relative performance of the two pointing stategies depend on the SNRs of the two targets and the number of subpulses, the simultaneous pointing strategy was found to be better for targets separated by less than one-half beamwidth, while the sequential pointing strategy was found to be better for targets that are separated by more than one-half of a beamwidth.

An estimation algorithm based on the Method of Moments (MM) was developed for the simultaneous DOA estimation of two unresolved Rayleigh targets with known relative amplitude. In the DOA estimation, the effects of the antenna gain pattern were treated as unknown and addressed in the DOA estimation with a one-step iteration on the DOA estimates. In other words, the initial DOA estimates obtained by ignoring the effects of the antenna gain were used to predict the effect of the antenna gain on the relative amplitude of the two targets for DOA estimation. The performances of the DOA estimators were studied via Monte Carlo simulations and compared to the MCRLB. The results of the Monte Carlo simulations confirmed the predicted benefits of frequency diversity and showed that frequency diversity also improves the efficiency [15] of the estimators. The results support the use of simultaneous DOA estimation when the targets are separated by less than one-half of a beamwidth and sequential DOA estimation when the targets are separated by more than one-half of a beamwidth.

The algorithms developed in this paper have two practical limitations: the uncertainty in the antenna gains at the two DOAs and the uncertainty in the relative RCS. The results show that the efficiency of the MM estimators is degraded rather significantly by the estimation of the effects of the antenna gain. If the two targets are under track prior the merged measurement,

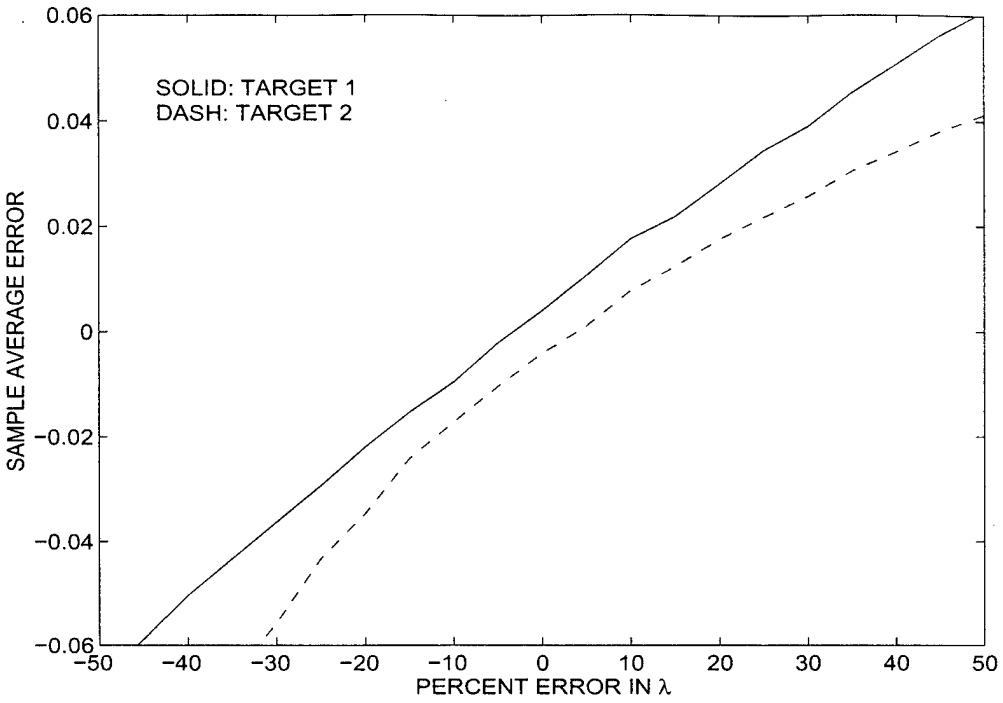

Figure 8(a) Averages of Errors in DOA Estimates for $N = 8$ and $\Delta\eta = 0.5\eta_{bw}$ with Error in λ

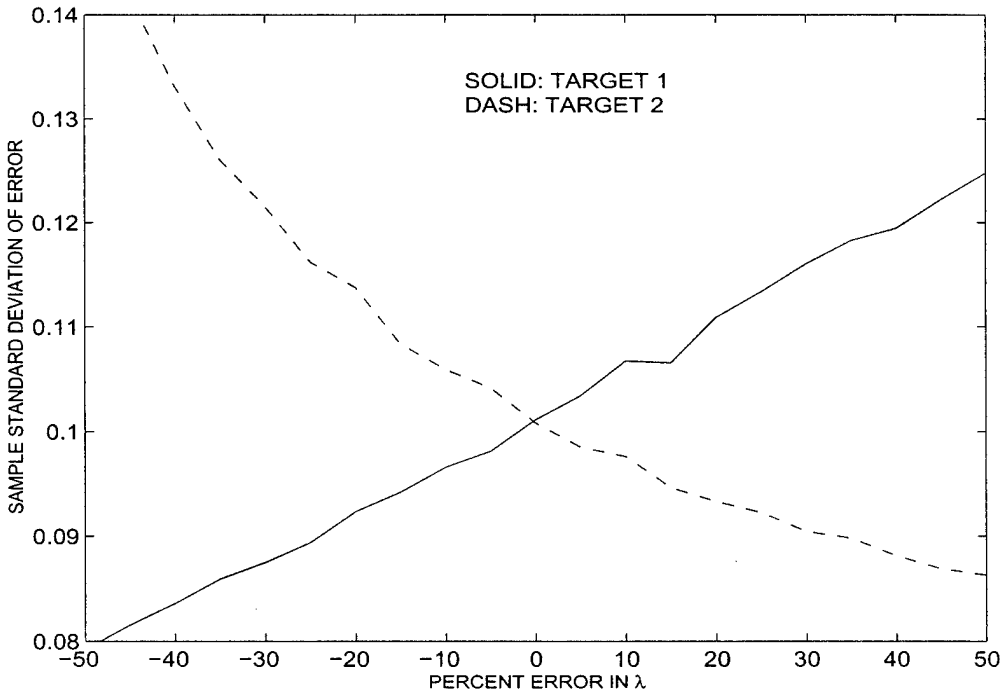

Figure 8(b) Standard Deviations of Errors in DOA Estimates for $N = 8$ and $\Delta\eta = 0.5\eta_{bw}$ with Error in λ

the target state estimates can be used to predict the individual DOAs so that the degradation due to the DOA dependent antenna gain can be reduced. Also, the tracks of the two targets can be used to estimate the relative RCS with sufficient accuracy. Thus, this paper provides practical algorithms for DOA estimation from unresolved measurements using estimated values for the required parameters (relative RCS and antenna gains) that can be obtained from the tracks on the two targets.

REFERENCES

1. F. Daum, "A System Approach to Multiple Target Tracking," in *Multitarget-Multisensor Tracking: Applications and Advances, Vol. II,* edited by Y. Bar-Shalom, Artech House, Inc., Norwood, MA, 1992.
2. Y. Bar-Shalom and X.R. Li, *Multitarget-Multisensor Tracking: Principles and Techniques,* YBS Publishers, Box U-157, Storrs, CT, 06296-3157, 1995.
3. K.C. Chang and Y. Bar-Shalom, "Joint Probabilistic Data Association for Multitarget Tracking with Possibly Unresolved Measurements and Maneuvers," *IEEE Trans. on Auto. Cont.,* July 1984, pp. 585-594.
4. Blackman, S.S., *Multiple-Target Tracking with Radar Applications,* Artech House, Inc., Norwood, MA, 1986.
5. W. Koch and G. Van Keuk, "Multiple Hypothesis Track Maintenance with Possibly Unresolved Measurements," *IEEE Trans. Aero. Elect. Sys.,* July 1997, pp. 883-892.
6. S.M. Sherman, *Monopulse Principles and Techniques,* Artech House, Inc., Dedham, MA, 1984.
7. F. E. Daum, "Angular Estimation Accuracy for Unresolved Targets," *Proc. of 1987 American Control Conference,* Minneapolis, MN, June 1987, pp. 1135-36.
8. W.D. Blair and M. Brandt-Pearce, "Unresolved Rayleigh Target Detection Using Monopulse Measurements," *IEEE Trans. Aero. Elect. Sys.,* April 1998, pp. 543-552.
9. A. A. Ksienski and R. B. McGhee, "A Decision Theoretic Approach to the Angular Resolution and Parameter Estimation Problem for Multiple Targets," *IEEE Trans. Aero. Elect. Sys.,* May 1968, pp. 443-455.
10. S. Haykin, J. Litva, and T.J. Shepherd, Eds., *Radar Array Processing,* Springer-Verlag, New York, NY, 1993.
11. P. Z. Peebles and R. S. Berkowitz, "Multiple-Target Monopulse Radar Processing Techniques," *IEEE Trans. Aero. Elect. Sys.,* Nov. 1968, pp. 845-854.
12. S. M. Sherman, "Complex Indicated Angles Applied To Unresolved Targets and Multipath," *IEEE Trans. Aero. and Elect. Sys.,* Jan. 1971, pp. 160-170.
13. R. S. Berkowitz and S. M. Sherman, "Information Derivable from Monopulse Radar Measurements of Two Unresolved Targets," *IEEE Trans. Aero. and Elect. Sys.,* Sept. 1971, pp. 1011-1013.
14. F. Gini, R. Reggiannini, and U. Mengali, "The Modified Cramer-Rao Bound in Vector Parameter Estimation," *IEEE Trans. on Communications,* vol. 46, No. 1, pp. 52-60, January 1998.
15. H. L., Van Trees, *Detection, Estimation, and Modulation Theory: Part I,* John Wiley & Sons, Inc., 1968.
16. Y. Bar-Shalom and X.R. Li, *Estimation and Tracking: Principles, Techniques, and Software,* Artech House, Inc., Dedham, MA, 1993. (Reprinted by YBS Publishering, Box U-157, Storrs, CT, 06296-3157, 1998).
17. W. D. Blair, G.A. Watson, and M. Brandt-Pearce, "Monopulse Tracking of Two Unresolved Rayleigh Targets," *Proceedings of the Signal and Data Processing of Small Targets 1997,* SPIE's International Symposium, San Diego, CA, July 1997.

18. D. K. Barton, Ed., *Radar Resolution and Multipath Effects*, Artech House, Inc., Dedham, MA, 1975.

Appendix

Derivation of DOA Estimator Variance

This appendix details the derivation of the estimate of the variance of $\hat{\eta}_1$ given in (41). The estimate of the variance of $\hat{\eta}_2$ given in (42) is derived similarly. Using $\hat{\eta}_1$ as defined in (38) and the orthogonality principle [15] gives

$$\begin{aligned}\mathrm{VAR}[\hat{\eta}_1|\Phi,\{\Re_{ok}\}_{k=1}^N] &= \mathrm{VAR}[\hat{y}_I|\Phi,\{\Re_{ok}\}_{k=1}^N] + \frac{\lambda}{\widehat{\Re}_R}\mathrm{VAR}[\sqrt{\hat{q}}|\Phi,\{\Re_{ok}\}_{k=1}^N] \\ &= \frac{q}{2NY_N} + \frac{\lambda}{\widehat{\Re}_R}\Big[E[\hat{q}] - \sigma_d^2\sigma_S^{-2}|\Phi,\{\Re_{ok}\}_{k=1}^N] + E^2[\sqrt{\hat{q}-\sigma_d^2\sigma_S^{-2}}|\Phi,\{\Re_{ok}\}_{k=1}^N]\Big] \quad (A.1)\end{aligned}$$

where the first term is given by (18) and $4\eta_{bw}^2\lambda\widehat{R}_R(1+\lambda)^{-2} \geq \hat{q} - \sigma_d^2\sigma_S^{-2} \geq 0$ from (40). From (33) through (36),

$$E[\hat{q}|\Phi,\{\Re_{ok}\}_{k=1}^N] = q \quad (A.2)$$

$$\mathrm{VAR}[\hat{q}|\Phi,\{\Re_{ok}\}_{k=1}^N] = \frac{2q^2}{2N-1} \quad (A.3)$$

Note that for a twice differentiable function $g(x)$,

$$E[g(x)] \approx g(\bar{x}) + \frac{1}{2}g''(\bar{x})\sigma_x^2 \quad (A.4)$$

where $\bar{x} = E[x]$, $\sigma_x^2 = \mathrm{VAR}[x]$, and $g''(\bar{x})$ is the second derivative of $g(x)$ with respect to x evaluated at $x = \bar{x}$. Using (A.2) through (A.4) gives

$$E[\sqrt{\hat{q}-\sigma_d^2\sigma_S^{-2}}|\Phi,\{\Re_{ok}\}_{k=1}^N] \approx \sqrt{q-\sigma_d^2\sigma_S^{-2}} - \frac{q^2}{4(2N-1)\sqrt{(q-\sigma_d^2\sigma_S^{-2})^3}} \quad (A.5)$$

Using (A.2) and (A.5) in (A.1) gives

$$\mathrm{VAR}[\hat{\eta}_1|\Phi,\{\Re_{ok}\}_{k=1}^N] = \frac{q}{2NY_N} + \frac{\lambda q^2}{2\widehat{\Re}_R(2N-1)(q-\sigma_d^2\sigma_S^{-2})}\Big[1 - \frac{q^2}{8(2N-1)(q-\sigma_d^2\sigma_S^{-2})}\Big] \quad (A.6)$$

For $q-\sigma_d^2\sigma_S^{-2} > 0.5$, which is satisfied by any nondegenerate case (*i.e.*, $\eta_1 \approx \eta_2$) of two unresolved targets, the last term of (A.6) can be ignored to obtain (41).

Track Management Technique for Electronically Scanned Radars

George C. Brown[†], William D. Blair[††], and Daniel A. Diaz[‡],

Air and Missile Defense Division
Sensors and Electromagnetic Applications Laboratory
Georgia Tech Research Institute
Georgia Institute of Technology, Atlanta, Georgia

ABSTRACT

A new method of track management for a phased array radar is proposed to simplify the data association and improve the allocation of radar resources. The tracks are organized into Association Groups and Dwell Groups. Association Groups are used for course gating when associating new measurement data with existing tracks, while Dwell Groups are used to efficiently schedule the next dwell on closely-spaced targets. By considering only closely-spaced tracks in the same Association Group, a form of coarse gating is inherently done to cull candidate tracks that are unlikely to associate with a measurement from a dwell directed by one of the members of the group. A Dwell Group contains tracks that are spaced sufficiently to allow one dwell to illuminate all of its members. Dwell groups lay the foundation for more systematic approaches to optimal allocation of the radar resources. Simulation results are presented to illustrate the new technique.

Keywords: Multitarget Tracking, Radar Signal Processing, Phased Array, Data Association

1. INTRODUCTION

In the past radar trackers have been designed with a keen eye on the computational throughput of the computers available. The designers justifiably traded radar resources for computational simplicity,[1] ,[2] ,[3] ,[4] and.[5] However, advances in computational hardware now make more sophisticated tracking algorithms feasible. A new method of track management for a phased array radar is proposed to make more efficient use of radar resources at the expense of added algorithm complexity and computational load.

The approach is based on classifying tracks into categories depending on one of two radar tasks– processing collected data or gathering new data. When new data has been collected, the measurements must be assigned to tracks according to some type of decision logic.[6] By categorizing the tracks into different Association Groups (AG's), the number of candidate tracks to be considered for association with new measurements is reduced, thus reducing the computational load similar to track partitioning. This is in essence a form of coarse gating that, while useful, is not all that note worthy. However, it does lay the stage for the second categorization, Dwell Groups (DG's). By first categorizing the tracks into AG's, the task of assigning membership to the DG is simplified. While the computational savings offered by AG's are attractive, the computational savings pale in comparison to the potential savings of radar resources offered by effective use of DG's.

The savings with DG's is seen when targets are sufficiently close that a single track dwell is capable of illuminating them so that fewer track dwells are required to maintain track. This in combination with measurements of opportunity from the search operations, track on search, offers significant radar resource savings. A full implementation of these strategies requires a sophisticated track management scheme that is capable of organizing the tracks into the different categories and making efficient use of the available measurements. A key feature of such a tracker is the ability to correctly suppress track dwell requests that have been earlier placed on the scheduling queue. These dwells are considered redundant before the dwell requests are granted due to measurements from other dwells. Many algorithmic

This work accomplished in part by funding from the Office of Naval Research, Arlington, Virginia through contract N00014-99-1-0553 and the Georgia Tech Research Institute's Faculty Leadership Program.

[†]E-mail: george.brown@gtri.gatech.edu

[††]E-mail: dale.blair@gtri.gatech.edu

[‡]E-mail: danny.diaz@gtri.gatech.edu

solutions of varying sophistication that exist solve the fundamental track goals. In terms of radar resource efficiency, the better ones are nontrivial.

The proposed approach offers notable improvements over simpler track management techniques when targets are closely-spaced. When multiple targets generate multiple detections from a single dwell, correctly associating them with current track files and making full use of the data at hand is a non-trivial task. Earlier approaches simplified this association problem by considering only the track that initiated the dwell. The closest measurement to this track is then selected and all other measurements discarded. Not only is this an inefficient method in that it does not make full use of all measurements, but it is prone to false tracks and cannot initiate new tracks except through search.

The paper is organized as follows: Section two describes the nomenclature and assumptions used to describe the problem. Issues such as the underlying assumptions behind the radar operation are discussed followed by the definitions of the Association Group and Dwell Group as well as track on search (ToS). Section three focuses on Dwell Group management issues such as the logic needed to properly implement this technique. The fourth section presents some computer simulations to illustrate the improvement of the proposed technique. Conclusions and areas for future work are discussed briefly in Section 5.

2. NOMENCLATURE/DEFINITIONS

In order to proceed, it is necessary to define the terms and assumptions pertaining to the problem at hand. This is done first with a brief overview of the assumptions concerning the radar followed by descriptions of association groups, dwell groups, and track on search.

2.1. Radar Assumptions

The radar model in question is a notational multi-faced phased array. The multiple arrays are knitted together into a single radar that is used to perform search, acquisition, and track. For all three modes, the radar obtains range and angle (azimuth and elevation) measurements for each detection.

2.2. Association Group

The definition of Association Groups is based on the distance between the tracks at a given time. Because the tracks are dynamic, the membership in the AG's must be reevaluated periodically. The optimal schedule for such reevaluation is currently an open issue. For simplicity, it can be assumed that this reevaluation occurs on each track dwell.

The distance used to define the AG's may be described either geometrically or statistically. If geometric distances are to be used, then the membership criteria is based on array-face coordinates. In addition to the natural relationship of array-face coordinates to radar measurements, there is the understanding that the targets must be within at least some multiple of a beamwidth of each other. Because the beamwidth in sine-space is independent of steer-direction, array-face coordinates are a convenient choice.[7] The array-face coordinates of the track are given as $\mathbf{tk}_{\mathrm{AFC}} = [r, k_x, k_y]^T$ where r denotes range and k_x and k_y denote the sine-space azimuth and elevation angles, respectively.

Let the distance between any two tracks be normalized to be either a logical 1 if near or a logical 0 if far. Thus, given M tracks the matrix of logical distance, $\mathbf{D} \in \mathbb{R}^{M \times M}$, is given as

$$[\mathbf{D}]_{j,k} = \begin{cases} 1, & \text{if } |r_k - r_j| \leq r_\Delta \text{ and } \sqrt{(k_{x_k} - k_{x_j})^2 + (k_{y_k} - k_{y_j})^2} \leq \theta_\Delta \\ 0, & \text{if } |r_k - r_j| > r_\Delta \text{ or } \sqrt{(k_{x_k} - k_{x_j})^2 + (k_{y_k} - k_{y_j})^2} > \theta_\Delta \end{cases} \tag{1}$$

where r_Δ denotes a range threshold, θ_Δ denotes angle separation threshold in sine-space, and $[\cdot]_{k,j}$ the k^{th}, j^{th} component of the matrix, $\mathbf{D}$. A good choice for θ_Δ is the 6 dB beamwidth and the track dwell range extent for r_Δ. If statistical distances are to be used, then the logical distance is defined in terms of track coordinates and covariance matrices in the East-North-Up (ENU) frame as

$$[\mathbf{D}]_{j,k} = \begin{cases} 1, & \text{if } (\mathbf{tk}_{\mathrm{ENU}_k} - \mathbf{tk}_{\mathrm{ENU}_j})^T (\mathbf{P}_k + \mathbf{P}_j)^{-1} (\mathbf{tk}_{\mathrm{ENU}_k} - \mathbf{tk}_{\mathrm{ENU}_j}) \leq \Delta \\ 0, & \text{if } (\mathbf{tk}_{\mathrm{ENU}_k} - \mathbf{tk}_{\mathrm{ENU}_j})^T (\mathbf{P}_k + \mathbf{P}_j)^{-1} (\mathbf{tk}_{\mathrm{ENU}_k} - \mathbf{tk}_{\mathrm{ENU}_j}) > \Delta \end{cases} \tag{2}$$

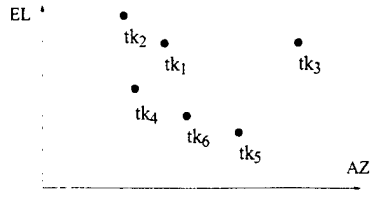

Figure 1. Association Group example.

where Δ is a distance threshold.

Once the matrix $\mathbf{D}$ is found, the AG's may be formed into either non-overlapping partitions, or overlapping groups. The advantage of forming non-overlapping partitions is easier implementation. While overlapping groups, form more AG's, they have fewer members and thus require a smaller processing load to evaluate the measurement/track assignment.

Intuitively, the groups describe a clustering of tracks such that there exists a connected covering of AG members with epsilon balls of radius defined by the logical distance metric. Thus, each AG contains members that are potential candidates for assignment with measurements derived from a dwell generated by any member of the AG.

Alternatively, the tracks may be partitioned into non-overlapping AG's by considering the structure of $\mathbf{D}$. With the proper bookkeeping, the rows and columns of $\mathbf{D}$ may be shuffled such that a modified matrix, $\bar{\mathbf{D}}$ has block diagonal form with the blocks corresponding to the different AG's. A track has membership into an AG if it also is an index into the corresponding block of $\bar{\mathbf{D}}$ (see the example described in Figure 1). Membership into overlapping groups requires that all tracks are within the threshold distance of each other. Tracks $\mathbf{tk_k}$ and $\mathbf{tk_j}$ are contained in the same overlapping AG if $[\mathbf{D}]_{k,j} = 1$.

An example is given in Figure 1 where the relative track positions are illustrated notationally. Using either of the two distance measures discussed above, it is possible to define the logical distance matrix shown below. Also shown is the block matrix $\bar{\mathbf{D}}$. Both matrices are bordered by rows and column of numbers that indicate the related track index.

$$\mathbf{D} = \begin{array}{c} \begin{matrix} 1 & 2 & 3 & 4 & 5 & 6 \end{matrix} \\ \left[\begin{array}{cccccc} 1 & 1 & 0 & 1 & 0 & 1 \\ 1 & 1 & 0 & 1 & 0 & 0 \\ 0 & 0 & 1 & 0 & 0 & 0 \\ 1 & 1 & 0 & 1 & 0 & 1 \\ 0 & 0 & 0 & 0 & 1 & 1 \\ 1 & 0 & 0 & 1 & 1 & 1 \end{array}\right] \end{array} \begin{matrix} 1 \\ 2 \\ 3 \\ 4 \\ 5 \\ 6 \end{matrix} \qquad \bar{\mathbf{D}} = \begin{array}{c} \begin{matrix} 1 & 2 & 4 & 6 & 5 & 3 \end{matrix} \\ \left[\begin{array}{cccccc|c} 1 & 1 & 1 & 1 & 0 & 0 & \\ 1 & 1 & 1 & 0 & 0 & 0 & \\ 1 & 1 & 1 & 1 & 0 & 0 & \\ 1 & 0 & 1 & 1 & 1 & 0 & \\ 0 & 0 & 0 & 1 & 1 & 0 & \\ \hline 0 & 0 & 0 & 0 & 0 & 1 & \end{array}\right] \end{array} \begin{matrix} 1 \\ 2 \\ 4 \\ 6 \\ 5 \\ 3 \end{matrix} \tag{3}$$

Thus, if the AG are allowed to overlap, the following groups may be formed: $AG_1 = \{tk_1, tk_2, tk_4, tk_6\}$, $AG_2 = \{tk_3\}$, and $AG_3 = \{tk_4, tk_5, tk_6\}$. From the block structure of $\bar{\mathbf{D}}$, it can be easily seen that there are only two groups that do not overlap: $AG_1 = \{tk_1, tk_2, tk_4, tk_5, tk_6\}$ and $AG_2 = \{tk_3\}$.

2.3. Dwell Group

Dwell Groups are an attempt to make better use of track dwells such that fewer are needed. The concept is simple– use a single dwell to illuminate multiple closely-spaced targets. Given a set of track states updated to the same time, the DG's are assigned such that there exists a covering of all tracks with dwell beams. The coverage can be defined in terms of the 3 dB beam contour, or a multiple.

There are two key features of a DG– its membership and its pointing direction. The membership is a critical part of the track management logic that deals with issues such as miss detections and drop/coast logic. Once the membership has been decided, the actual beam pointing direction must be determined. While the optimal solution is beyond the scope of this paper, it must take into account the probability of detections, estimated RCS, target model dynamics, and track preferences. One suboptimal method that is easy to implement is to simply point the beam in the direction given by the centroid of the DG track members.

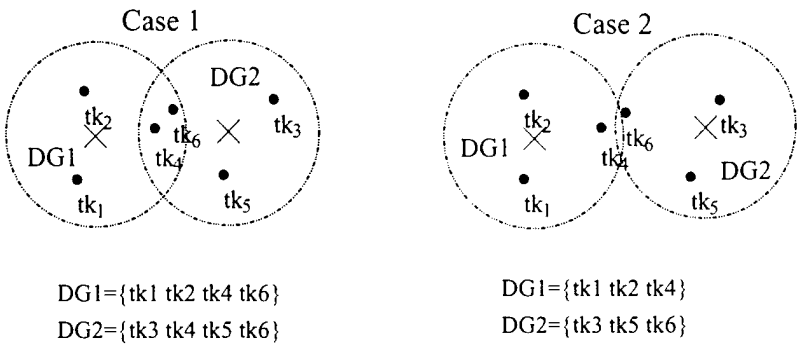

Figure 2. Example of two Dwell Group memberships for the same cluster of tracks. The open large circle represents a dwell beam where the small closed circles denote track positions and the cross-hair denotes beam center.

Figure 2 illustrates some of the concerns in optimally assigning membership into the DG's and in pointing the dwell beam as well. In case 1, the memberships are not a partition since $\mathbf{tk_4}$ and $\mathbf{tk_6}$ are in both DG1 and DG2. Case 2 is a strict partition. However, it could be argued that it is not desirable since $\mathbf{tk_4}$ and $\mathbf{tk_6}$ are close to the beam shoulder. Case 1, on the other hand, does not put these tracks much closer to the beam center, but it may be possible to combine the measurements from the two dwells, DG1 and DG2, to improve the quality of the overall measurements.

Even though the positioning of the DG may require that some tracks fall into more than one DG, it is possible to force a partition structure to simplify the dwell logic. This is simply done by arbitrarily assigning membership to one DG.

Given that the optimal solution is currently beyond reach, consider a simple strategy to form the dwell groups and position the resulting dwell beams. Using the same track positions in Figure 2, the simple algorithm is illustrated in three steps in Figure 3. To simplify the process, only tracks in an AG are candidates for membership into the DG's in question. In other words, since tracks in separate AG's are unlikely to associate with each other, it is unlikely that they are close enough to be adequately illuminated with a few closely-spaced beams. Note that the algorithm below speaks of pointing beams, it is understood that no actual beams are scheduled while assigning membership to DG's.

step 1: Form cluster of tracks of interest
Point beam at centroid of cluster– the tracks that are covered are in DG_k
step 2: Point DG_{k+1} at the track that is furtherest from DG_k
The tracks that DG_{k+1} covers are in DG_{k+1}
Redirect DG_k beam at the tracks not in DG_{k+1}
step 3: Center the beams about the DG members.
If all tracks are covered, stop, else eliminate the tracks in DG_{k+1} and go to step 1.

2.4. Track on Search

Track on search makes use of measurements collected during the normal search operations of the radar to update existing tracks. This is made possible because both range and AoA estimates are available in search mode. While it is a good idea to make use of all available measurements from the radar, ToS measurements are not without drawbacks. In addition to the added complexity in the track management logic to handle ToS measurements, they may also be of reduced quality compared to normal track dwell measurements. This reduced quality is because the search beam pointing location is not directed at a DG. It is not expected that all members of the DG will be centered in the beam such that they all will be sufficiently illuminated to produce detections. Similarly, since the quality of many angle of arrival (AoA) estimates degrade as the target moves off beam center into the shoulder, the resulting ToS measurements will not be of the same quality as the normal track dwells. This reduction in ToS measurement quality over track dwell measurements has not been adequately analyzed for the problem at hand and may prove to be insignificant. It is mentioned for completeness.

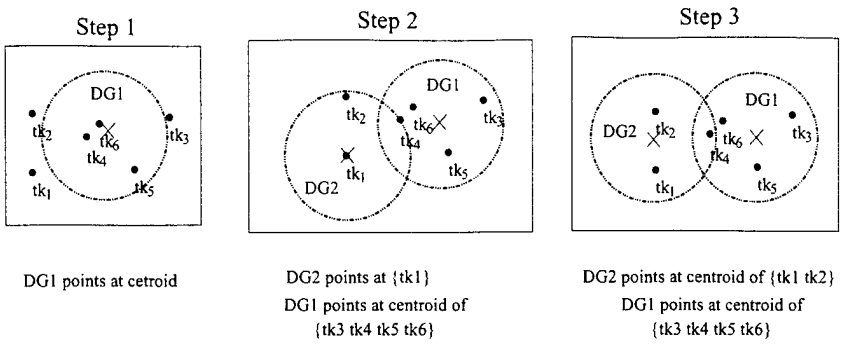

Figure 3. A simple method of generating DG and beam pointing directions.

3. DWELL GROUP MANAGEMENT ISSUES

As should be expected, the improved efficiency of dwell groups comes at the expense of additional computational complexity. There are more bookkeeping issues in dealing with missed detections, coasting, and drop decisions. Additionally, the adaptive revisit time logic must be reassessed because of the dynamic nature of DG's.

3.1. Track Management Logic

The logic associated with this type of track management is a bit more involved than with conventional methods in which a dwell is keyed to a track index. In traditional track logic, if a dwell generates no measurements that associate with its parent track, then a decision is made to either coast or schedule another dwell. However, with dwell groups, it is not that simple since several tracks are keyed to a dwell and the membership can change between dwells. Some of the important issues that must be addressed before the DG strategy can be correctly implemented are:

- **acquisition**: the initiation of multiple new tracks within a DG may require a different dwell sequence than singletons.
- **missed detections**: the probability of miss detections of multiple tracks in a DG must be understood as it impacts coasting and drop track logic.
- **coasting and drop track logic**: decisions to drop track may be influenced if the track is a member of multiple DG's. It may be more appropriate to coast longer than if the track were a singleton. If the track were a singleton, additional radar resources may be needed to re-acquire than if it were coasted in a DG.
- **merge track decisions**: when to join multiple tracks together should depend on DG membership.
- **scheduling track dwells**: DG's influence the track beam positions and their timing. To fully capture the efficiencies offered by DG's, it is necessary to have proper logic that will inhibit previously scheduled dwells that are considered redundant because of measurements from other nearby dwell groups that associate with the tracks.

There exist many possible choices regarding the implementation details for these items that will result in a working tracker, and a detailed discussion will not be given here.

3.2. Next Dwell-time Request (Adaptive Revisit)

In scheduling dwell times, there are two choices: adaptive revisit time and periodically scheduled. In attempting to make the most economical use of dwells, adaptive revisit time is the better choice. The adaptive revisit time is computed to maximize the time between dwells such that the target dynamics model is constrained to be illuminated by the dwell when it is sent.[5] Issues that must be taken into account include the beamwidth, range extent of the dwell, and accuracies of the target state estimates as well as the maximum thrust and turn acceleration of the target.

Since the targets are free to maneuver, the DG membership may change before the dwell if the adaptive revisit period (*i.e.* time between two consecutive DG dwells) is too long. Because of poor track maintenance performance

observed through simulation studies, it was noted that this should be avoided. Thus, if it is observed that the DG memberships change before the next scheduled dwell, the adaptive time is reduced by roughly half.

To further simplify the tracker's task, adaptive revisits are only allowed for DG's with only one member (*i.e.* singleton). These singletons can capitalize on the throughput gains offered by adaptive revisit times. For DG's with more than one member, periodically scheduled revisit times proved to provide more robust track maintenance.

4. COMPUTER SIMULATIONS

To illustrate the concept of the proposed AG/DG strategy, computer simulations are presented. The radar model used to derive the plots is a notational ship based radar of medium fidelity level . The radar operates at 3.4 to 4.0 GHz with four planar arrays that provide 360° of azimuthal coverage and 75° in elevation. Each of the four arrays is tilted back 15° and faces 90° apart from each other to give full azimuthal coverage. The field of view of each array is such that any two arrays overlap in azimuth by about 10°. Linear motion of the platform is modeled as well as roll, pitch, and yaw. The four arrays are knitted together into a single radar that is used to perform search, acquisition, and track. For simplicity the same suite of waveforms are assumed used for each task with individual waveforms varying in frequency and pulsewidth. After a track has been established, the proper pulsewidth is selected to adjust the energy on target. The range estimates are based on a discrete-phase coded pulse compression model while the AoA measurements are generated with sum and difference monopulse for both azimuth and elevation. As a result, if range resolution is lost, the monopulse estimates will be corrupted due to the fact that multiple targets within a single range cell contaminate monopulse AoA estimates. Monopulse estimates are available in all modes of operation such that data collected during search may be efficiently used in ToS.

High fidelity issues such as element level effects are not modeled, instead an analytic expression is used to represent the sum and difference antenna patterns. This level of fidelity allows issues such as multiple detections in adjacent search beams to be studied along with attenuation effects due to off-boresight beams.

Figures 4-6 present different views of the same simulation run. The simulation starts with two aircraft in flight, with the ship denoted by the **S** at location (0,0) as seen in Figure 4. The aircraft then join and fly in formation until the end of the simulation. In all of these figures, the truth trajectories are denoted with a broken line while the solid lines represent tracks.

Figures 5 and 6 depict sub-regions of Figure 4 to illustrate finer detail. These figures also show beam pointing track dwells and the resulting measurements along with ToS measurements. The ToS dwells are not shown, because there is no equivalent range component of the search dwell– it does not carry the same meaning as it does in the track dwell and would clutter the figures. The track dwell beam pointing directions for tracks 1 and 2 are shown with circles and diamonds while $\times$ and $+$ denote measurements and the square is used to show ToS measurements.

In Figure 5 the targets are in separate AG's and separate DG's resulting in separate track dwells for each target. Adaptive revisit time is used so that the spacing of the track dwells is aperiodic. The ToS dwells which are not shown are periodic. Their resulting measurements may be seen to overlap the track dwells on occasion. It is these times where the ToS dwells may be considered redundant to the track dwells, because the search dwells must be scheduled and never inhibited. Conversely, isolated ToS measurements may be seen where the search dwell happened just before a scheduled track dwell, inhibiting it and giving some of the promised radar resource efficiency. Also of note is where the targets transition from one array face to another. This array face hand-off can be seen as the two closely-spaced ToS measurements on each track.

A closeup of the region where the aircraft come together is shown in Figure 6. The targets are close enough to be in the same AG since Track 1 dwells are suppressed because Track 2 is being fed by measurements from Track 1 dwells. The two tracks are in the same DG, DG_1, at the region where the Track 1 dwells straddle the two tracks. Because of an artifact due to the plot's scale, it appears that the dwell favors Track 2, but it really is in the middle. Also note that the track logic implemented in the simulation moves from adaptive to periodic revisits when the DG has more than one member.

5. CONCLUSIONS/FUTURE WORK

A new track management technique that makes efficient use of radar resources has been presented along with computer simulations to illustrate its operation. Key features of this strategy involve the use of association groups and dwell groups. Several different methods of structuring the AG's and DG's were presented along with track logic

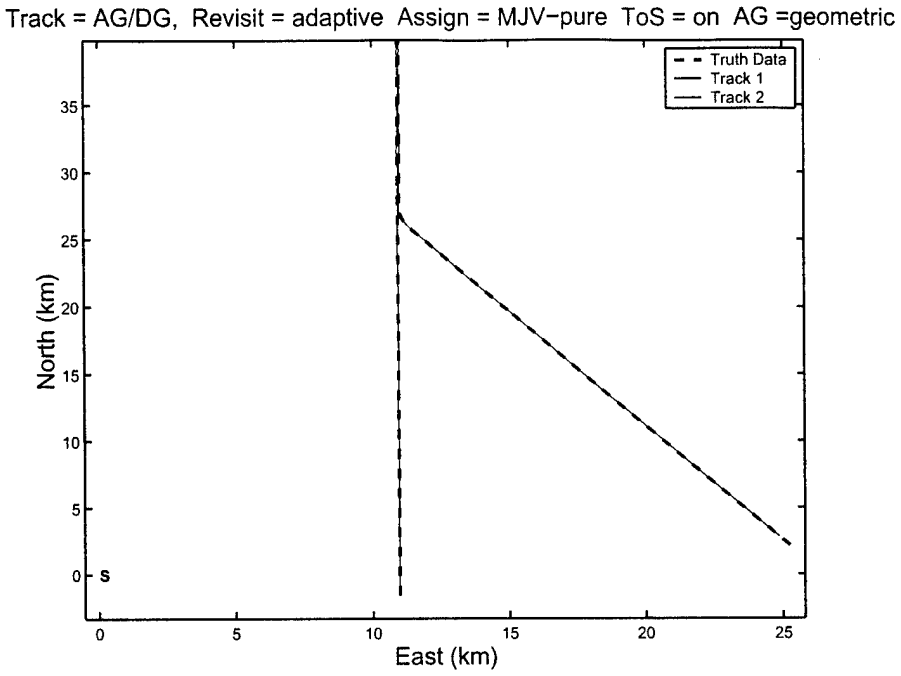

Figure 4. Two tracks merging with AG/DG tracker and ToS enabled, AG uses geometric distance.

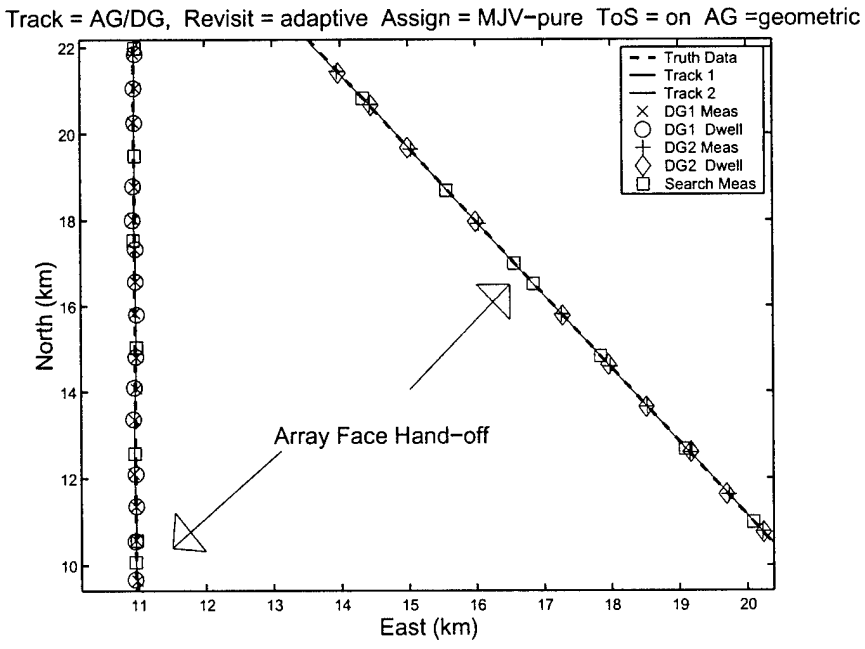

Figure 5. Two tracks merging with AG/DG tracker and ToS enabled, AG uses geometric distance.

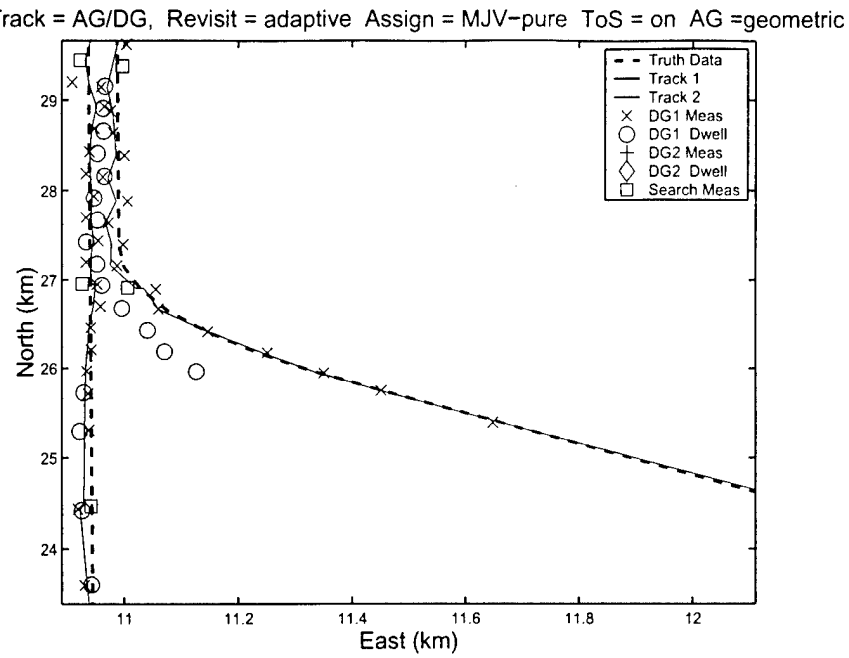

Figure 6. Close up view of tracks after the targets join and the AG/DG technique comes into play.

and management issues that are of concern when implementing these methods. Many issues are left open and promise to be rich areas of future research. Performance analysis of the different AG/DG structures discussed along with the optimal DG beam positions are obvious areas for further study. Also a detailed performance analysis is needed to compare the new algorithm with existing ones with regard to track metrics and, of course, radar resource efficiency. Other areas of interest involve further refinement of the management logic to make the tracker with respect to radar resources more efficient and robust to both noise and smart jammers.

REFERENCES

1. R. A. Baugh, *Computer Control of Modern Radars*, RCA, 1973.
2. Y. Bar-Shalom and X. R. Li, *Estimation and Tracking: Principles, Techniques and Software*, Artech House, Dedham, Ma, 1998.
3. Y. Bar-Shalom and X. R. Li, *Multitarget-Multisensor Tracking: Principles and Techniques*, YBS Publishing, Storrs, CT, 1998.
4. S. S. Blackman, *Multiple-Target Tracking with Radar Applications*, Artech House, Dedham, Ma, 1986.
5. S. S. Blackman and R. Popoli, *Design and Analysis of Modern Tracking Systems*, Artech House, Norwood, Ma, 1999.
6. W. D. Blair, *et al*, "2D Assignment Algorithms for Tracking Combat Maneuvering Aircraft With an Electronically Scanned Radar," in *SPIE*, (Orlando, FL), April 2000.
7. R. J. Mailloux, *Phased Array Antenna Handbook*, Artech House, Norwood, MA, 1994.

Effects of Diffuse Multipath on the Statistics of Monopulse Measurements

W. D. Blair
Georgia Tech Research Institute
Georgia Institute of Technology
Atlanta, Georgia 30332-0800
dale.blair@gtri.gatech.edu

M. Brandt-Pearce
Dept. of Electrical Engineering
University of Virginia
Charlottesville, Virginia 22903-2442
mb-p@virginia.edu

Extended Abstract

Monopulse is a simultaneous lobing technique for determining the angular location of a source of radiation or of a "target" that reflects part of the energy incident upon it [1]. In an amplitude comparison monopulse radar system, a pulse of energy is transmitted directly at the predicted position of the target, and the target echo is received with two beams that are squinted relative to the predicted position of the target (note that two beams are required for each angular coordinate). Traditionally, the Direction-Of-Arrival (DOA) of a target is estimated with the in-phase part (*i.e.*, the real part) of the monopulse ratio, which is formed by dividing the difference of the two received signals by their sum. However, the presence of reflections from the sea surface in the main lobe of the antenna pattern can cause severe errors, when using the monopulse ratio as the target DOA estimate. While the problem of tracking low elevation targets has been studied extensively in the last 30 years [1-8], the statistics of monopulse measurements of a target in the presence of sea-surface induced multipath were not available in the literature until [9,10].

In tracking of low elevation targets with a monopulse radar, the presence of reflections from the sea surface can cause severe errors in the DOA measurements of the target. Since the target echoes that are received directly and via the sea surface are unresolved in time and frequency, tracking targets in the presence of sea-surface induced multipath is a special case of tracking unresolved targets. The sea-surface reflection is modeled by a specular (coherent) component and a diffuse (noncoherent) component. The probability density function (PDF) of the measured amplitude of the sum signal and the amplitude-conditioned means and variances of the in-phase and quadrature monopulse ratios are given in [9,10] for low elevation, fixed-amplitude targets in the presence of sea-surface induced

Submitted to the 2001 IEEE Radar Conference, September 2000.

multipath. The PDF and the means and variances include the effects of both diffuse and specular multipath and the means and variances of the monopulse ratios are studied for radars operating at S, X, and Ku bands.

The diffuse reflection coefficients in [9,10] that were taken from [11] were found to be inconsistent with the diffuse reflection coefficients given by [12]. The use of diffuse reflection coefficients of [11] has been found to exaggrate the impacts of the diffuse multipath compared to the effects found in real radar data. In this paper, the inconsistencies in the diffuse reflection coefficients will be reconciled and the means and variances of the monopulse ratios will be studies for various operating frequencies. The discrepancies between predicted and actual monopulse measurements for targets in the presence of multipath in [4] are thought to be the result of diffuse multipath, and the paper include the results of an investigation into these discrepancies.

Additional Background

The sea-surface reflection is modeled with a specular (coherent) component and a diffuse (noncoherent) component. The specular reflection is caused by a smooth ("mirror-like") surface and the diffuse reflection is caused by the surface irregularities. While the specular reflection coefficient is a deterministic number which depends on several unknown parameters, the diffuse reflection has a random nature that is often modeled as a complex Gaussian process. Generally, the sea surface is perturbed by small irregularities, and both reflection components are present.

The signal received from a low elevation target in the presence of sea-surface induced multipath includes four components. The first part travels directly to the target and returns directly to the radar, while the second part travels to the target via the sea surface and returns directly to the radar. The third part travels directly to the target and returns to the radar via the sea surface, while the fourth part travels to the target via the sea surface and returns to the radar via the sea surface. In the presence of sea-surface induced multipath, the in-phase and quadrature portions of the sum and difference signals for elevation measurements are given by

$$\begin{aligned} s_I &= \alpha_t \cos\phi + 2\alpha_t g\rho_S \cos(\phi + \Delta\phi) + \alpha_t (g\rho_S)^2 \cos(\phi + 2\Delta\phi) + 2\alpha_t g\rho_d \cos(\phi_d + \Delta\phi) \\ &\quad + \alpha_t (g\rho_d)^2 \cos(2\phi_d + 2\Delta\phi) + n_{SI} \qquad (1) \\ s_Q &= \alpha_t \sin\phi + 2\alpha_t g\rho_S \sin(\phi + \Delta\phi) + \alpha_t (g\rho_S)^2 \sin(\phi + 2\Delta\phi) + 2\alpha_t g\rho_d \sin(\phi_d + \Delta\phi) \end{aligned}$$

$$+\alpha_t(g\rho_d)^2 \sin(2\phi_d + 2\Delta\phi) + n_{SQ} \tag{2}$$

$$d_I = \alpha_t\eta_t \cos\phi + \alpha_t(\eta_t + \eta_I)g\rho_S \cos(\phi + \Delta\phi) + \alpha_t\eta_I(g\rho_S)^2 \cos(\phi + 2\Delta\phi)$$
$$+ \alpha_t(\eta_t + \eta_I)g\rho_d \cos(\phi_d + \Delta\phi) + \alpha_t\eta_I(g\rho_d)^2 \cos(2\phi_d + 2\Delta\phi) + n_{dI} \tag{3}$$

$$d_Q = \alpha_t\eta_t \sin\phi + \alpha_t(\eta_t + \eta_I)g\rho_S \sin(\phi + \Delta\phi) + \alpha_t\eta_I(g\rho_S)^2 \sin(\phi + 2\Delta\phi)$$
$$+ \alpha_t(\eta_t + \eta_I)g\rho_d \sin(\phi_d + \Delta\phi) + \alpha_t\eta_I(g\rho_d)^2 \sin(2\phi_d + 2\Delta\phi) + n_{dQ} \tag{4}$$

where

$$\alpha_t = \sqrt{\kappa}A_t G_\Sigma^2(\theta_t)p_0$$
$$\kappa = \text{ proportional to the transmitted power}$$
$$A_t = \text{ voltage amplitude of the target backscatter}$$
$$G_\Sigma(\theta) = \text{ sum channel antenna gain at angle } \theta$$
$$G_\Delta(\theta) = \text{ difference channel antenna gain at angle } \theta$$
$$\theta_t = \text{ off-boresight angle of the target}$$
$$p_0 = \text{ matched filter gain}$$
$$\phi = \text{ phase of the directly returned signal echo}$$
$$\eta_t = \frac{G_\Delta(\theta_t)}{G_\Sigma(\theta_t)} = \text{ DOA of the target}$$
$$\eta_I = \frac{G_\Delta(\theta_I)}{G_\Sigma(\theta_I)} = \text{ DOA of the target's image}$$
$$\theta_I = \text{ off-boresight angle of the target's image}$$
$$g = \frac{G_\Sigma(\theta_I)}{G_\Sigma(\theta_t)}$$
$$\Delta\phi = \text{ phase difference between the direct and specular reflections}$$
$$\phi_d = \text{ uniformly distributed phase of the diffuse reflection}$$
$$\rho_S = \text{ specular reflection coefficient}$$
$$\rho_d = \text{ Rayleigh diffuse reflection coefficient with parameter } \rho_{d0}$$
$$n_{SI} \sim N(0, \sigma_S^2) \qquad n_{SQ} \sim N(0, \sigma_S^2)$$
$$n_{dI} \sim N(0, \sigma_d^2) \qquad n_{dQ} \sim N(0, \sigma_d^2)$$

The α_t is the voltage amplitude of the target echo in the absence of multipath reflections. Note that $\Delta\phi$ includes the phase difference due to both the Path Length Difference (PLD) and the specular reflection at the sea surface, which is approximately π. The receiver errors n_{SI}, n_{SQ}, n_{dI}, and n_{dQ} are assumed independent. Both ρ_S and ρ_{d0} depend on the sea state,

properties of the seawater, polarization of the transmitted waveform, grazing angle at the point of the sea-surface reflection, and wavelength λ of the carrier.

The first term on the right side of (1) and (2) corresponds to the echo received directly from the target, while the second and third terms correspond to the three echoes that are the result of the specular reflection at the sea surface. The fourth and fifth terms represent three echoes that result from the diffuse reflections at the sea surface. The phase information associated with ϕ in the fourth and fifth terms is lost due to the presence of the random phase, ϕ_d. In the difference signals of (3) and (4), the second and fourth terms on the right side of (3) and (4) include echoes from two different DOAs, η_t and η_I.

The specular reflection coefficient is computed as

$$\rho_S = \begin{cases} \Gamma \exp(-8\pi^2 g_o^2), & 0 < g_o < 0.1 \\ \Gamma \dfrac{0.81254}{1 + 8\pi^2 g_o^2}, & g_o \geq 0.1 \end{cases} \tag{5}$$

where

$$g_o = \frac{\sigma_h}{\lambda} \sin \psi_{ga} \tag{6}$$

$$\Gamma = \begin{cases} \Gamma_V, & \text{vertical polarization} \\ \Gamma_H, & \text{horizontal polarization} \end{cases}$$

$$\Gamma_H = \frac{\sin \psi_{ga} - \sqrt{\epsilon_c - \cos^2 \psi_{ga}}}{\sin \psi_{ga} + \sqrt{\epsilon_c - \cos^2 \psi_{ga}}}$$

$$\Gamma_V = \frac{\epsilon_c \sin \psi_{ga} - \sqrt{\epsilon_c - \cos^2 \psi_{ga}}}{\epsilon_c \sin \psi_{ga} + \sqrt{\epsilon_c - \cos^2 \psi_{ga}}}$$

$$\epsilon_c = \frac{\epsilon_S - \epsilon_0}{1 + \omega_c^2 \tau^2} - j\left(\frac{(\epsilon_S - \epsilon_0)\omega_c \tau}{1 + \omega_c^2 \tau^2} - 4\pi \frac{\sigma_i}{\omega_c}\right)$$

$\omega_c = \dfrac{2\pi}{\lambda} =$ carrier frequency

$\lambda =$ wavelength of the carrier frequency

$\sigma_h =$ RMS sea-surface elevation above the mean level

$\psi_{ga} =$ grazing angle

$\epsilon_S =$ static dielectric parameter of the seawater

$\epsilon_0 =$ 4.9 for seawater

$\tau =$ relaxation time of the seawater

$\sigma_i =$ ionic conductivity of the seawater

According to [11], the Rayleigh parameter for the diffuse reflection coefficient is computed as

$$\rho_{d0} = \begin{cases} \sqrt{2}|\Gamma|3.68 g_o, & 0 < g_o < 0.1 \\ \sqrt{2}|\Gamma|\big(0.454 - 0.858 g_o\big), & 0.1 \le g_o < 0.5 \\ \sqrt{2}|\Gamma|0.025, & g_o \ge 0.5 \end{cases} \tag{7}$$

Letting Λ and ψ denote the measured amplitude and phase of the sum signal gives

$$s_I = \Lambda \cos \psi \qquad s_Q = \Lambda \sin \psi \tag{8}$$

Also, let

$$\Re = \frac{\alpha_t^2}{2\sigma_S^2} \qquad \Re_o = \frac{\Lambda^2}{2\sigma_S^2} \tag{9}$$

where $\Re$ denotes the Signal-to-Noise Ratio (SNR) of a fixed-amplitude target in the absence of multipath and $\Re_o$ denotes the observed SNR.

Let Φ denote the parameters $\{\alpha_t, \Delta\phi, \rho_S, \rho_{d0}, \sigma_S, \sigma_d\}$. With $E[\cdot]$ denoting the expected value and VAR[$\cdot$] denoting the variance, then [9,10]

$$E[\Re_o|\Phi] = \left[(1 + 2\rho_S g \cos\Delta\phi + \rho_S^2 g^2)^2 + 8\rho_{d0}^2 g^2 (1 + \rho_{d0}^2 g^2)\right]\Re + 1 \tag{10}$$

$$\begin{aligned} \mathrm{VAR}[\Re_o^2|\Phi] = &\left[8\rho_{d0}^2 g^2 (1 + \rho_{d0}^2 g^2)\Re + 1\right] \\ &\times \left[\left[2(1 + 2\rho_S g \cos\Delta\phi + \rho_S^2 g^2)^2 + 8\rho_{d0}^2 g^2 (1 + \rho_{d0}^2 g^2)\right]\Re + 1\right] \end{aligned} \tag{11}$$

Denoting $s = s_I + j s_Q$ and $d = d_I + j d_Q$, the in-phase and quadrature parts of the monopulse ratio are given by

$$y_I = \mathrm{Re}\Big(\frac{d}{s}\Big) = \frac{d_I s_I + s_Q d_Q}{s_I^2 + s_Q^2} \tag{12}$$

$$y_Q = \mathrm{Im}\Big(\frac{d}{s}\Big) = \frac{d_Q s_I - d_I s_Q}{s_I^2 + s_Q^2} \tag{13}$$

The expected value of the monopulse measurements [9.10] are given by

$$E[y_I|\Lambda,\Phi] = \frac{p_{12}}{p_{11}} + I_{1|0}\Big(\frac{\Lambda\alpha_t}{p_{11}}\big(1 + 2\rho_S g\ \cos\Delta\phi + \rho_S^2 g^2\big)\Big)\frac{\alpha_t}{\Lambda}\Bigg[\Big(\eta_t - \frac{p_{12}}{p_{11}}\Big) + (\rho_S g)^2\Big(\eta_I - \frac{p_{12}}{p_{11}}\Big) + \Big(\eta_t + \eta_I - 2\frac{p_{12}}{p_{11}}\Big)\rho_S g\ \cos\Delta\phi\Bigg] \tag{14}$$

$$E[y_Q|\Lambda,\Phi] = I_{1|0}\Big(\frac{\Lambda\alpha_t}{p_{11}}\big(1 + 2\rho_S g\ \cos\Delta\phi + \rho_S^2 g^2\big)\Big)\frac{\alpha_t\rho_S g}{\Lambda}\Big(\eta_I - \eta_t\Big)\ \sin\Delta\phi \tag{15}$$

where

$$\frac{p_{12}}{p_{11}} = \frac{2\alpha_t^2\rho_{d0}^2 g^2\big[\eta_t + (1 + 2\rho_{d0}^2 g^2)\eta_I\big]}{4\alpha_t^2\rho_{d0}^2 g^2[1 + \rho_{d0}^2 g^2] + \sigma_S^2} \tag{16}$$

$$I_{1|0}(x) = \frac{I_1(x)}{I_0(x)} \tag{17}$$

The $I_0(x)$ and $I_1(x)$ are the zero and first order modified Bessel function of first kind. The form of (14) suggests that separating the bias in the monopulse ratio (*i.e.*, as a DOA estimate of the target) into diffuse and specular components as in [8] may not be appropriate. For example, when measured amplitude of the sum signal is rather small, the bias in the monopulse ratio will result from the diffuse multipath. On the other hand, when the measured amplitude of the sum signal is very large, the effects of the diffuse multipath will be very small.

Since the statistics of the monopulse ratios as presented above are a function of the measured amplitude, Λ, of each pulse or subpulse, the statistics will be illustrated by using the expected value of the observed SNR in (10) for the $\Re_o$. Using the $\Re_o = E[\Re_o|\Phi]$ of (10) and the sea-surface reflection model above, trajectories of $E[y_I|\Lambda,\Phi]$, $E[y_Q|\Lambda,\Phi]$, and the variances were generated for low-elevation targets, with the antenna boresight pointing directly at the target. Trajectories were generated for a radar operating at 4 GHz in S band. For all cases, the sea surface was assumed to have a RMS wave height of 0.25 m, and the radar is vertically polarized and 20 m above the sea surface. Also, for all cases, the use of Sensitivity Time Control (STC) will be assumed so that the SNR of the target only, $\Re$, is independent of range.

For the S band case, the radar was modeled to have a one-way beamwidth of 2.5° and a squint angle of 1.05°. The target travels from a range of 20 km to a range of 5 km at an altitude 80 m. The means of y_I and y_Q and the associated standard deviations are shown in Figures 1 through 3 for a 16-dB target (*i.e.*, 16 dB in the absence of multipath). The

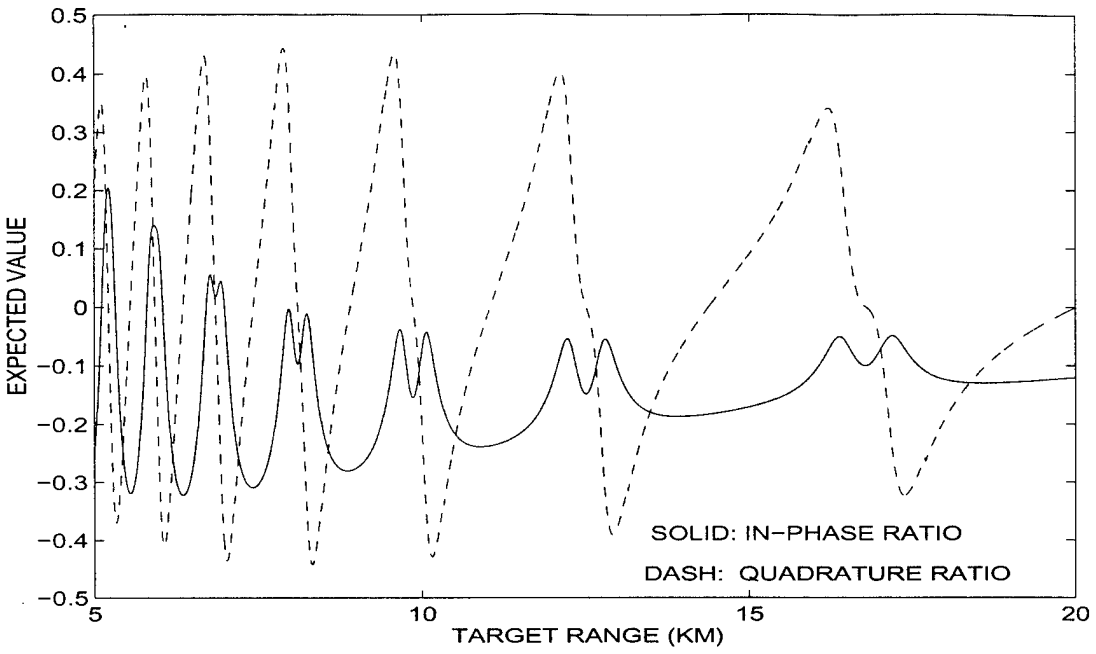

Figure 1. Means of Monopulse Ratios for 16-dB Target at an Altitude of 80 m and S Band

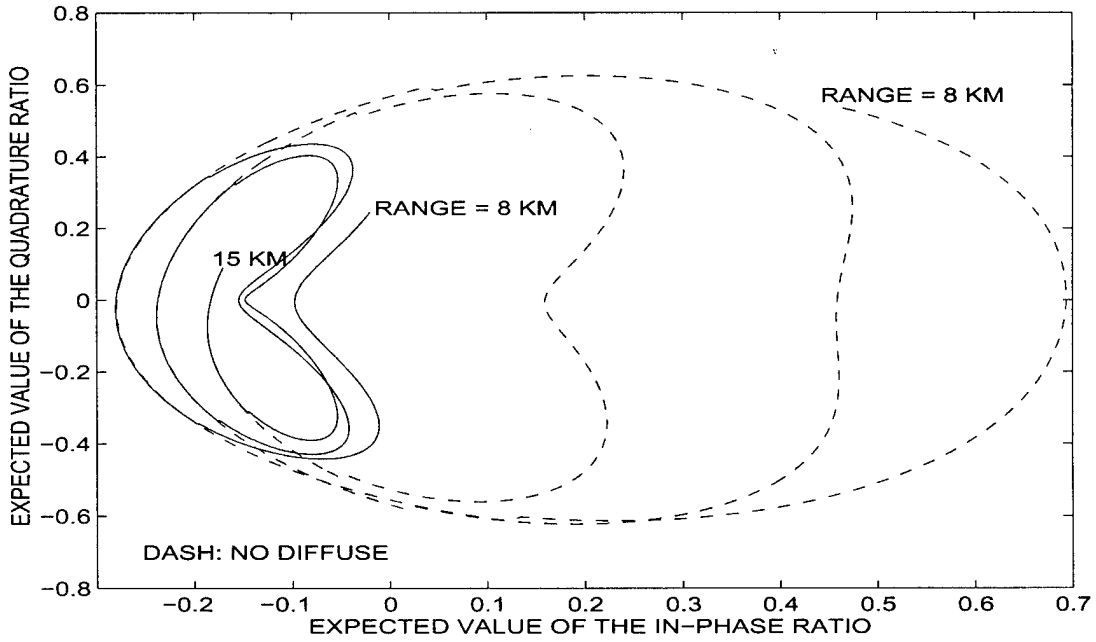

Figure 2 Means of the Complex Monopulse Ratios for 16-dB Target at an Altitude of 80 m and S Band

oscillatory form of y_I and y_Q in Figure 1 is the result of changes in $\Delta\phi$. The dips in the

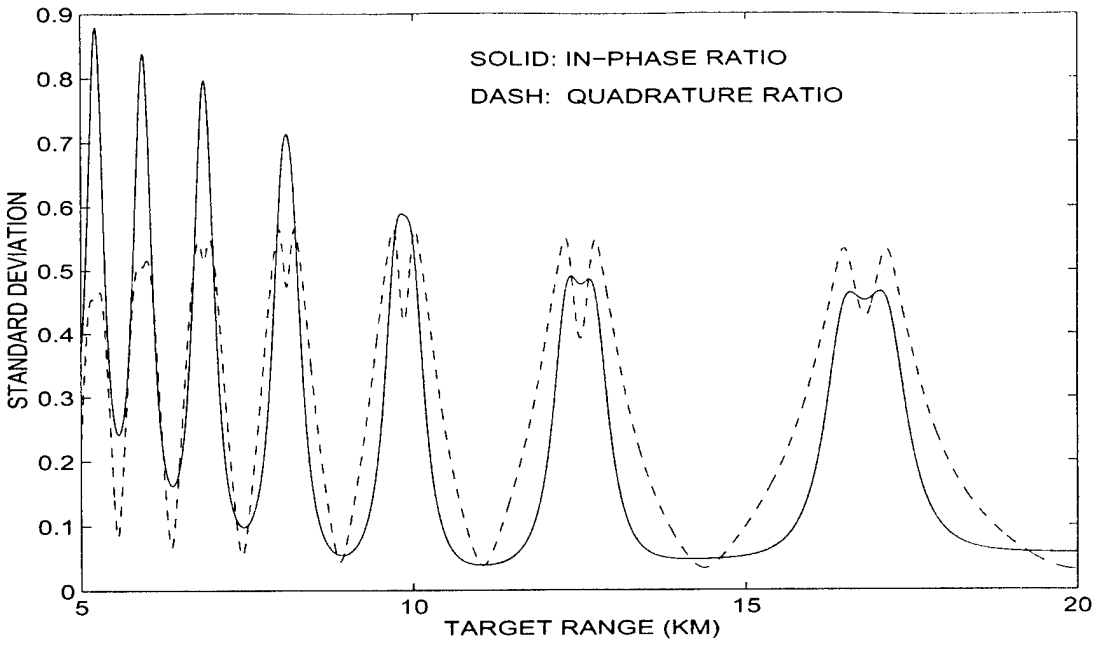

Figure 3. Standard Deviations of Monopulse Ratios for 16-dB Target at an Altitude of 80 m and S Band

peaks of $E[y_I|\Lambda, \Phi]$ are the result of the diffuse multipath dominating the return signal when the direct and reflected signals almost cancel. The results of Figures 1 are given in the complex plane in Figure 2 along with the same results for $\rho_{d0} = 0$. Note that Figure 2 gives only the results for the target ranges of 15 km to 8 km. The dash lines in Figure 2 give the means of y_I and y_Q for specular-only reflections at the sea surface. Figure 2 shows that ignoring the effects of the diffuse reflections will result in significant errors in the DOA estimation for a target in the presence of sea-surface-induced multipath. Note that these curves utilize teh diffuse reflection coefficients of [11]. Based on the examination of actual radar data, the effects of the diffuse multipath appears to be too large. Figure 3 shows that the standard deviations of the in-phase monopulse ratios are significantly less when the target is out of the multipath nulls (*i.e.*, peaks in the expected value of the in-phase monopulse ratios) and at longer ranges, where the specular reflections are relatively strong, and the angles between the target and the image are rather small.

REFERENCES

[1] S.M. Sherman, *Monopulse Principles and Techniques*, Artech House, Inc., Dedham, MA, 1984.

[2] D.D. Howard, J.T. Nessmith, and S.M. Sherman, "Monopulse Tracking Errors Due to Multipath: Causes and Remedies," *IEEE Eascon Record '71*, pp. 175-82.

[3] M.D. Symonds and J.M. Smith, "Multi-Frequency Complex Angle Tracking of Low Elevation Targets," *Proc. of IEE international Conf. on Radar*, Oct 1973.

[4] D.D. Howard, S.M. Sherman, and D.N. Thomas, "Experimental Results of the Complex Indicated Angle Technique for Elevation Measurements in the Multipath Region," *Proc. of 19th Tri-Service Radar Symposium*, Jul 1973, 329-46.

[5] D.K. Barton, "Low Angle Radar Tracking," *Proceedings of IEEE*, Jun 1974, pp. 687-704.

[6] D.K. Barton, Ed., *Radar Resolution and Multipath Effects*, Artech House, Inc., Dedham, MA, 1978.

[7] J.A. Bruder and J.A. Saffold, "Multipath Propagation Effects on Low-Angle Tracking at Milimeter-Wave Frequencies," *IEE Proceedings - F*, Apr, 1991.

[8] E. Daeipour, W.D. Blair, and Y. Bar-Shalom, "Bias Compensation and Tracking with Monopulse Radars in the Presence of Multipath," *IEEE Trans. Aero. Elect. Sys.*, Jul 1997.

[9] W. D. Blair, and M. Brandt-Pearce, *Monopulse Processing for Tracking Unresolved Targets*, Naval Surface Warfare Center Dahlgren Division, Technical Report NSWCDD/TR-97/167, Dahlgren, Virginia, Sep 1997.

[10] W. D. Blair, and M. Brandt-Pearce, "Statistics of Monopulse Measurements for Tracking Target in the Presence of Sea-Surface Induced Multipath," *Proc. of the 1998 Aerospace Conference*, Snowmass, Colorado, March 21-28, 1998.

[11] D. Y. Northam, *A Stochastic Simulation of Low Grazing Angle, Forward Scatter, Over-Water Multipath Effects*, Naval Research Laboratory, NRL Techical Report 8568, Washington, DC, Dec 1981.

[12] C. I. Beard, "Coherent and Incoherent Scattering of Microwaves from the Ocean," *IRE Trans. on Antennas and Propagation*, Vol. AP-9, No. 5, Sept. 1961, pp. 470-483.

Steady-State Tracking with LFM Waveforms*

Winnie Wong
Georgia Tech Research Institute
Georgia Institute of Technology
Atlanta, Georgia 30332-0857

W. D. Blair
Georgia Tech Research Institute
Georgia Institute of Technology
Atlanta, Georgia 30332-0857
dale.blair@gtri.gatech.edu

Abstract–The steady-state gains and error covariance are derived for a two-state Kalman filter (i.e., an α, β filter) for tracking with linear frequency modulated (LFM) waveforms. A procedure is given for calculating the α, β gains from the tracking index, Γ, the sample period, T, and the range-Doppler coupling coefficient, Δt. The steady-state error covariance is found to be a simple function of α, β, Δt, T and the measurement noise variance, σ_v^2. A gain scheduling technique for α and β during filter initialization is also given.

I. INTRODUCTION

The Kalman filter produces an optimal estimate of the target state when given the motion model and a sequence of sensor measurements corrupted with white Gaussian errors. The computational burden of maintaining the Kalman filter may prohibit its use when many targets are being tracked. Steady-state filters are also good for filter design and analysis. Constant data rate and constant error covariances required for steady-state filters are not typically true in real systems, so approximate gains are typically used. The gains are based on the steady-state gains of the Kalman filter and implemented either using a fixed gain or an easily generated gain schedule. The resultant filter for tracking range and range rate is called the α, β filter, where approximate filter gains α, β may be used instead of the optimal Kalman gains [1]. In [2], the range-Doppler coupling of linear frequency modulated (LFM) waveforms is shown to have a significant effect on tracking accuracy. In the Appendix of [1] and in [3], the steady-state gains and error covariance are derived for range measurements without range-Doppler coupling. In this paper, the range-Doppler coupling associated with LFM waveforms is included in the measurement equation, and expressions for the steady-state gains and error covariance are calculated.

II. MATHEMATICAL MODEL

The dynamics model commonly assumed for a target in track is given by

$$X_{k+1} = F_k X_k + G_k w_k \tag{1}$$

where $w_k \sim N(0, Q_k)$ is the process noise, F_k defines a linear constraint on the dynamics and G_k is the input matrix for maneuver. The target state vector X_k contains the range and range rate of the target at time k. The linear measurement model is given by

$$Y_k = H_k X_k + v_k \tag{2}$$

where Y_k is typically the target position measurement and $v_k \sim N(0, R_k)$ is the measurement noise, and H_k is the output matrix that will include range-Doppler coupling coefficient.

The measured range and the variance for a LFM waveform and the range-Doppler coupling coefficient for a LFM waveform are given by [2] as

$$y_k = r_k + \Delta t \dot{r}_k + v_k \tag{3}$$

$$\sigma_v^2 = E[v_k^2] = \frac{\Delta t^2 c^2}{8 f_o^2 \tau^2 \Re} = \frac{c^2}{8 \mathcal{B}^2 \Re} \tag{4}$$

$$\Delta t = \frac{f_0 \tau}{f_2 - f_1} = \frac{f_0 \tau}{\mathcal{B}} \tag{5}$$

where r_k is the true range at time k, $\Re$ is the signal-to-noise ratio, c is the speed of light, f_0 is the nominal carrier frequency, f_1 is the initial frequency, and f_2 is the final frequency. Also $|\mathcal{B}|$ is the bandwidth of the LFM waveform and τ is the pulse length. Note that the demodulation frequency can be modified with the range rate estimate to reduce the bias in the range measurement due to range-Doppler coupling. However, if the range rate estimate is used to remove the bias in the range measurements, the measurement errors become correlated with the state estimate and the typical Kalman filter must be modified to account for the state correlated measurement errors.

The Kalman filtering equations associated with the state model in (1) and the measurement model in (2) are given by the following equations.

Time Update:

$$X_{k|k-1} = F_{k-1} X_{k-1|k-1} \tag{6}$$

$$P_{k|k-1} = F_{k-1} P_{k-1|k-1} F_{k-1}^T + G_{k-1} Q_{k-1} G_{k-1}^T \tag{7}$$

Measurement Update:

$$K_k = P_{k|k-1} H_k^T [H_k P_{k|k-1} H_k^T + R_k]^{-1} = P_{k|k} H_k^T R_k^{-1} \tag{8}$$

$$X_{k|k} = X_{k|k-1} + K_k [Y_k - H_k X_{k|k-1}] \tag{9}$$

$$P_{k|k} = [I - K_k H_k] P_{k|k-1} \tag{10}$$

* This research was accomplished through funding from the Faculty Leadership Program of the Georgia Tech Research Institute, Atlanta Georgia.

where the subscript notation $(k|j)$ denotes the state estimate for time t_k when given measurements through time t_j. The K_k is the Kalman gain that minimizes the mean square error in the state estimate. Also, note that $X_k \sim N(X_{k|k}, P_{k|k})$ with $X_{k|k}$ and $P_{k|k}$ denoting the mean and error covariance of the state estimate, respectively.

III. THE α, β FILTER

For the Kalman filter in steady-state conditions, $P_{k|k} = P_{k-1|k-1}$, $P_{k+1|k} = P_{k|k-1}$, and $K_k = K_{k-1}$. For a Kalman filter to achieve these steady-state conditions, the error processes, w_k and v_k, must have stationary statistics and the data rate must be constant. When the noise processes are not stationary or the data rate is not constant, a filter using the steady-state gains will provide suboptimal estimates. The α, β filter is the steady-state Kalman filter for tracking nearly constant range rate targets. The α, β filter is a single coordinate filter that is based on the assumption that the target is moving with constant range rate plus zero-mean, white Gaussian acceleration errors. Given this assumption, the filter gains α and β are chosen as the steady-state Kalman gains that minimize the mean-square error in the range and range rate estimates.

For the α, β filter for piecewise constant acceleration errors,

$$X_k = \begin{bmatrix} r_k & \dot{r}_k \end{bmatrix}^T \tag{11}$$

$$F_k = F = \begin{bmatrix} 1 & T \\ 0 & 1 \end{bmatrix} \tag{12}$$

$$G_k = G = \begin{bmatrix} \frac{T^2}{2} & T \end{bmatrix}^T \tag{13}$$

$$H_k = H = \begin{bmatrix} 1 & \Delta t \end{bmatrix} \tag{14}$$

$$R_k = R = \sigma_v^2 \tag{15}$$

$$Q_k = Q = \sigma_w^2 \tag{16}$$

$$K_k = K = \begin{bmatrix} \alpha & \frac{\beta}{T} \end{bmatrix}^T \tag{17}$$

where r_k and $\dot{r}_k$ are the range and range rate of the target, respectively, σ_v^2 and σ_w^2 are the variances of measurement noise and process noise, respectively, T is the sample period between measurements, and Δt is the range-Doppler coupling coefficient.

Let the steady-state error covariance matrix of the filtered estimates for the α, β filter be denoted as

$$P_{k+1|k+1} = P_{k|k} = P = \begin{bmatrix} p_{11} & p_{12} \\ p_{12} & p_{22} \end{bmatrix} \tag{18}$$

Using (14), (15), and (18) in (8) gives the steady-state gain as

$$K_k = K_{k-1} = K = PH^T R^{-1} = \begin{bmatrix} p_{11} + p_{12}\Delta t \\ p_{12} + p_{22}\Delta t \end{bmatrix} \sigma_v^{-2} \tag{19}$$

Using (17) with (19) gives

$$\alpha = (p_{11} + p_{12}\Delta t)\sigma_v^{-2} \tag{20}$$

$$\beta = (p_{12} + p_{22}\Delta t)T\sigma_v^{-2} \tag{21}$$

Inserting (7) into (10) and setting $P_{k|k} = P_{k-1|k-1} = P$ for steady-state conditions gives

$$[I - KH]^{-1} P = FPF^T + GG^T\sigma_w^2 \tag{22}$$

Equating the (1,2) and (2,2) elements of (22) gives expressions for p_{12} and p_{22}. Substituting p_{12} and p_{22} into (21) gives

$$\Gamma^2 = \frac{T^4\sigma_w^2}{\sigma_v^2} = \frac{\beta^2}{1 - \alpha - \beta\frac{\Delta t}{T}} \tag{26}$$

where Γ is the tracking or maneuvering index. Using (26) to eliminate σ_w^2 in the expressions of p_{12} and p_{22} gives

$$p_{12} = \frac{\beta\sigma_v^2}{T\left(1 - \alpha - \beta\frac{\Delta t}{T}\right)}\left[1 - \alpha - \left(\frac{2\alpha + \beta}{2}\right)\frac{\Delta t}{T}\right] \tag{27}$$

$$p_{22} = \frac{\beta\sigma_v^2(2\alpha - \beta)}{2T^2\left(1 - \alpha - \beta\frac{\Delta t}{T}\right)} \tag{28}$$

Substituting p_{12} into (20) gives

$$p_{11} = \alpha\sigma_v^2 - \frac{\beta\sigma_v^2}{1 - \alpha - \beta\frac{\Delta t}{T}}\left[1 - \alpha - \left(\frac{2\alpha + \beta}{2}\right)\frac{\Delta t}{T}\right]\frac{\Delta t}{T} \tag{29}$$

The steady-state error covariance is then given by (27) through (29). Equating the (1,1) elements of (22) and using (27) through (29) gives

$$a_3\beta^3 + a_2\beta^2 + a_1\beta + a_0 = 0 \tag{30}$$

where

$$a_3 = -\left(\frac{\Delta t}{T}\right)^2 - \frac{\Delta t}{4T} \tag{31}$$

$$a_2 = -2\alpha\left(\frac{\Delta t}{T}\right)^2 - 2\alpha\frac{\Delta t}{T} + 3\frac{\Delta t}{T} + \frac{1 - \alpha}{4} \tag{32}$$

$$a_1 = -3\alpha^2\frac{\Delta t}{T} - \alpha^2 + 2\alpha\frac{\Delta t}{T} + 3\alpha - 2 \tag{33}$$

$$a_0 = \alpha^2 - \alpha^3 \tag{34}$$

There are three solutions for (30). By comparing with the Kalman filter numerical results, the valid solutions of (31) for β are given by

$$\beta_\pm = \frac{2}{(1 + 4\frac{\Delta t}{T})} \times \left(-\alpha\left(1 + 2\frac{\Delta t}{T}\right) + 2 \pm 2\sqrt{\left(1 - \alpha\frac{\Delta t}{T}\right)^2 - \alpha}\right) \tag{35}$$

For $\frac{\Delta t}{T} > 0$, both solutions of (35) are valid for β depending on the selection of Γ and $\frac{\Delta t}{T}$. The β_- (i.e., minus sign in the front of the radical) is used for β with increasing α until the maximum α is reached, which is given by

$$\alpha_{max} = \frac{\frac{2\Delta t}{T} + 1 - \sqrt{\frac{4\Delta t}{T} + 1}}{2\left(\frac{\Delta t}{T}\right)^2} \tag{36}$$

Then β_+ (i.e., plus sign in the front of the radical) is used for β from α_{max} with decreasing α and it is valid as long as $1 - \alpha - \beta_+ \frac{\Delta t}{T} > 0$, that is, Γ in (26) is a real number. For $\frac{\Delta t}{T} \leq 0$, β_- is the only solution for β. If $\frac{\Delta t}{T} = -\frac{1}{4}$, (30) becomes a quadratic equation given by

$$b_2\beta^2 + b_1\beta + b_0 = 0 \tag{37}$$

where

$$b_2 = \frac{\alpha}{8} - \frac{1}{2} \tag{38}$$

$$b_1 = -\frac{\alpha^2}{4} + \frac{5\alpha}{2} - 2 \tag{39}$$

$$b_0 = \alpha^2 - \alpha^3 \tag{40}$$

If there is no range-Doppler coupling (i.e., $\frac{\Delta t}{T} = 0$) [3], (26) through (29), and β_- of (35) give

$$P_{k|k} = \sigma_v^2 \begin{bmatrix} \alpha & \frac{\beta}{T} \\ \frac{\beta}{T} & \frac{\beta^2(2\alpha - \beta)}{2(1-\alpha)T^2} \end{bmatrix} \tag{41}$$

$$\Gamma^2 = \frac{T^4\sigma_w^2}{\sigma_v^2} = \frac{\beta^2}{1-\alpha} \tag{42}$$

$$\beta = 2(2 - \alpha) - 4\sqrt{1-\alpha} \tag{43}$$

These results of (41) through (43) agree with that derived in the Appendix of [1] and Kalata's paper [3].

Inserting (26) into (30) to eliminate α and expressing a polynomial equation of β in terms of Γ, Δt and T gives

$$\beta^4 - \Gamma^2\beta^3 + \left[\frac{\Gamma^4}{4} - \left(\frac{\Delta t}{T}\right)^2\Gamma^4 - 2\Gamma^2\right]\beta^2 - \Gamma^4\beta + \Gamma^4 = 0 \tag{44}$$

Note that (44) does not depend on the sign of Δt. Newton's method with a good initial guess of β can be used to find a zero of (44). A good initial guess of β is given by the case of $\Delta t = 0$, where the initial β is computed with (43) and α is given by [4]

$$\alpha = -\frac{1}{8}\left(\Gamma^2 + 8\Gamma - (\Gamma + 4)\sqrt{\Gamma^2 + 8\Gamma}\right) \tag{45}$$

After β is found by utilizing Newton's method, the steady-state gain, α and the error covariance are then calculated for the given Γ and $\frac{\Delta t}{T}$ using (26) through (29).

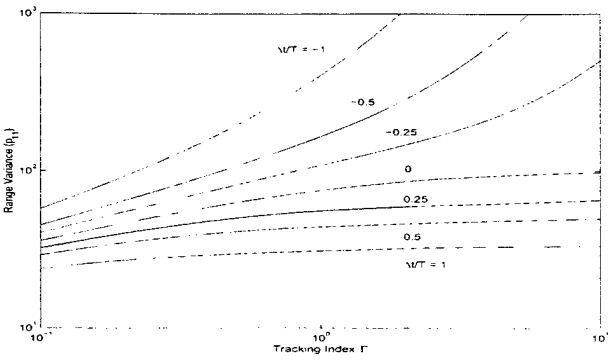

Fig. 1. Range Variance Versus Γ with $T = 1$ s and $\sigma_v = 10$ m

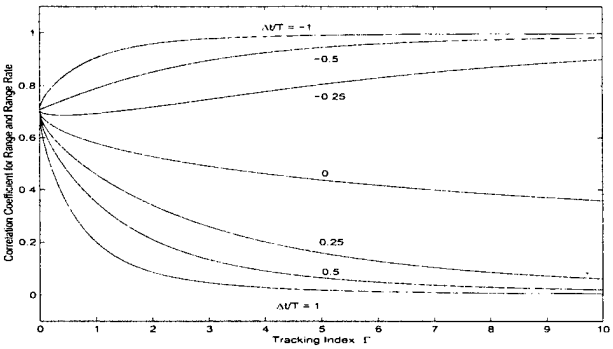

Fig. 2. Correlation Coefficient for Range and Range Rate Versus Γ with $T = 1$ s and $\sigma_v = 10$ m

Various results for the α, β filter are shown in Figures 1 through 7 and the results were confirmed by iterating the Kalman filtering algorithm until the steady-state conditions were achieved. Figure 1 shows that the variance of the range estimate decreases with increasing Δt for a given Γ. Figure 2 shows that the correlation coefficients for range and range rate estimates are between zero and one. Note that as Δt becomes more positive, the correlation coefficient for range and range rate goes to zero at higher Γ. This means that the range and range rate estimates are less correlated to each other at higher Γ. Thus the accuracy of the predicted measurements will be improved at more positive Δt. Figure 3 shows that the variance of range rate decreases with increasing Δt. Figure 4 shows that α decreases with increasing Δt. For the case of $\Delta t = 0$, α will go to one as Γ approaches infinity. Figure 5 shows that β

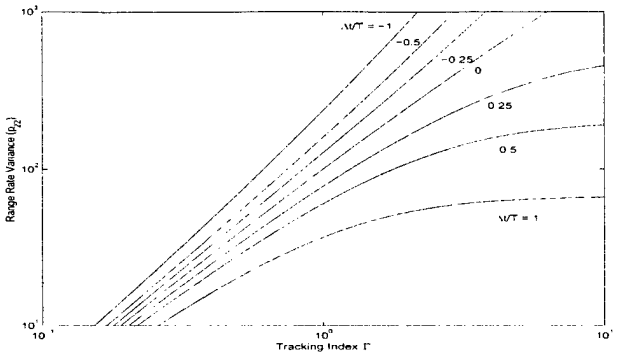

Fig. 3. Range Rate Variance Versus Γ with $T = 1$ s and $\sigma_v = 10$ m

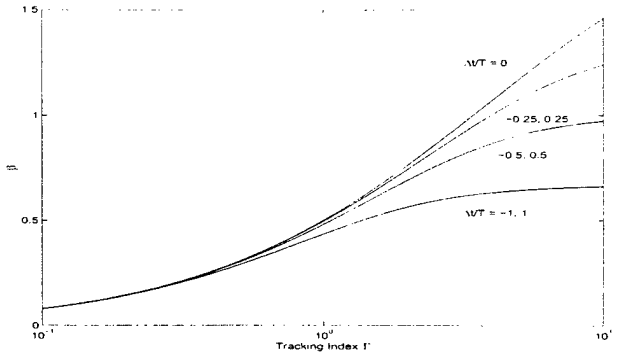

Fig. 5. β Versus Γ with $T = 1$ s and $\sigma_v = 10$ m

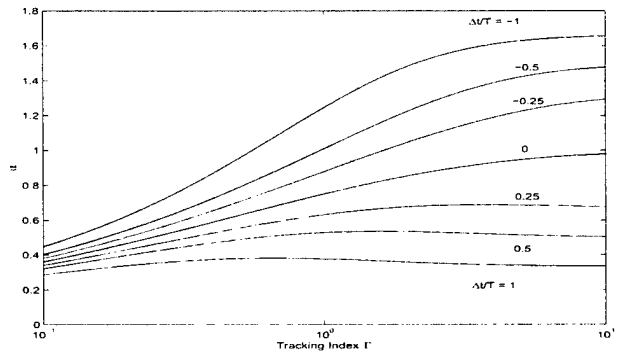

Fig. 4. α Versus Γ with $T = 1$ s and $\sigma_v = 10$ m

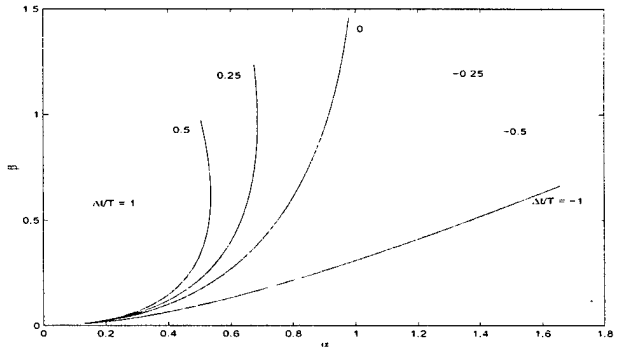

Fig. 6. β Versus α with $T = 1$ s, $\sigma_v = 10$ m and $0.01 \leq \Gamma \leq 10.0$ for various values of $\frac{\Delta t}{T}$

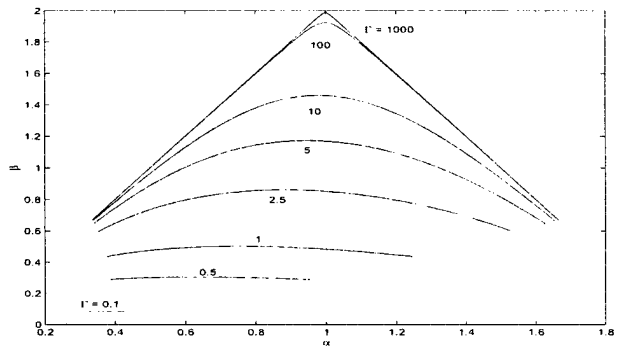

Figure 7. β Versus α with $T = 1$ s, $\sigma_v = 10$ m and $-1.0 < \frac{\Delta t}{T} < 1.0$ for various values of Γ

is maximized for no range-Doppler coupling (i.e., $\Delta t = 0$) and β does not depend on the sign of Δt as indicated by (44). For the case of $\Delta t = 0$, β will go to two as Γ approaches infinity. In Figure 6, β is plotted versus α for various values of $\frac{\Delta t}{T}$. Note that there may be two solutions of β for a given α when $\Delta t > 0$, and there is only one solution of β for a given α when $\Delta t \leq 0$. Figure 7 shows the contours of constant Γ for β versus α for $-1.0 < \frac{\Delta t}{T} < 1.0$. Comparing Figures 6 and 7, the curve for $\frac{\Delta t}{T} = 0$ passes through the peak of the contours of constant Γ. Note that for $\frac{\Delta t}{T} = 0$, the values of α and β will go to one and two as Γ approaches infinity, respectively.

IV. INITIALIZATION GAINS

Least-squares estimation can be used to derive the gains for initializing an α, β filter. For linear least-squares estimation, an equation formulating the measurement vector Z as a linear function of the parameter vector X to be estimated is given by

$$Z = WX + V \tag{46}$$

where $E[V] = 0$ and $E[VV^T] = \sigma_v^2 I_N$ for $N + 1$ measurements with I_N denoting the $(N + 1)$ x $(N + 1)$ identity matrix. The least-squares estimate $\hat{X}$ [4] is given

$$\hat{X} = (W^T W)^{-1} W^T Z \tag{47}$$

with error covariance

$$P_N = COV[\hat{X}] = \sigma_v^2 (W^T W)^{-1} \tag{48}$$

A current state estimate of X denoted by $\hat{X}_0 = [\hat{r}_0 \quad \hat{\dot{r}}_0]^T$ can be obtained from the current measurement

plus the N previous measurements as

$$Z_N = W_N X_0 + V_N \tag{49}$$

where

$$Z_N = [\, y_{-N} \quad y_{-N+1} \quad \cdots \quad y_{-1} \quad y_0 \,] \tag{50}$$

$$V_N = [\, v_{-N} \quad v_{-N+1} \quad \cdots \quad v_{-1} \quad v_0 \,] \tag{51}$$

$$W_N = \begin{bmatrix} 1 & 1 & \cdots & 1 \\ \Delta t - NT & \Delta t + (-N+1)T & \cdots & \Delta t \end{bmatrix}^T \tag{52}$$

where $E[V_N] = 0$, $E[V_N V_N^T] = \sigma_v^2 I_N$, Δt is the range-Doppler coupling coefficient in (14) and W_N is a combination of the state transition matrix and the output matrix. The error covariance of the least-squares state estimate $\widehat{X}_0$ with an LFM waveform is given by

$$COV[\widehat{X}_0] = P_N = \sigma_v^2 (W_N^T W_N)^{-1} \tag{53}$$

where

$$(W_N^T W_N) = \begin{bmatrix} \frac{1}{N+1} & \frac{\Delta t}{N+1} - \frac{N}{N+1}\frac{T}{2} \\ \Delta t - \frac{N}{N+1}\frac{T}{2} & \frac{(\Delta t)^2 - \Delta t NT}{N+1} + \frac{N(2N+1)}{N+1}\frac{T^2}{6} \end{bmatrix} \tag{54}$$

Then

$$P_N = \frac{2\sigma_v^2}{d_N} \begin{bmatrix} 2N+1-6\frac{\Delta t}{T} + \frac{6}{N}\left(\frac{\Delta t}{T}\right)^2 & \frac{3}{T}(1 - \frac{2\Delta t}{NT}) \\ \frac{3}{T}(1 - \frac{2\Delta t}{NT}) & \frac{6}{NT^2} \end{bmatrix} \tag{55}$$

where $d_N = (N+1)(N+2)$. Note that Δt cannot be selected to minimize the determinant of P_N, $|P_N|$, because $|P_N|$ is not a function of Δt. Also note that for $\frac{\Delta t}{T} = \frac{N}{2}$, the variance of range is minimized and the range and range rate estimates are uncorrelated.

Let the scheduled gains for initialization for the α, β filter be denoted by

$$K_k = \begin{bmatrix} \alpha_k & \frac{\beta_k}{T} \end{bmatrix}^T \tag{56}$$

where k denotes the gains for processing the $k+1^{st}$ measurement.

Letting $P_{k|k} = P_k$ of (55) in (8) provides a simple gain scheduling procedure for α and β during initialization that is given by

$$\alpha_k = max\left\{ \frac{2(2k+1) - 6\frac{\Delta t}{T}}{(k+1)(k+2)}, \alpha \right\} \tag{57}$$

$$\beta_k = max\left\{ \frac{6}{(k+1)(k+2)}, \beta \right\} \tag{58}$$

with $X_{0|-1} = [\, 0 \quad 0 \,]^T$. Note that as k approaches infinity, the functions of k for α_k and β_k go to zero. This is because the least-squares estimation assumes there is no process noise. However, the steady-state gains, α and β are nonzero in the Kalman filter, which takes process noise into consideration. If $\sigma_w = 0$ (e.g., exoatmospheric ballistic target), and $\alpha = \beta = 0$, α_k and β_k are valid for longer periods. Using the range measurement at $t = 0$, y_0, and the range measurement at $t = T$, y_1, the initial state estimate and error covariance based on two measurements with an LFM waveform are given by

$$\widehat{X}_{1|1} = \begin{bmatrix} y_1 - \frac{\Delta t}{T}(y_1 - y_0) \\ \frac{y_1 - y_0}{T} \end{bmatrix} \tag{59}$$

$$P_{1|1} = \sigma_v^2 \begin{bmatrix} \left(\frac{\Delta t}{T} - 1\right)^2 + \left(\frac{\Delta t}{T}\right)^2 & \frac{1}{T}\left(1 - 2\frac{\Delta t}{T}\right) \\ \frac{1}{T}\left(1 - 2\frac{\Delta t}{T}\right) & \frac{2}{T^2} \end{bmatrix} \tag{60}$$

The $\widehat{X}_{1|1}$ and $P_{1|1}$ are the result of the least-squares estimation with the first two measurements.

V. CONCLUDING REMARKS

The steady-state gains and error covariance for the α, β filter are presented as a simple function of $\alpha, \beta, \Delta t, T$ and σ_v^2. The results for the α, β filter were confirmed with the Kalman filtering equations. The initialization equations of (60) and (61) assume two identical LFM waveforms at $t = 0$ and $t = T$. However, in a phased array radar, the confirmation dwell may include a LFM waveform with up-chirp and down-chirp to achieve range and range rate measurements from a single dwell.

REFERENCES

1. Blair, W.D., *Fixed-Gain, Two-Stage Estimators for Tracking maneuvering targets*, Naval Surface Warfare Center, Dahlgren Divison, Dahlgren, Virginia 22448-5000, July 1992.
2. Fitzgerald, R.J., "Effects of Range-Doppler Coupling on Chirp Radar Tracking Accuracy," *IEEE Transactions on Aerospace and Electronic Systems*, July 1974, pp. 528-532.
3. Kalata, P.R., "The Tracking Index: A Generalized Parameter for $\alpha - \beta$ and $\alpha - \beta - \gamma$ Target Trackers," *IEEE Transactions on Aerospace and Electronic Systems*, Vol. AES-20, March 1984, pp. 174-182. Corrections: Vol. AES-20, Nov. 1984, pp. 845.
4. Bar-Shalom, Y., and Li, X.R., *Estimation and Tracking: Principles, Techniques and Software*, Dedham, MA: Artech Hourse, 1993.

Correspondence

The steady-state gains and error covariance are derived for a two-state Kalman filter (i.e., an α, β filter) for tracking with linear frequency modulated (LFM) waveforms. A procedure is given for calculating the α, β gains from the tracking index Γ, the sample period T, and the range-Doppler coupling coefficient Δt. The steady-state error covariance is found to be a simple function of α, β, Δt, T and the measurement noise variance σ_v^2. The expressions for the steady-state gains and error covariance were confirmed numerically with the Kalman filtering equations. A gain scheduling technique for α and β during initialization is also given.

INTRODUCTION

The Kalman filter produces an optimal estimate of the target state when given the motion model and a sequence of sensor measurements corrupted with white Gaussian errors. The computational burden of maintaining the Kalman filter may prohibit its use when many targets are being tracked. Steady-state filters are also good for filter design and analysis. Constant data rate and constant covariances required for steady-state filters are not typically true in real systems, so approximate gains are typically used. The gains are based on the steady-state gains of the Kalman filter and implemented either using a fixed gain or an easily generated gain schedule. The resultant filter for tracking range and range rate is called the α, β filter, where approximate filter gains α, β may be used instead of the optimal Kalman gains [1]. In [2], the range-Doppler coupling of linear frequency modulated (LFM) waveforms is shown to have a significant effect on tracking accuracy. In [3] and the Appendix of [1], the steady-state gains and error covariance are derived for range measurements without range-Doppler coupling. Here, the range-Doppler coupling associated with LFM waveforms is included in the measurement equation, and expressions for the steady-state gains and error covariance are calculated.

Manuscript received September 18, 1999; revised November 20, 1999; released for publication November 27, 1999.

IEEE Log No. T-AES/36/2/05240.

Refereeing of this contribution was handled by G. I. Friedman.

This research was accomplished through the Faculty Leadership Program of the Georgia Tech Research Institute, Georgia Institute of Technology, Atlanta, GA.

MATHEMATICAL MODEL

The dynamics model commonly assumed for a target in track is given by

$$X_{k+1} = F_k X_k + G_k w_k \tag{1}$$

where $w_k \sim N(0, Q_k)$ is the process noise, F_k defines a linear constraint on the dynamics, and G_k is the input matrix for maneuver. The target state vector X_k contains the range and range rate of the target at time k. The linear measurement model is given by

$$Y_k = H_k X_k + v_k \tag{2}$$

where Y_k is typically the target position measurement and $v_k \sim N(0, R_k)$ is the measurement noise, and H_k is the output matrix that includes range-Doppler coupling coefficient.

The measured range and the variance for an LFM waveform and the range-Doppler coupling coefficient for an LFM waveform are given by [2] as

$$y_k = r_k + \Delta t \dot{r}_k + v_k \tag{3}$$

$$\sigma_v^2 = E[v_k^2] = \frac{\Delta t^2 c^2}{8 f_o^2 \tau^2 \Re} = \frac{c^2}{8 \mathcal{B}^2 \Re} \tag{4}$$

$$\Delta t = \frac{f_0 \tau}{f_2 - f_1} = \frac{f_0 \tau}{\mathcal{B}} \tag{5}$$

where r_k is the true range at time k, $\Re$ is the signal-to-noise ratio, c is the speed of light, f_0 is the nominal carrier frequency, f_1 is the initial frequency, and f_2 is the final frequency. Also $|\mathcal{B}|$ is the bandwidth of the LFM waveform and τ is the pulse length. Note that the demodulation frequency can be modified with the range rate estimate to reduce the bias in the range measurement due to range-Doppler coupling. However, if the range rate estimate is used to remove the bias in the range measurements, the measurement errors become correlated with the state estimate and the typical Kalman filter must be modified to account for the state correlated measurement errors.

The Kalman filtering equations associated with the state model in (1) and the measurement model in (2) are given by the following equations.

Time Update:

$$X_{k|k-1} = F_{k-1} X_{k-1|k-1} \tag{6}$$

$$P_{k|k-1} = F_{k-1} P_{k-1|k-1} F_{k-1}^T + G_{k-1} Q_{k-1} G_{k-1}^T. \tag{7}$$

Measurement Update:

$$K_k = P_{k|k-1} H_k^T [H_k P_{k|k-1} H_k^T + R_k]^{-1} = P_{k|k} H_k^T R_k^{-1} \tag{8}$$

$$X_{k|k} = X_{k|k-1} + K_k [Y_k - H_k X_{k|k-1}] \tag{9}$$

$$P_{k|k} = [I - K_k H_k] P_{k|k-1} \tag{10}$$

where the subscript notation $(k \mid j)$ denotes the state estimate for time t_k when given measurements through time t_j. The K_k is the Kalman gain that minimizes the mean square error in the state estimate. Also, note that $X_k \sim N(X_{k|k}, P_{k|k})$ with $X_{k|k}$ and $P_{k|k}$ denoting the mean and error covariance of the state estimate, respectively.

THE α,β FILTER

For the Kalman filter in steady-state conditions, $P_{k|k} = P_{k-1|k-1}$, and $P_{k+1|k} = P_{k|k-1}$, and $K_k = K_{k-1}$. For a Kalman filter to achieve these steady-state conditions, the error processes, w_k and v_k, must have stationary statistics and the data rate must be constant. When the noise processes are not stationary or the data rate is not constant, a filter using the steady-state gains provides suboptimal estimates. The α,β filter is the steady-state Kalman filter for tracking nearly constant range rate targets. The α,β filter is a single coordinate filter that is based on the assumption that the target is moving with constant range rate plus zero-mean, white Gaussian acceleration errors. Given this assumption, the filter gains α and β are chosen as the steady-state Kalman gains that minimize the mean-square error in the range and range rate estimates.

For the α,β filter for piecewise constant acceleration errors,

$$X_k = [r_k \quad \dot{r}_k]^T \tag{11}$$

$$F_k = F = \begin{bmatrix} 1 & T \\ 0 & 1 \end{bmatrix} \tag{12}$$

$$G_k = G = \left[\frac{T^2}{2} \quad T\right]^T \tag{13}$$

$$H_k = H = [1 \quad \Delta t] \tag{14}$$

$$R_k = R = \sigma_v^2 \tag{15}$$

$$Q_k = Q = \sigma_w^2 \tag{16}$$

$$K_k = K = \left[\alpha \quad \frac{\beta}{T}\right]^T \tag{17}$$

where r_k and $\dot{r}_k$ are the range and range rate of the target, respectively, σ_v^2 and σ_w^2 are the variances of measurement noise and process noise, respectively, T is the sample period between measurements, Δt is the range-Doppler coupling coefficient, and α and β/T are the steady-state Kalman filter gains.

Let the steady-state error covariance matrix of the filtered estimates for the α, β filter be denoted as

$$P_{k+1|k+1} = P_{k|k} = P = \begin{bmatrix} p_{11} & p_{12} \\ p_{12} & p_{22} \end{bmatrix}. \tag{18}$$

Using (14), (15), and (18) in (8) gives the steady-state gain as

$$K_k = K_{k-1} = K = PH^T R^{-1} = \begin{bmatrix} p_{11} + p_{12}\Delta t \\ p_{12} + p_{22}\Delta t \end{bmatrix} \sigma_v^{-2}. \tag{19}$$

Using (17) with (19) gives

$$\alpha = (p_{11} + p_{12}\Delta t)\sigma_v^{-2} \tag{20}$$

$$\beta = (p_{12} + p_{22}\Delta t)T\sigma_v^{-2}. \tag{21}$$

Inserting (7) into (10) and setting $P_{k|k} = P_{k-1|k-1} = P$ for steady-state conditions gives

$$[I - KH]^{-1}P = FPF^T + GG^T\sigma_w^2. \tag{22}$$

Then

$$[I - KH]^{-1}P = \frac{1}{1 - \alpha - \frac{\beta\Delta t}{T}} \begin{bmatrix} \left(1 - \frac{\beta\Delta t}{T}\right)p_{11} + \alpha\Delta t p_{12} & \left(1 - \frac{\beta\Delta t}{T}\right)p_{12} + \alpha\Delta t p_{22} \\ \frac{\beta}{T}p_{11} + (1-\alpha)p_{12} & \frac{\beta}{T}p_{12} + (1-\alpha)p_{22} \end{bmatrix} \tag{23}$$

$$FPF^T = \begin{bmatrix} p_{11} + 2Tp_{12} + T^2p_{22} & p_{12} + Tp_{22} \\ p_{12} + Tp_{22} & p_{22} \end{bmatrix} \tag{24}$$

$$GG^T\sigma_w^2 = \sigma_w^2 \begin{bmatrix} \frac{T^4}{4} & \frac{T^3}{2} \\ \frac{T^3}{2} & T^2 \end{bmatrix}. \tag{25}$$

Equating the (1,2) and (2,2) elements of (22) gives expressions for p_{12} and p_{22}. Substituting p_{12} and p_{22} into (21) gives

$$\Gamma^2 = \frac{T^4\sigma_w^2}{\sigma_v^2} = \frac{\beta^2}{1 - \alpha - \beta\frac{\Delta t}{T}} \tag{26}$$

where Γ is the tracking or maneuvering index. Using (26) to eliminate σ_w^2 in the expressions of p_{12} and p_{22} gives

$$p_{12} = \frac{\beta\sigma_v^2}{T\left(1 - \alpha - \beta\frac{\Delta t}{T}\right)}\left[1 - \alpha - \left(\frac{2\alpha + \beta}{2}\right)\frac{\Delta t}{T}\right] \tag{27}$$

$$p_{22} = \frac{\beta\sigma_v^2(2\alpha - \beta)}{2T^2\left(1 - \alpha - \beta\frac{\Delta t}{T}\right)}. \tag{28}$$

Substituting p_{12} into (20) gives

$$p_{11} = \alpha\sigma_v^2 - \frac{\beta\sigma_v^2}{\left(1 - \alpha - \beta\frac{\Delta t}{T}\right)} \times \left[1 - \alpha - \left(\frac{2\alpha + \beta}{2}\right)\frac{\Delta t}{T}\right]\frac{\Delta t}{T}. \tag{29}$$

The steady-state error covariance is then given by

$$P_{k|k} = \sigma_v^2 \begin{bmatrix} \alpha - \frac{\beta}{\left(1 - \alpha - \beta\frac{\Delta t}{T}\right)}\left[1 - \alpha - \left(\frac{2\alpha + \beta}{2}\right)\frac{\Delta t}{T}\right]\frac{\Delta t}{T} & \frac{\beta}{T\left(1 - \alpha - \beta\frac{\Delta t}{T}\right)}\left[1 - \alpha - \left(\frac{2\alpha + \beta}{2}\right)\frac{\Delta t}{T}\right] \\ \frac{\beta}{T\left(1 - \alpha - \beta\frac{\Delta t}{T}\right)}\left[1 - \alpha - \left(\frac{2\alpha + \beta}{2}\right)\frac{\Delta t}{T}\right] & \frac{\beta(2\alpha - \beta)}{T^2\left(1 - \alpha - \beta\frac{\Delta t}{T}\right)} \end{bmatrix}. \tag{30}$$

Equating the (1,1) elements of (22) and using (27) through (29) gives

$$a_3\beta^3 + a_2\beta^2 + a_1\beta + a_0 = 0 \tag{31}$$

where

$$a_3 = -\left(\frac{\Delta t}{T}\right)^2 - \frac{\Delta t}{4T} \tag{32}$$

$$a_2 = -2\alpha\left(\frac{\Delta t}{T}\right)^2 - 2\alpha\frac{\Delta t}{T} + 3\frac{\Delta t}{T} + \frac{1 - \alpha}{4} \tag{33}$$

$$a_1 = -3\alpha^2\frac{\Delta t}{T} - \alpha^2 + 2\alpha\frac{\Delta t}{T} + 3\alpha - 2 \tag{34}$$

$$a_0 = \alpha^2 - \alpha^3. \tag{35}$$

There are three solutions for (31). By comparing with the Kalman filter numerical results, the valid solutions of (31) for β are given by

$$\beta_{\pm} = \frac{2}{\left(1+4\frac{\Delta t}{T}\right)} \times \left(-\alpha\left(1+2\frac{\Delta t}{T}\right)+2\pm 2\sqrt{\left(1-\alpha\frac{\Delta t}{T}\right)^2-\alpha}\right). \tag{36}$$

For $\Delta t/T > 0$, both solutions of (36) are valid for β depending on the selection of Γ and $\Delta t/T$. The β_- (i.e., minus sign in the front of the radical) is used for β with increasing α until the maximum α is reached, which is given by

$$\alpha_{\max} = \frac{\frac{2\Delta t}{T}+1-\sqrt{\frac{4\Delta t}{T}+1}}{2\left(\frac{\Delta t}{T}\right)^2}. \tag{37}$$

Then β_+ (i.e., plus sign in the front of the radical) is used for β from $\alpha_{\max}$ with decreasing α and it is valid as long as $1-\alpha-\beta_+\Delta t/T > 0$, that is, Γ in (26) is a real number. For $\Delta t/T \le 0$, β_- is the only solution for β. If $\Delta t/T = -\frac{1}{4}$, (31) becomes a quadratic equation given by

$$b_2\beta^2 + b_1\beta + b_0 = 0 \tag{38}$$

where

$$b_2 = \frac{\alpha}{8} - \frac{1}{2} \tag{39}$$

$$b_1 = -\frac{\alpha^2}{4} + \frac{5\alpha}{2} - 2 \tag{40}$$

$$b_0 = \alpha^2 - \alpha^3. \tag{41}$$

If there is no range-Doppler coupling (i.e., $\Delta t/T = 0$) [1, 3, 7], (30), (26) and β_- of (36) give

$$P_{k|k} = \sigma_v^2\begin{bmatrix}\alpha & \frac{\beta}{T}\\ \frac{\beta}{T} & \frac{\beta^2(2\alpha-\beta)}{2(1-\alpha)T^2}\end{bmatrix} \tag{42}$$

$$\Gamma^2 = \frac{T^4\sigma_w^2}{\sigma_v^2} = \frac{\beta^2}{1-\alpha} \tag{43}$$

$$\beta = 2(2-\alpha) - 4\sqrt{1-\alpha}. \tag{44}$$

These results of (42)–(44) agree with that derived from [1, Appendix] and Kalata's papers [3, 4].

Inserting (26) into (31) to eliminate α and expressing a polynomial equation of β in terms of Γ, Δt and T gives

$$\beta^4 - \Gamma^2\beta^3 + \left[\frac{\Gamma^4}{4} - \left(\frac{\Delta t}{T}\right)^2\Gamma^4 - 2\Gamma^2\right]\beta^2 - \Gamma^4\beta + \Gamma^4 = 0. \tag{45}$$

Note that (45) does not depend on the sign of Δt. Newton's method with a good initial guess of β can be used to find a zero of (45) when Γ and $\Delta t/T$ are given. A good initial guess of β is given by the case of $\Delta t = 0$, where the initial β is computed with (44) and α is given by [6]

$$\alpha = -\tfrac{1}{8}(\Gamma^2 + 8\Gamma - (\Gamma+4)\sqrt{\Gamma^2+8\Gamma}). \tag{46}$$

After β is found by utilizing Newton's method, the steady-state gain, α, and the error covariance are then calculated for the given Γ and $\Delta t/T$ using (26) and (30). These results were confirmed with the Kalman filtering equations.

Various results for the α,β filter are shown in Figs. 1–7 and the results were comfirmed by iterating the Kalman filtering algorithm until the steady-state conditions were achieved. Fig. 1 shows that the variance of the range estimate decreases with increasing Δt for a given Γ. Fig. 2 shows that the correlation coefficients for range and range rate estimates are between zero and one. Note that as Δt becomes more positive, the correlation coefficient for range and range rate goes toward zero at higher Γ. This means that the range and range rate estimates are less correlated with each other at higher Γ. Thus the accuracy of the predicted measurements will be improved at more positive Δt. Fig. 3 shows that the variance of range rate decreases with increasing Δt. Fig. 4 shows that α decreases with increasing Δt. For the case of $\Delta t = 0$, α will go to one as Γ approaches infinity. Fig. 5 shows that β is maximized for no range-Doppler coupling (i.e., $\Delta t = 0$) and β does not depend on the sign of Δt as indicated by (45). For the case of $\Delta t = 0$, β will go to two as Γ approaches infinity. In Fig. 6, β is plotted versus α for various values of $\Delta t/T$. Note that there may be two solutions of β for a given α when $\Delta t > 0$, and there is only one solution of β for a given α when $\Delta t \le 0$. Fig. 7 shows the contours of constant Γ for β versus α for $-1.0 < \Delta t/T < 1.0$. Comparing Figs. 6 and 7, the curve for $\Delta t/T = 0$ passes through the peak of the contours of constant Γ. Note that for $\Delta t/T = 0$, the values of α and β will go to one and two as Γ approaches infinity, respectively.

INITIALIZATION GAINS

Least-squares estimation can be used to derive the gains for initializing an α,β filter. For linear least-squares estimation, an equation formulating the measurement vector Z as a linear function of the parameter vector X to be estimated is given by

$$Z = WX + V \tag{47}$$

where $E[V] = 0$ and $E[VV^T] = \sigma_v^2 I_N$ for $N+1$ measurements with I_N denoting the $(N+1)\times(N+1)$ identity matrix. The least-squares estimate $\hat{X}$ [5] is

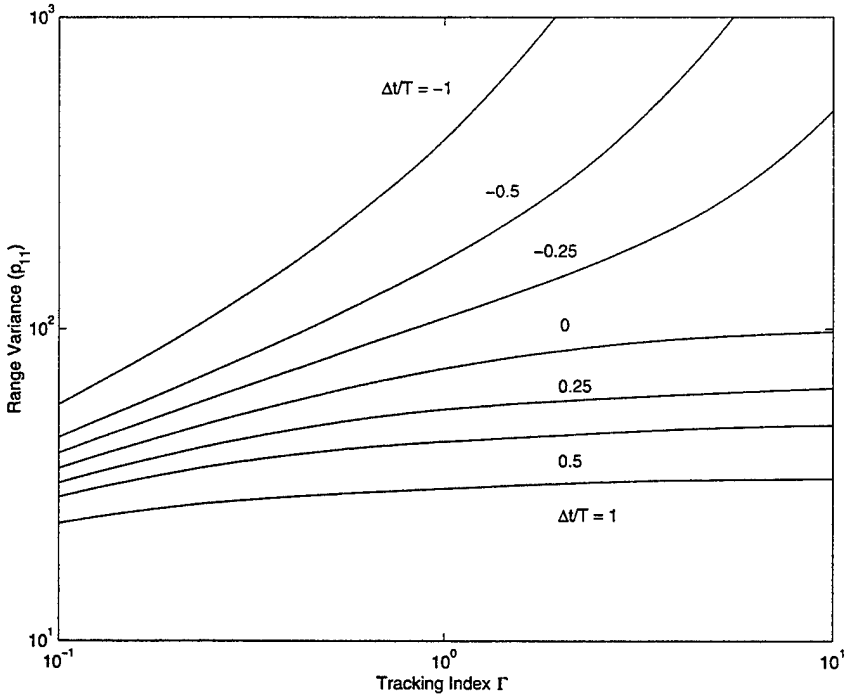

Fig. 1. Range variance versus Γ with $T = 1$ s and $\sigma_v = 10$ m.

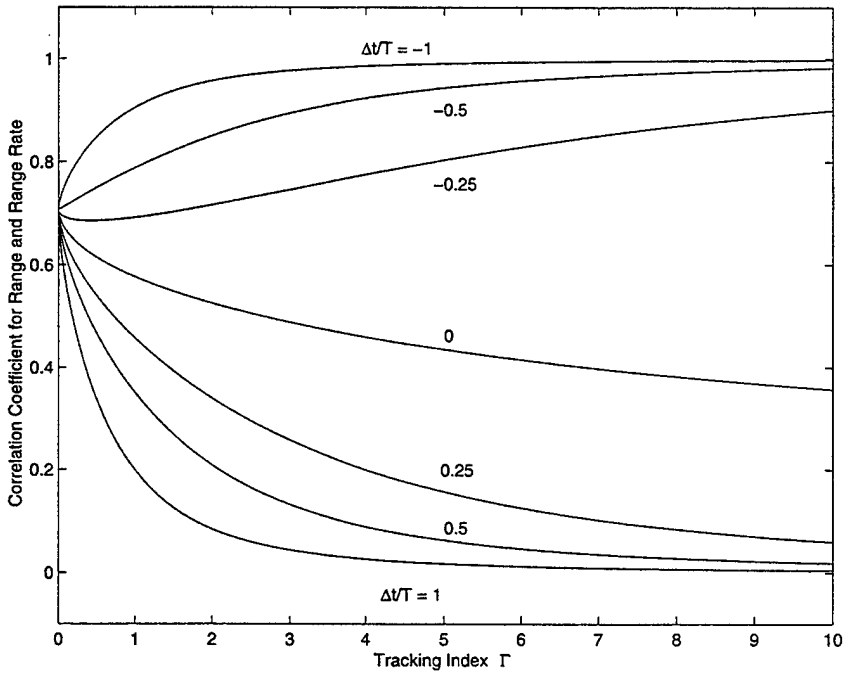

Fig. 2. Correlation coefficient for range and range rate versus Γ with $T = 1$ s and $\sigma_v = 10$ m.

given

$$\hat{X} = (W^T W)^{-1} W^T Z \tag{48}$$

with error covariance

$$P_N = \text{cov}[\hat{X}] = \sigma_v^2 (W^T W)^{-1}. \tag{49}$$

A current state estimate of X denoted by $\hat{X}_0 = [\hat{r}_0 \quad \dot{\hat{r}}_0]^T$ can be obtained from the current measurement plus the N previous measurements as

$$Z_N = W_N X_0 + V_N \tag{50}$$

where

$$Z_N = [y_{-N} \quad y_{-N+1} \quad \cdots \quad y_{-1} \quad y_0] \tag{51}$$

$$V_N = [v_{-N} \quad v_{-N+1} \quad \cdots \quad v_{-1} \quad v_0] \tag{52}$$

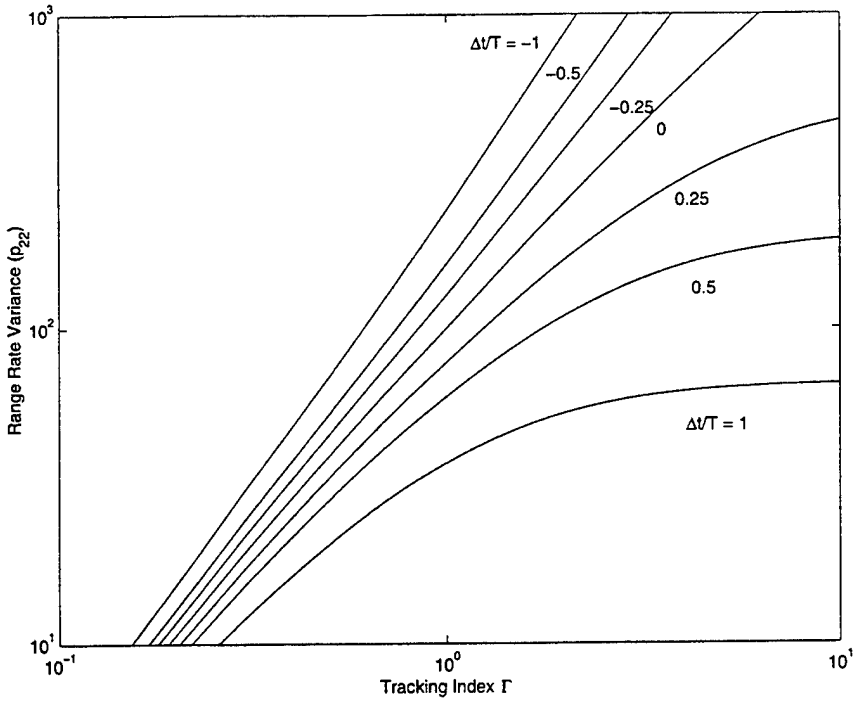

Fig. 3. Range rate variance versus Γ with $T = 1$ s and $\sigma_v = 10$ m.

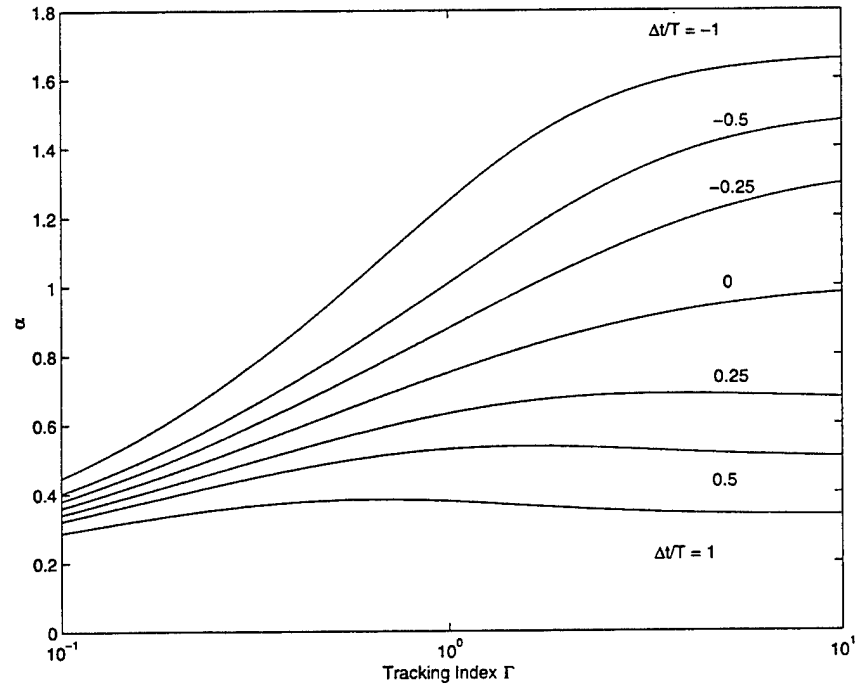

Fig. 4. α versus Γ with $T = 1$ s and $\sigma_v = 10$ m.

$$W_N = \begin{bmatrix} 1 & 1 & \cdots & 1 & 1 \\ \Delta t - NT & \Delta t + (-N+1)T & \cdots & \Delta t - T & \Delta t \end{bmatrix}^T \tag{53}$$

where $E[V_N] = 0$, $E[V_N V_N^T] = \sigma_v^2 I_N$, Δt is the range-Doppler coupling coefficient in (14) and W_N is a combination of the state transition matrix and the output matrix. The error covariance of the least-squares state estimate $\hat{X}_0$ with an LFM waveform is given by

$$\text{cov}[\hat{X}_0] = P_N = \sigma_v^2 (W_N^T W_N)^{-1} \tag{54}$$

where

$$(W_N^T W_N) = (N+1) \begin{bmatrix} 1 & \Delta t - N\dfrac{T}{2} \\ \Delta t - N\dfrac{T}{2} & (\Delta t)^2 - \Delta t NT + N(2N+1)\dfrac{T^2}{6} \end{bmatrix}. \tag{55}$$

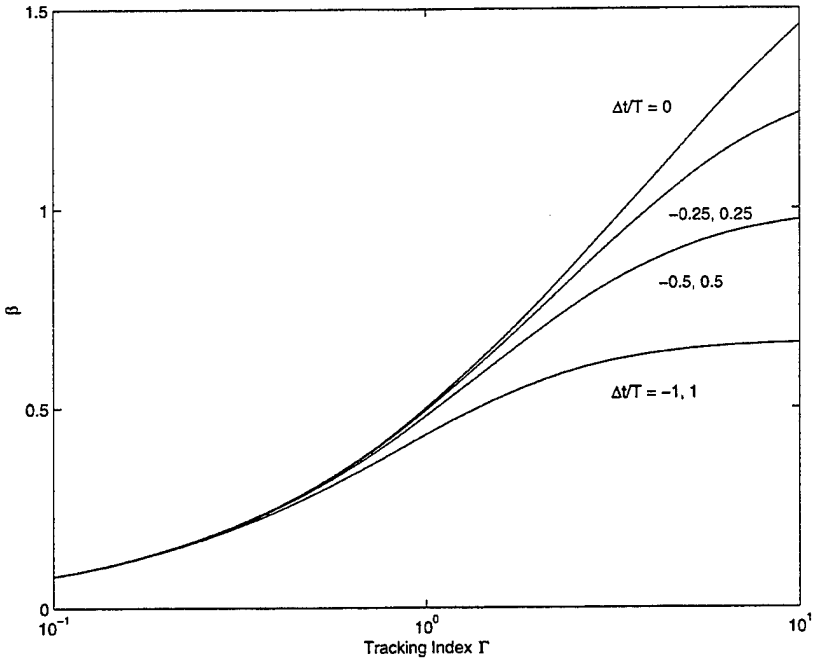

Fig. 5. β versus Γ with $T = 1$ s and $\sigma_v = 10$ m.

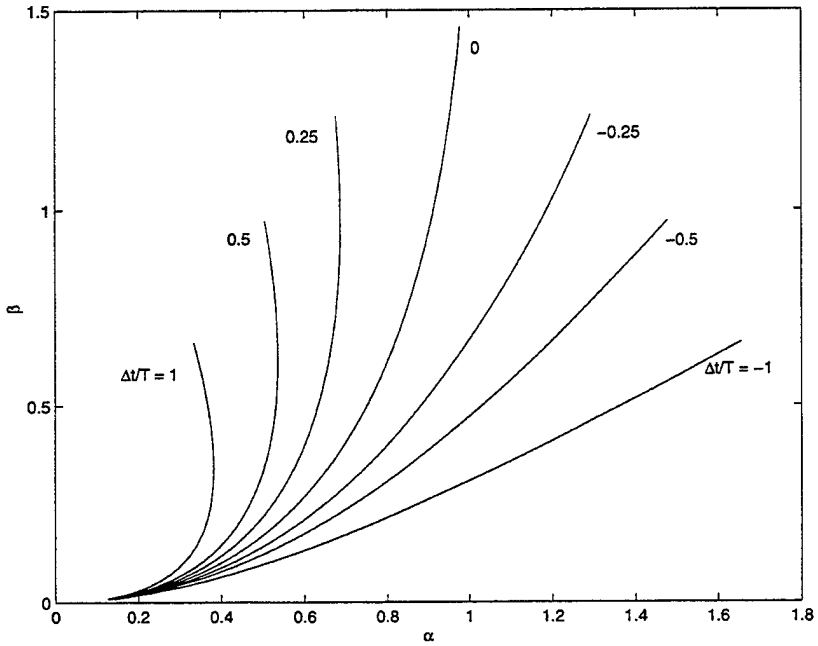

Fig. 6. β versus α with $T = 1$ s, $\sigma_v = 10$ m, $0.001 \leq \Gamma \leq 10.0$ for various values of $\Delta t/T$.

Then

$$\operatorname{cov}[\hat{X}_0] = P_N = \frac{2\sigma_v^2}{(N+1)(N+2)} \times \begin{bmatrix} 2N+1-6\frac{\Delta t}{T}+\frac{6}{N}\left(\frac{\Delta t}{T}\right)^2 & \frac{3}{T}\left(1-\frac{2\Delta t}{NT}\right) \\ \frac{3}{T}\left(1-\frac{2\Delta t}{NT}\right) & \frac{6}{NT^2} \end{bmatrix}. \tag{56}$$

Note that Δt cannot be selected to minimize the determinant of P_N, $|P_N|$, because $|P_N|$ is not a function of Δt. Also note that for $\Delta t/T = N/2$, the variance of range is minimized and the range and range rate estimates are uncorrelated.

Let the scheduled gains for initialization for the α, β filter be denoted by

$$K_k = \begin{bmatrix} \alpha_k & \frac{\beta_k}{T} \end{bmatrix}^T \tag{57}$$

where k denotes the gains for processing the $k+1$st measurement.

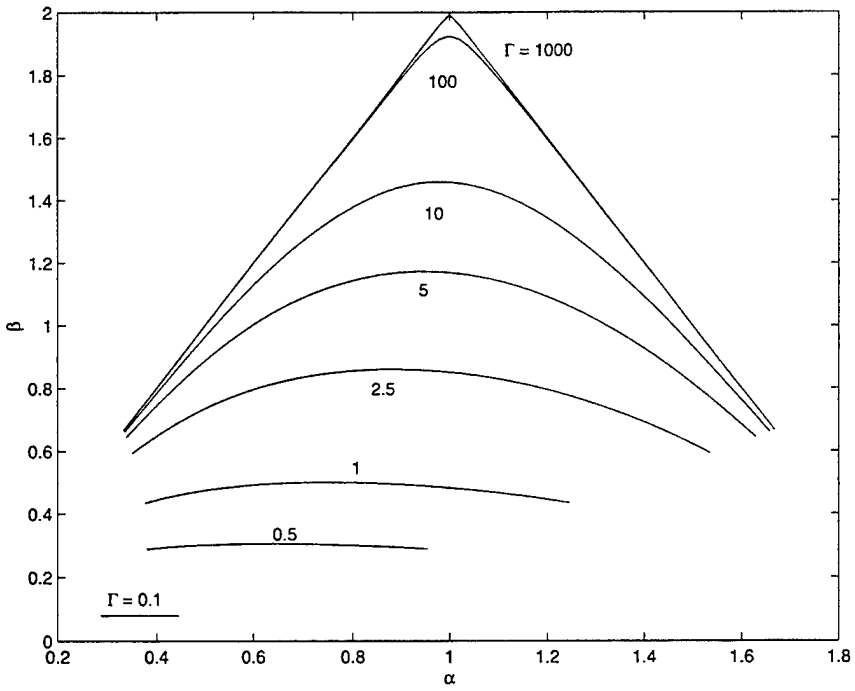

Fig. 7. β versus α with $T = 1$ s, $\sigma_v = 10$ m, $-1.0 < \Delta t/T < 1.0$ for various values of Γ.

Letting $P_{k|k} = P_k$ of (56) in (8) provides a simple gain scheduling procedure for α and β during initialization that is given by

$$\alpha_k = \max\left\{\frac{2(2k+1) - 6\frac{\Delta t}{T}}{(k+1)(k+2)}, \alpha\right\} \tag{58}$$

$$\beta_k = \max\left\{\frac{6}{(k+1)(k+2)}, \beta\right\} \tag{59}$$

with $X_{0|-1} = [0 \quad 0]^T$. Note that as k approaches infinity, the functions of k for α_k and β_k go to zero. This is because the least-squares estimation assumes there is no process noise. However, the steady-state gains, α and β, are non-zero in the Kalman filter, which takes process noise into consideration. If $\sigma_w = 0$ (e.g., exoatmospheric ballistic target), and $\alpha = \beta = 0$, α_k and β_k are valid for longer periods. Using the range measurement at $t = 0$, y_0, and the range measurement at $t = T$, y_1, the initial state estimate and error covariance based on two measurements with an LFM waveform are given by

$$\hat{X}_{1|1} = \begin{bmatrix} y_1 - \frac{\Delta t}{T}(y_1 - y_0) \\ \frac{y_1 - y_0}{T} \end{bmatrix} \tag{60}$$

$$P_{1|1} = \sigma_v^2 \begin{bmatrix} \left(\frac{\Delta t}{T} - 1\right)^2 + \left(\frac{\Delta t}{T}\right)^2 & \frac{1}{T}\left(1 - 2\frac{\Delta t}{T}\right) \\ \frac{1}{T}\left(1 - 2\frac{\Delta t}{T}\right) & \frac{2}{T^2} \end{bmatrix}. \tag{61}$$

The $\hat{X}_{1|1}$ and $P_{1|1}$ are the result of the least-squares estimation with the first two measurements.

CONCLUDING REMARKS

The steady-state gains and error covariance for the α,β filter are presented as a simple function of α, β, Δt, T, and σ_v^2. The results for the α,β filter were confirmed with the Kalman filtering equations. The initialization equations of (60) and (61) assume two identical LFM waveforms at $t = 0$ and $t = T$. However, in a phased-array radar, the confirmation dwell may include an LFM waveform with up-chirp and down-chirp to achieve range and range rate measurements from a single dwell.

WINNIE WONG
Georgia Tech Research Institute
Georgia Institute of Technology
Atlanta, GA 30332-0857

W. D. BLAIR
Georgia Tech Research Institute
7220 Richardson Rd.
Smyrna, GA 30080
E-mail: (dale.blair@gtri.gatech.edu)

REFERENCES

[1] Blair, W. D. (1992)
Fixed-gain, two-stage estimators for tracking maneuvering targets.
Naval Surface Warfare Center, Dahlgren Divison, Dahlgren, VA 22448-5000, July 1992.

[2] Fitzgerald, R. J. (1974)
Effects of range-Doppler coupling on chirp radar tracking accuracy.
IEEE Transactions on Aerospace and Electronic Systems (July 1974), 528–532.

[3] Kalata, P. R. (1992)
α–β target tracking systems: A survey.
1992 ACC, 832–836.

[4] Kalata, P. R. (1984)
The tracking index: A generalized parameter for α–β and α–β–γ target trackers.
IEEE Transactions on Aerospace and Electronic Systems, **AES-20** (Mar. 1984), 174–182. Corrections: **AES-20** (Nov. 1984), 845.

[5] Bar-Shalom, Y., and Li, X. R. (1993)
Estimation and Tracking: Principles, Techniques and Software.
Dedham, MA: Artech Hourse, 1993.

[6] Blair, W. D., and Bar-Shalom, Y. (1996)
Tracking maneuvering targets with multiple sensors: Does more data always mean better estimates?
IEEE Transactions on Aerospace and Electronic Systems, **32**, 1 (Jan. 1996), 450–455.

[7] Friedland, B. (1973)
Optimum steady-state position and velocity estimation using noisy sampled position data.
IEEE Transactions on Aerospace and Electronic Systems, **AES-9**, 6 (Nov. 1973), 906–911.

Georgia Tech Research Institute

A PERSPECTIVE ON MULTISENSOR FUSION

William Dale Blair, Ph.D.

Air and Missile Defense Division
Georgia Tech Research Institute
Georgia Institute of Technology

dale.blair@.gtri.gatech.edu
(770) 528-7934

Introduction

- Fusion is only a supporting process and it is unlikely that any customer is going for pay for "fusion for the sake of fusion."
- In many typical systems, the developers of the components (e.g., sensors) and system integrators most often do not understand fusion algorithms nor appreciate their value.
- Critical to develop and apply fusion algorithms in a systems context and optimize the system-level performance.
- Demonstrations of the potential for improvements in system-level performance will encourage system developers to take the risk associated with implementing fusion algorithms.
- Promising areas for potential improvements in system-level performance of sensor systems is the use fusion for efficient utilization of sensor resources and control of sensor modes.

Georgia Tech Research Institute

Introduction

- **Tracking benchmark is a set of scenarios and associated simulation environment that**
  - Captures salient features of the tracking system of interest
  - Provides a "level playing field" for evaluation and comparison of candidate tracking algorithms
- **Expected benefits of benchmark process**
  - Promote research and development with respect to many "real-world" issues associated with the deployment of the tracking system of interest
  - Development of algorithms that optimize system-level performance metrics of the tracking system of interest

Georgia Tech Research Institute

Tracking Requirements

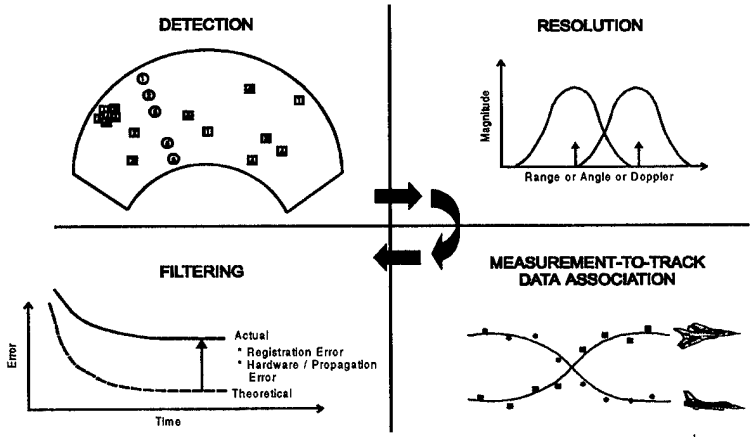

Georgia Tech Research Institute

Tracking In Legacy Simulations

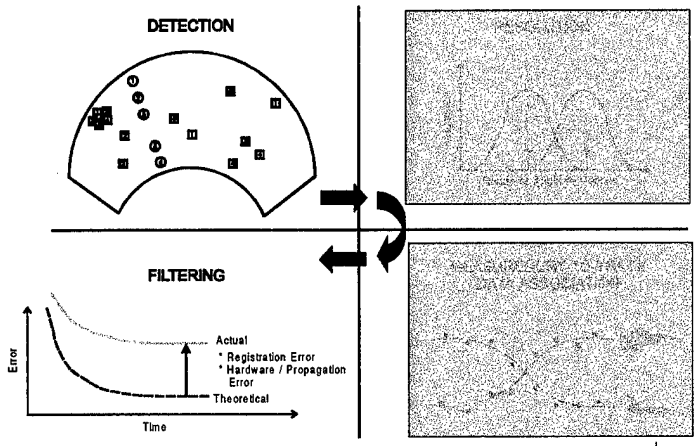

Georgia Tech Research Institute

NSWC Tracking Benchmark I

Target	Max. Acc. (m/s^2)	Man. Den. (%)	Average Sample Period(s)	Lost Tracks (%)
Anti-Ship Missile	69	44	1.9	1.5
Commercial Aircraft	6	37	3.6	0.1
Military Aircraft	75	98	1.6	0.5
Military Aircraft	77	91	1.9	2.4
Military Aircraft	68	67	1.9	0.2
Military Aircraft	68	83	1.9	0.2

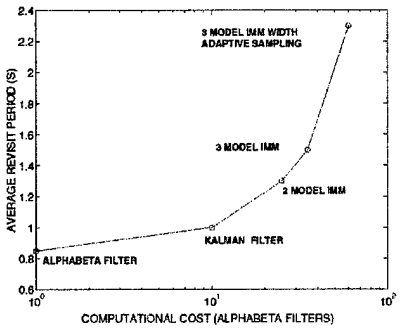

Average Sample Periods versus Computational Cost

Georgia Tech Research Institute

NSWC Tracking Benchmark II

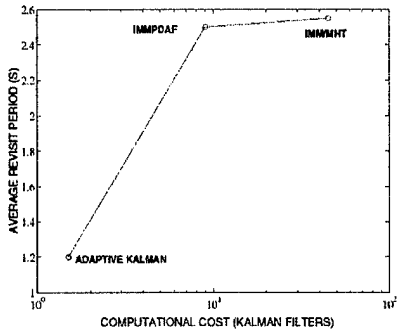

Average Radar Revisit Period

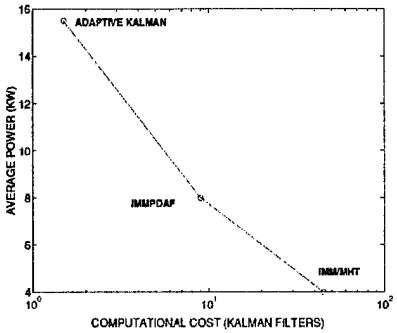

Average Radar Power

See W. D. Blair, et. al., "Benchmark for Radar Allocation and Tracking in ECM," IEEE Transactions on Aerospace and Electronic Systems, October 1998, pp. 1097-1114.

Georgia Tech Research Institute

Multiplatform/Multisensor Fusion

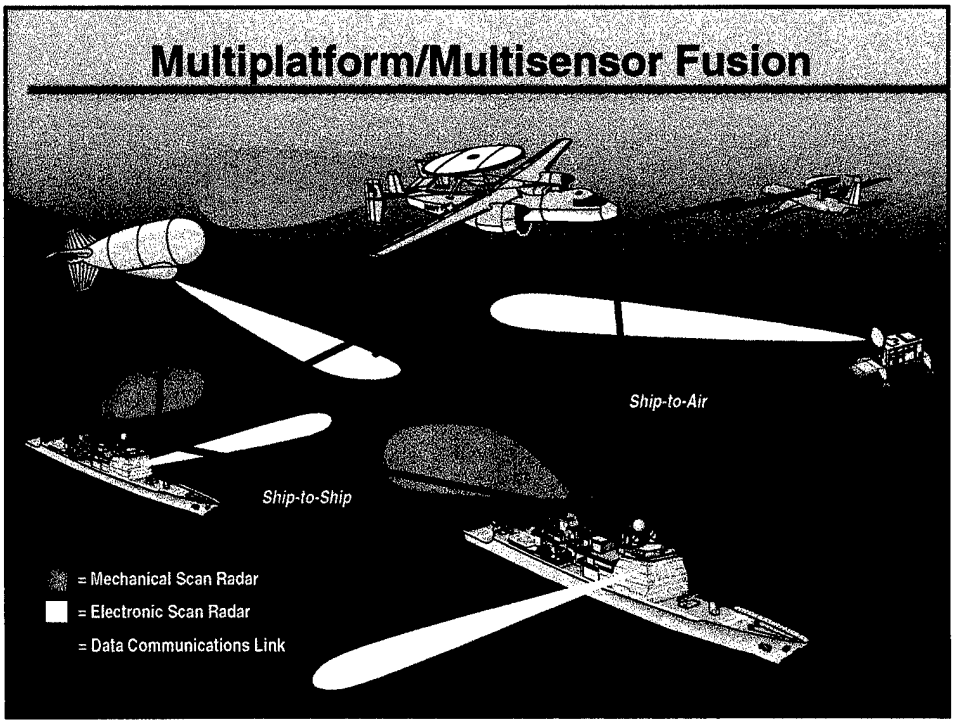

Performance Metrics

- **Completeness history**
  - Composite completeness (implemented)
  - Relative completeness
- **Timeliness**
  - Composite track initiation time (implemented)
  - Composite track relative initiation time
  - Composite track convergence time
- **Track continuity**
  - Cumulative swaps of composite tracks (implemented)
  - Cumulative broken composite tracks (implemented)
- **Ambiguity**
  - Composite track redundant track mean ratio (implemented)
  - Composite track spurious track mean ratio (implemented)
- **Accuracy**
  - Composite track accuracy (implemented)
  - Composite track covariance consistency (implemented)
- **Cross-platform commonality history**
  - Ratio of non-common composite track numbers (implemented)
  - Composite track state estimate differences
- **JCTN loading**
  - Communication data loading (implemented)
  - Processor loading

Georgia Tech Research Institute

Reporting Responsibility

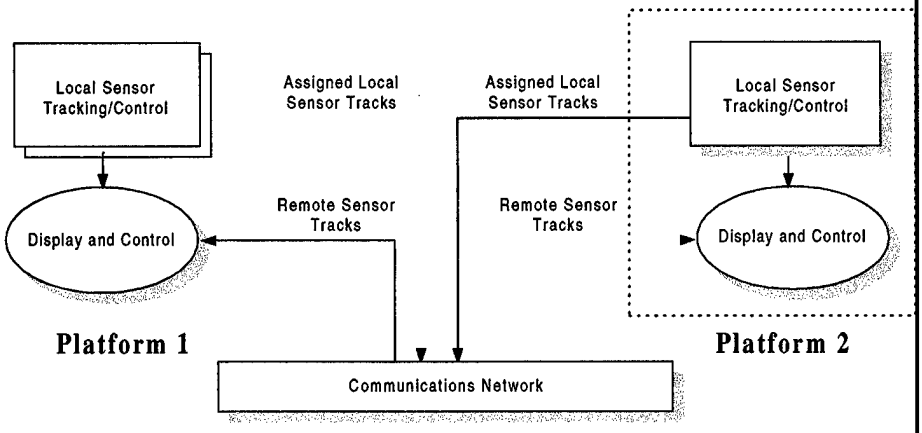

Georgia Tech Research Institute

Distributed Composite Tracking

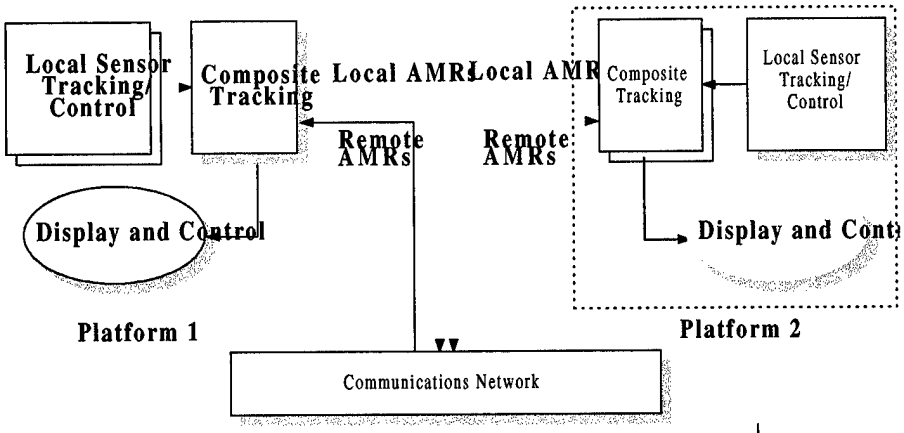

Georgia Tech Research Institute

Purpose/Goals of Benchmark

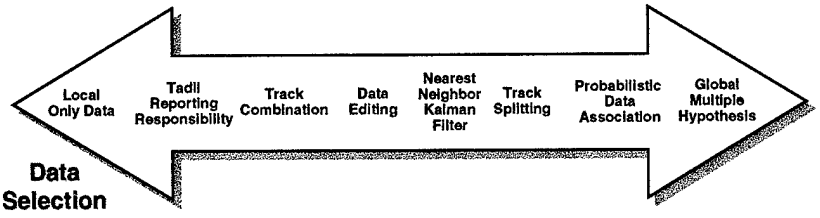

Velocity Insensitive to Biases	Maximum Accuracy
Heuristic	Systematic
Slow Responses	Fast Response
Less Computer Resources	More Computer Resources

Georgia Tech Research Institute

Concluding Remarks

Three areas critical to sensor fusion are:

- Optimization of system-level performance through the use of fusion
- Extension of fusion algorithm to address sensor phenomenology
- Characterization of the performance of different fusion algorithms versus the cost of implementation via benchmark problems

Georgia Tech Research Institute

Multiplatform-Multisensor Tracking

Dale Blair

September 15, 2000

Georgia Tech Research Institute
Georgia Institute of Technology
Atlanta, GA 30332-0857
dale.blair@gtri.gatech.edu

Outline

- Introduction
- Multiplatform-Multisensor Architectures
- Coordinate Systems
- Multiplatform-Multisensor Track Filtering
  - Target Motion Modeling
  - Radar Measurements
  - Extended Kalman Filter
  - Processing Local Measurements
  - Processing Remote Measurements
  - Processing Time-delay, Out-of-Sequence Measurements
  - Interacting Multiple Model (IMM) Estimator
- Conclusion Remarks

Introduction

- Target Tracking includes two types of uncertainty
  - Target Motion Uncertainty: magnitude and mode
  - Measurement Uncertainty: magnitude and mode
- **Local Measurement** refers to any sensor measurements that originate on the platform where the track processor resides.
- **Remote Measurement** refers to any sensor measurements that originate on a platform other than the platform where the track processor resides.
- **Local Track** refers to any track that includes only local measurements.
- **Remote Track** refers to any track that includes only remote measurements.
- **Composite Track** refers to any track that includes measurements from more than one sensor.

Introduction

- **Gridlock** refers to the process by which data from one frame of reference is transformed to another frame of reference. The frame of reference may be the tracking frame of reference and/or the sensor frame of reference. This process will include a geometric transformation component and an intersensor bias estimation and removal component. The term gridlock may be used interchangeably with **sensor data registration.**
- **Platform-centric Tracking** refers to those tracking systems where the sensors are all located at a single site or on a single platform (e.g., a ship or an aircraft). In these cases, the transformation of data from one frame of reference to another, which is the first step in the gridlock process, can be accomplished by rather simple transformations that change very slowly with time. The data passing from the various sensors to the tracker can be accomplished in a relatively simple manner as well (e.g., over a local area network).
- **Network-centric Tracking** refers to those tracking systems where sensors may be located at significant distances from one another as in the case of radar data from multiple ships or a ship and an aircraft. In these cases, the transformation of data from one site to another is more involved, and the existence of a communication link is implied.

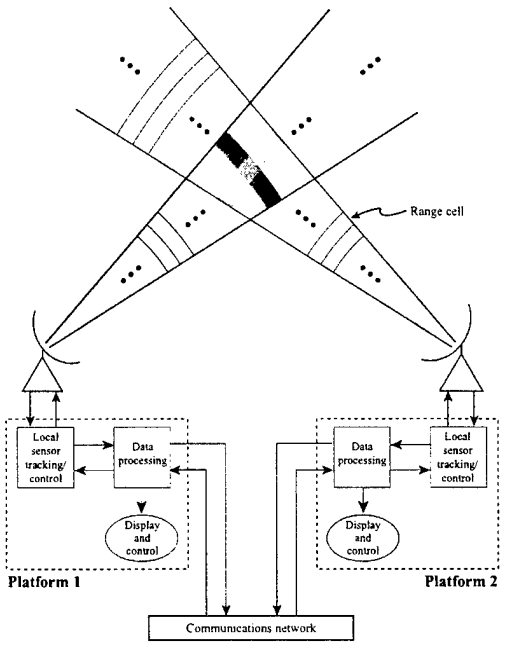

Figure 1: Illustration of network-centric tracking

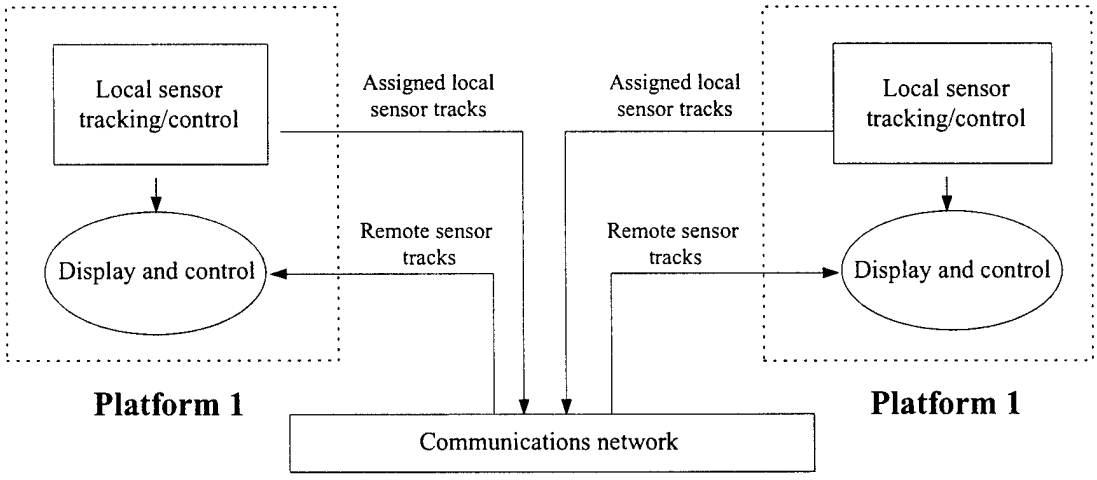

Figure 2: Assigned reporting responsibility

Architectures

Table 1: Assumptions for Hypothetical Network-Centric Tracking Systems

Max position = 500 km	Position LSB = 1m
Max velocity = 1,000 m/s	Velocity LSB = 0.1 m/s
Max range = 500 km	Range LSB = 1m
Range accuracy = 1 - 300m	
Max bearing = 360°	Bearing LSB = 0.05°
Max elevation = 90°	Elevation LSB = 0.05°
Bearing accuracy = 0.05 - 5°	Elevation accuracy = 0.05 - 5°
Max time = 86,400 s	Time LSB = 0.1 s
Max track number (N_{tracks})= 1,000	Track number LSB = 1
Number of platforms = 5	Tracking interval (I_{track}) = 5 s

Assigned Reporting Responsibility

Number of bits required to represent each quantity can be computed as follows:

$$n_{\text{pos}} \geq \log_2\left(\frac{\text{Max position}}{\text{Position LSB}}\right) \Rightarrow n_{\text{pos}} = 19 \text{ bits } + 1 \text{ sign bit} \quad (1)$$

$$n_{\text{vel}} \geq \log_2\left(\frac{\text{Max velocity}}{\text{Velocity LSB}}\right) \Rightarrow n_{\text{vel}} = 14 \text{ bits } + 1 \text{ sign bit} \quad (2)$$

$$n_{\text{time}} \geq \log_2\left(\frac{\text{Max time}}{\text{Time LSB}}\right) \Rightarrow n_{\text{time}} = 20 \text{ bits} \quad (3)$$

$$n_{\text{number}} \geq \log_2\left(\frac{\text{Max track number}}{\text{Track number LSB}}\right) \Rightarrow n_{\text{number}} = 10 \text{ bits} \quad (4)$$

Thus, 20 bits are necessary for each position quantity, 15 bits for each rate (velocity) quantity, 20 bits for the time quantity, and 10 bits for the track number. Thus, the total data rate required to support the hypothetical system is given by

$$R_{\text{DistRR}} = \frac{N_{\text{tracks}}}{I_{\text{track}}}\left(3n_{\text{pos}} + 3n_{\text{vel}} + n_{\text{time}} + n_{\text{number}}\right) \quad (5)$$

which results in a data rate requirement of 27 kbps.

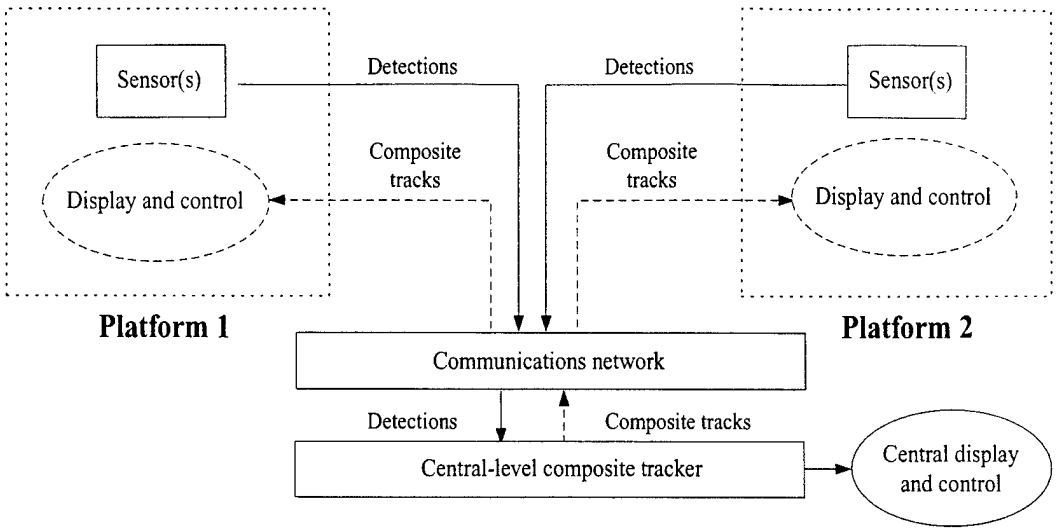

Figure 3: Central-level composite tracking: pure

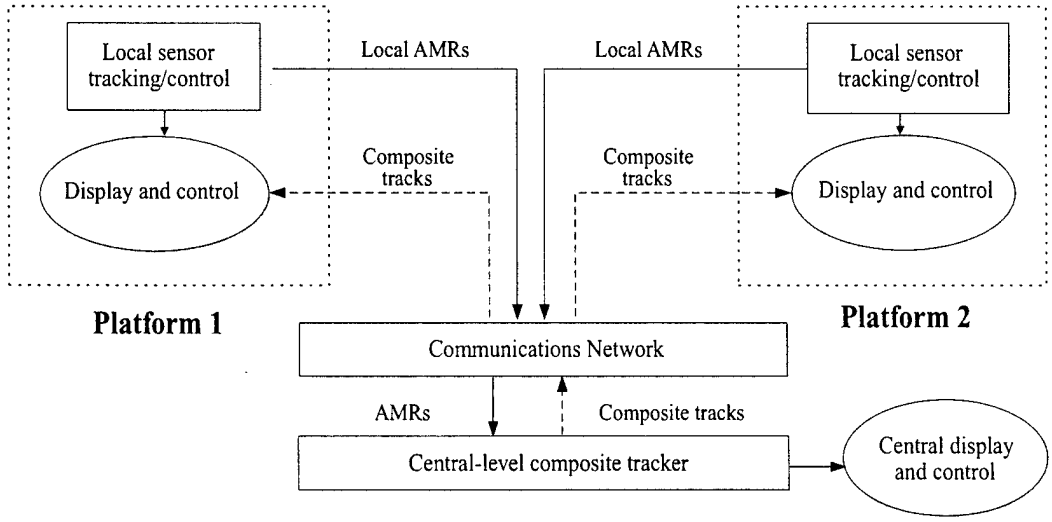

Figure 4: Central-level composite tracking: practical

Central-level Composite Tracking: Practical

Data rate required to pass just the measurements and associated accuracies with a valid time tag is computed with

$$n_{\text{range}} = 19 \text{ bits} \qquad n_{\text{r\_acc}} = 9 \text{ bits} \tag{6}$$

$$n_{\text{bearing}} = 13 \text{ bits} \qquad n_{\text{b\_acc}} = 7 \text{ bits} \tag{7}$$

$$n_{\text{elevation}} = 12 \text{ bits} \quad \text{(including a sign bit)} \tag{8}$$

$$n_{\text{e\_acc}} = 7 \text{ bits} \qquad n_{\text{time}} = 20 \text{ bits} \tag{9}$$

For this approach, the data rate required to pass all measurements from legitimate target returns is given by

$$n_{\text{meas}} = n_{\text{range}} + n_{\text{bearing}} + n_{\text{elevation}} \tag{10}$$

$$n_{\text{meas\_acc}} = n_{\text{r\_acc}} + n_{\text{b\_acc}} + n_{\text{e\_acc}} \tag{11}$$

$$R_{\text{practical central}} = \frac{N_{\text{platforms}} N_{\text{meas/scan}}}{I_{\text{track}}} \left(n_{\text{meas}} + n_{\text{meas\_acc}} + n_{\text{time}} \right) \tag{12}$$

To support the passing of AMRs associated with the maximum number of targets ($N_{\text{meas/scan}} = 1,000$), the data rate requirement is 17.4 kbps per platform and 87 kbps for the entire five-platform network.

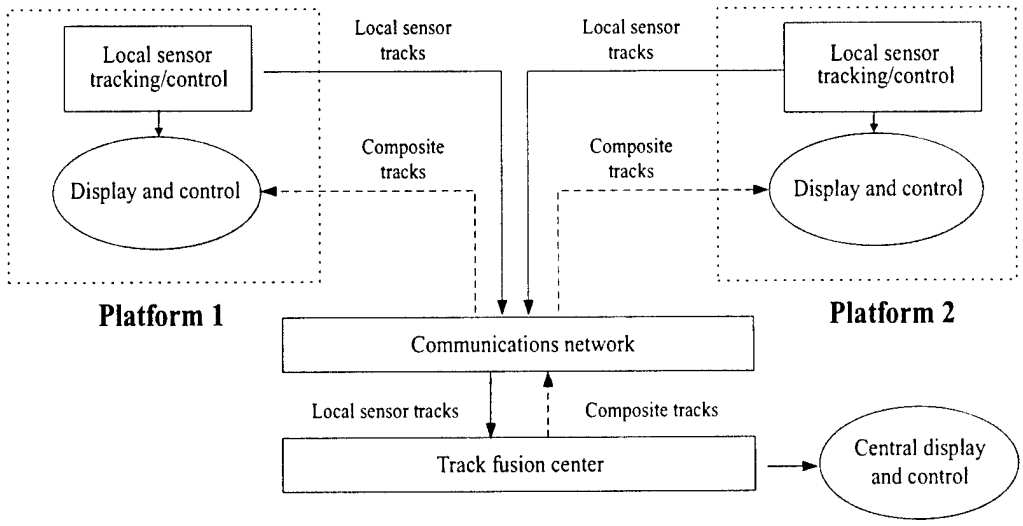

Figure 5: Distributed tracking with track fusion for composite tracking: central-level track fusion

Central-level Track Fusion

Continuing the example from above, with the added assumption that the elements of the covariance matrix will all be represented as 32-bit quantities, the data rate requirement can be estimated as

$$R_{\text{track fusion}} = \frac{N_{\text{platforms}} N_{\text{meas/scan}}}{I_{\text{track}}} \times \left(3n_{\text{pos}} + 3n_{\text{vel}} + n_{\text{number}} + n_{\text{time}} + 21n_{\text{acc}}\right) \quad (13)$$

where n_{acc} is the number of bits required to accurately represent the elements of the covariance matrix. The minimum data rate required to pass the track data is 161.4 kbps per platform or 807 kbps for the five-platform network.

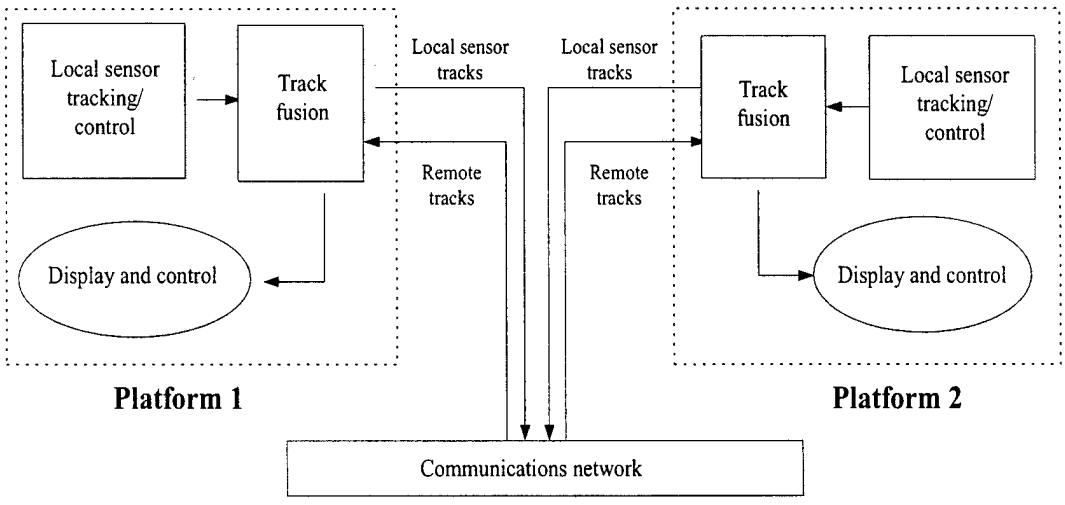

Figure 6: Distributed tracking with track fusion for composite tracking: distributed track fusion

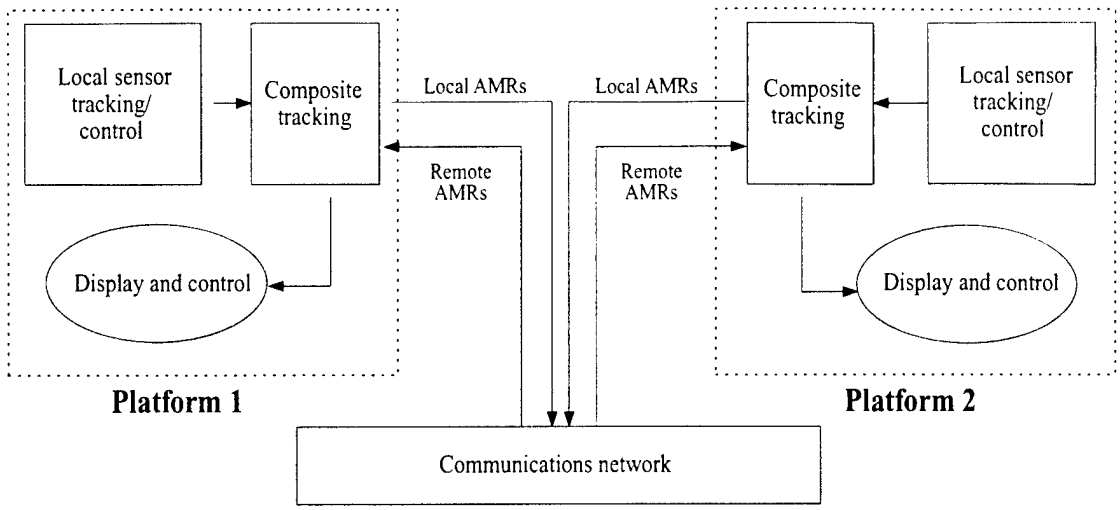

Figure 7: Distributed composite tracking

Distributed Composite Tracking

The data rate for passing measurement and accuracy data for the distributed composite tracking approach is given by

$$R_{\text{dist composite}} = \frac{N_{\text{platforms}} N_{\text{meas/scan}}}{I_{\text{track}}} \times \left(n_{\text{meas}} + n_{\text{meas\_acc}} + n_{\text{number}} + n_{\text{time}}\right) \quad (14)$$

Using the assumptions for the previous examples, the data rate for this approach is determined to be 19.4 kbps per unit or 97 kbps for the five-platform network.

Table 2: Data Rate Requirements for Hypothetical Network-Centric Tracking Systems

Architecture	AMR or state vector Update (bits)	Accuracy Update (bits)	Total rate Unit (kbps)	Total rate Network (kbps)
Reporting responsibility	135	NA	NA	27
Cent. tracking:				
Pure	–	–	–	–
Practical	64	23	17.4	87
Dist. tracking:				
Cent. Track Fusion	135	672	161.4	807
Dist. Track Fusion	135	672	161.4	807
Tracklets (4:1)	135	672	40.4	202
Composite Track	74	23	19.4	97

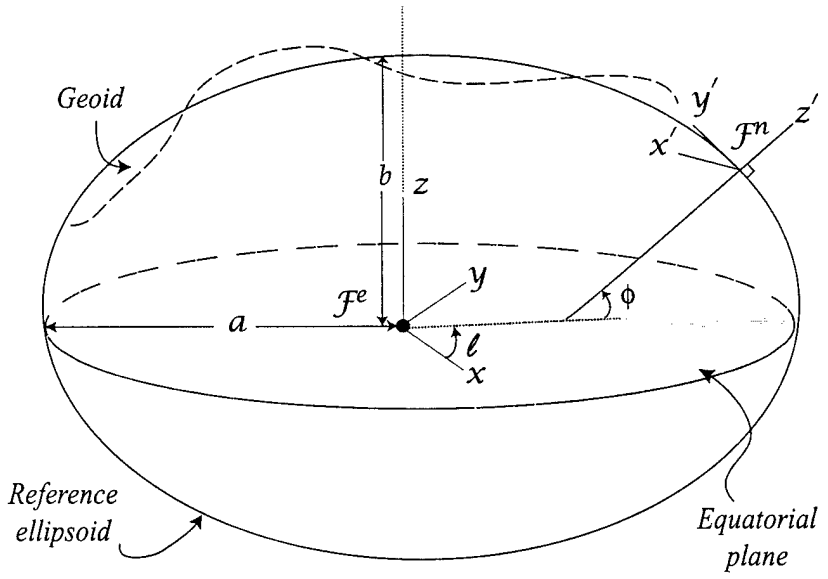

Figure 8: Earth-centered, Earth-fixed (ECEF) coordinate frame

Coordinate Systems

The defining parameters are the length of the semi-major axis, a, of the generating ellipse and, either the length of the semi-minor axis, b, the eccentricity, e, where

$$e^2 = \frac{a^2 - b^2}{a^2} \tag{15}$$

or the flattening

$$f = \frac{a - b}{a} \tag{16}$$

The ellipsoid is a very good fit to the geoid; the root-mean-square (RMS) deviation of the geoid from the ellipsoid is 30.5 m based on a 1° by 1° worldwide grid.

Coordinate Systems

Table 3: WGS-84 Parameters

Parameter	**Value**
semi-major axis (a)	6,378,137m
eccentricity (e)	0.08181919
flattening (f)	$\frac{1}{298.2572}$
Earth's rotation rate (ω_e)	7.292115×10^{-5} rad/s

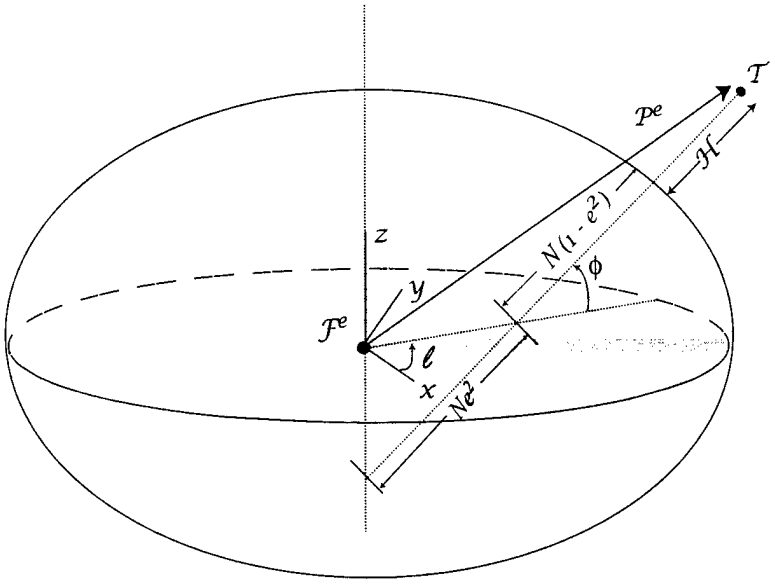

Figure 9: ECEF coordinates in terms of latitude, longitude, and altitude

Coordinate Systems

Position vector $\mathcal{P}^e$ to a point above Earth's surface can be specified in frame $\mathcal{F}^e$ as

$$\mathcal{P}^e = \begin{bmatrix} (N+\mathcal{H})\ \mathrm{c}\phi\ \mathrm{c}\ell \\ (N+\mathcal{H})\ \mathrm{c}\phi\ \mathrm{s}\ell \\ (N(1-e^2)+\mathcal{H})\ \mathrm{s}\phi \end{bmatrix} \tag{17}$$

where ϕ is the geodetic latitude, ℓ is the geodetic longitude, $\mathcal{H}$ is the geodetic height, N is the prime vertical radius of curvature (PVRC).

The PVRC is a function of the geodetic latitude and is calculated from

$$N = \frac{a}{\sqrt{1-e^2\ \mathrm{s}^2\phi}} \tag{18}$$

where a is the length of the semi-major axis of the WGS-84 generating ellipse and e the eccentricity.

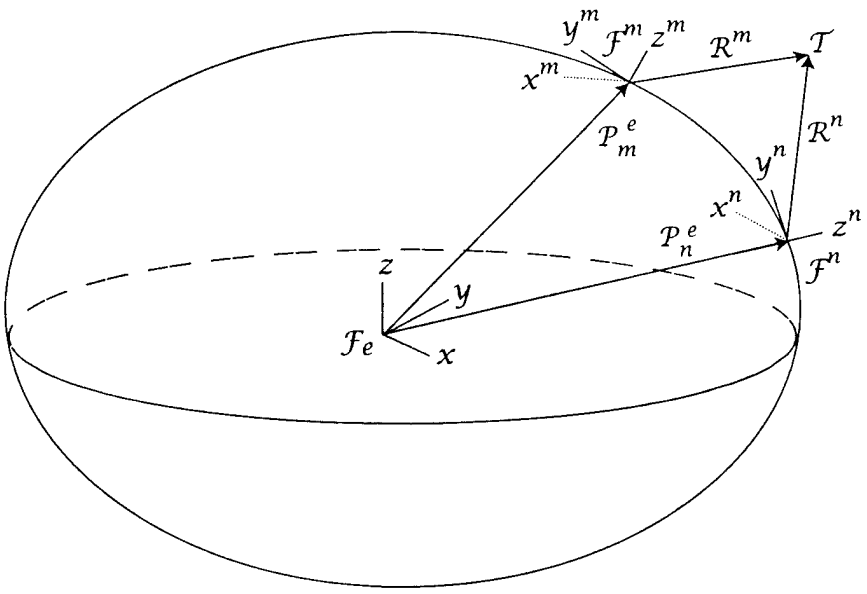

Figure 10: Two platforms in ECEF coordinates

Coordinate Systems

The composite rotation or direction cosine matrix from ECEF to frame m is given by

$$C^{m|e} = \begin{bmatrix} -\,\mathrm{s}\ell^m & \mathrm{c}\ell^m & 0 \\ -\,\mathrm{s}\phi^m\,\mathrm{c}\ell^m & -\,\mathrm{s}\phi^m\,\mathrm{s}\ell^m & \mathrm{c}\phi^m \\ \mathrm{c}\phi^m\,\mathrm{c}\ell^m & \mathrm{c}\phi^m\,\mathrm{s}\ell^m & \mathrm{s}\phi^m \end{bmatrix} \tag{19}$$

where ϕ^m and ℓ^m are the latitude and longitude of frame m.

The position of target $\mathcal{T}$ relative to platform n is denoted by position vector $\mathcal{R}^n$. The corresponding position vector from platform m is given by

$$\mathcal{R}^m = C^{m|n}\mathcal{R}^n + D^{m|n} \tag{20}$$

where

$$C^{m|n} = C^{m|e}C^{e|n} = C^{m|e}(C^{n|e})^{-1} = C^{m|e}(C^{n|e})^T \tag{21}$$

$$D^{m|n} = C^{m|e}(\mathcal{P}_n^e - \mathcal{P}_m^e) \tag{22}$$

Coordinate Systems

The elements of $C^{m|n}$ are given by

$$C^{m|n}(1,1) = \mathrm{c}\Delta\ell^{m|n} \quad (23)$$
$$C^{m|n}(1,2) = -\mathrm{s}\phi^n\ \mathrm{s}\Delta\ell^{m|n} \quad (24)$$
$$C^{m|n}(1,3) = \mathrm{c}\phi^n\ \mathrm{s}\Delta\ell^{m|n} \quad (25)$$
$$C^{m|n}(2,1) = \mathrm{s}\phi^m\ \mathrm{s}\Delta\ell^{m|n} \quad (26)$$
$$C^{m|n}(2,2) = \mathrm{s}\phi^m\ \mathrm{s}\phi^n\ \mathrm{c}\Delta\ell^{m|n} + \mathrm{c}\phi^m\ \mathrm{c}\phi^n \quad (27)$$
$$C^{m|n}(2,3) = -\mathrm{s}\phi^m\ \mathrm{c}\phi^n\ \mathrm{c}\Delta\ell^{m|n} + \mathrm{c}\phi^m\ \mathrm{s}\phi^n \quad (28)$$
$$C^{m|n}(3,1) = -\mathrm{c}\phi^n\ \mathrm{s}\Delta\ell^{m|n} \quad (29)$$
$$C^{m|n}(3,2) = -\mathrm{c}\phi^m\ \mathrm{s}\phi^n\ \mathrm{c}\Delta\ell^{m|n} + \mathrm{s}\phi^m\ \mathrm{c}\phi^n \quad (30)$$
$$C^{m|n}(3,3) = \mathrm{c}\phi^m\ \mathrm{c}\phi^n\ \mathrm{c}\Delta\ell^{m|n} + \mathrm{s}\phi^m\ \mathrm{s}\phi^n \quad (31)$$

where $\Delta\ell^{m|n} = \ell^n - \ell^m$.

Coordinate Systems

The elements of $D^{m|n}$ are given by

$$D^{m|n}(1) = (N^n + \mathcal{H}^n)\ \mathrm{c}\phi^n\ \mathrm{s}\Delta\ell^{m|n} \quad (32)$$
$$D^{m|n}(2) = -(N^n + \mathcal{H}^n)\ \mathrm{c}\phi^n\ \mathrm{s}\phi^m\ \mathrm{c}\Delta\ell^{m|n} + (N^n(1-e^2) + \mathcal{H}^n)\ \mathrm{c}\phi^m\ \mathrm{s}\phi^n + N^m e^2\ \mathrm{c}\phi^m\ \mathrm{s}\phi^m \quad (33)$$
$$D^{m|n}(3) = (N^n + \mathcal{H}^n)\ \mathrm{c}\phi^n\ \mathrm{c}\phi^m\ \mathrm{c}\Delta\ell^{m|n} - (N^m + \mathcal{H}^m) + (N^n(1-e^2) + \mathcal{H}^n)\ \mathrm{s}\phi^m\ \mathrm{s}\phi^n + N^m e^2(\mathrm{s}\phi^m)^2 \quad (34)$$

Coordinate Systems

The deck frame is colocated with the ship's ENU frame with the x-axis starboard, the y-axis forward, and the z-axis up. This sequence of plane rotations for roll, pitch, and heading for platform n denoted by θ_r^n, θ_p^n, and θ_h^n is given by

$$C^{\mathcal{D}n|n}(1,1) = \mathrm{c}\theta_r^n\,\mathrm{c}\theta_h^n + \mathrm{s}\theta_r^n\,\mathrm{s}\theta_p^n\,\mathrm{s}\theta_h^n \quad (35)$$

$$C^{\mathcal{D}n|n}(1,2) = -\mathrm{c}\theta_r^n\,\mathrm{s}\theta_h^n + \mathrm{s}\theta_r^n\,\mathrm{s}\theta_p^n\,\mathrm{c}\theta_h^n \quad (36)$$

$$C^{\mathcal{D}n|n}(1,3) = \mathrm{s}\theta_r^n\,\mathrm{c}\theta_p^n \quad (37)$$

$$C^{\mathcal{D}n|n}(2,1) = \mathrm{c}\theta_p^n\,\mathrm{s}\theta_h^n \quad (38)$$

$$C^{\mathcal{D}n|n}(2,2) = \mathrm{c}\theta_p^n\,\mathrm{c}\theta_h^n \quad (39)$$

$$C^{\mathcal{D}n|n}(2,3) = -\mathrm{s}\theta_p^n \quad (40)$$

$$C^{\mathcal{D}n|n}(3,1) = -\mathrm{s}\theta_r^n\,\mathrm{c}\theta_h^n + \mathrm{c}\theta_r^n\,\mathrm{s}\theta_p^n\,\mathrm{s}\theta_h^n \quad (41)$$

$$C^{\mathcal{D}n|n}(2,3) = \mathrm{s}\theta_r^n\,\mathrm{s}\theta_h^n + \mathrm{c}\theta_r^n\,\mathrm{s}\theta_p^n\,\mathrm{c}\theta_h^n \quad (42)$$

$$C^{\mathcal{D}n|n}(3,3) = \mathrm{c}\theta_r^n\,\mathrm{c}\theta_p^n \quad (43)$$

Coordinate Systems

For two platforms with positions $\mathcal{P}_n^e$ and $\mathcal{P}_m^e$ relative to $\mathcal{F}^e$ and reference coordinate frames $\mathcal{F}^n$ and $\mathcal{F}^m$, respectively, the position of target $\mathcal{T}$ relative to platform n is denoted by position vector $\mathcal{R}^n$ and the corresponding position vector from platform m is given in deck coordinates by

$$\mathcal{R}^{\mathcal{D}m} = C^{\mathcal{D}m|m}\mathcal{R}^m = C^{\mathcal{D}m|n}\mathcal{R}^n + D^{\mathcal{D}m|n} \quad (44)$$

where

$$C^{\mathcal{D}m|n} = C^{\mathcal{D}m|m}C^{m|n} \quad (45)$$

$$D^{\mathcal{D}m|n} = C^{\mathcal{D}m|m}D^{m|n} \quad (46)$$

Coordinate Systems

For two platforms with positions $\mathcal{P}_n^e$ and $\mathcal{P}_m^e$ relative to $\mathcal{F}^e$ and reference coordinate frames $\mathcal{F}^n$ and $\mathcal{F}^m$, respectively, the position of target $\mathcal{T}$ relative to platform n is denoted by position vector $\mathcal{R}^n$ and the corresponding position vector from platform m is given in deck coordinates by

$$\mathcal{R}^{\mathcal{D}m} = C^{\mathcal{D}m|m}\mathcal{R}^m = C^{\mathcal{D}m|n}\mathcal{R}^n + D^{\mathcal{D}m|n} \tag{47}$$

where

$$C^{\mathcal{D}m|n} = C^{\mathcal{D}m|m}C^{m|n} \tag{48}$$

$$D^{\mathcal{D}m|n} = C^{\mathcal{D}m|m}D^{m|n} \tag{49}$$

Coordinate Systems

The Cartesian coordinates of a position vector in $\mathcal{F}^m$ are given in terms of the spherical coordinates by

$$\mathcal{R}^m = \begin{bmatrix} x^m \\ y^m \\ z^m \end{bmatrix} = \begin{bmatrix} r^m \cos e^m \sin b^m \\ r^m \cos e^m \cos b^m \\ r^m \sin e^m \end{bmatrix} \tag{50}$$

Because the deck frame is colocated with the local geographic frame, the sensors may measure the range $r^{\mathcal{D}n}$, bearing $b^{\mathcal{D}n}$ and elevation $e^{\mathcal{D}n}$ in deck coordinates.

Coordinate Systems

From (50), the spherical coordinates are given in terms of the Cartesian coordinates by

$$r^m = \sqrt{(x^m)^2 + (y^m)^2 + (z^m)^2} \tag{51}$$

$$b^m = \begin{cases} \tan^{-1}\left(\frac{x^m}{y^m}\right), & |y^m| > |x^m| \\ \frac{\pi}{2} - \tan^{-1}\left(\frac{y^m}{x^m}\right), & |x^m| > |y^m| \end{cases} \tag{52}$$

$$e^m = \begin{cases} \tan^{-1}\left(\frac{z^m}{\sqrt{(x^m)^2 + (y^m)^2}}\right), & |\sqrt{(x^m)^2 + (y^m)^2}| > |z^m| \\ \frac{\pi}{2} - \tan^{-1}\left(\frac{\sqrt{(x^m)^2 + (y^m)^2}}{z^m}\right), & |z^m| > |\sqrt{(x^m)^2 + (y^m)^2}| \end{cases} \tag{53}$$

The radial velocity or range rate is given by

$$\dot{r}^m = \frac{x^m \dot{x}^m + y^m \dot{y}^m + z^m \dot{z}^m}{\sqrt{(x^m)^2 + (y^m)^2 + (z^m)^2}} \tag{54}$$

Target Motion Model

The dynamical equation that is commonly used to represent the motion of the target relative to the platform is given by

$$X_{k+1} = F_k X_k + V_k \tag{55}$$

where

$$\begin{aligned} X_k &= \text{target state vector at time } t_k \\ F_k &= \text{linear constraint on the target dynamics at time } t_k \\ V_k &= \text{white noise error in the state process with } V_k \sim \mathcal{N}(0, Q_k) \end{aligned} \tag{56}$$

The $N(\bar{x}, P)$ denotes the Gaussian distribution with mean $\bar{x}$ and covariance P.

Target Motion Model

The state vector for a nearly constant velocity motion model is given by

$$X_k = \begin{bmatrix} x_k & \dot{x}_k & y_k & \dot{y}_k & z_k & \dot{z}_k \end{bmatrix}^T \tag{57}$$

where (x_k, y_k, z_k) represents the position of the target in Cartesian coordinates at time t_k and $(\dot{x}_k, \dot{y}_k, \dot{z}_k)$ represents the velocity of the target. The dynamical constraint for nearly constant velocity motion is given by

$$F_k = \begin{bmatrix} A_k & 0_{2\times 2} & 0_{2\times 2} \\ 0_{2\times 2} & A_k & 0_{2\times 2} \\ 0_{2\times 2} & 0_{2\times 2} & A_k \end{bmatrix} \quad \text{where} \quad A_k = \begin{bmatrix} 1 & \delta_k \\ 0 & 1 \end{bmatrix} \tag{58}$$

$\delta_k = t_k - t_{k-1}$ denotes the sample period, t_k denotes the time of measurement k, and $0_{2\times 2}$ denotes a two-by-two matrix of zeros.

Target Motion Model

For the nearly constant velocity motion model, the process noise covariance matrix for discretized continuous-time, white acceleration errors is given by

$$Q_k = \begin{bmatrix} \tilde{q}^x C_k & 0_{2\times 2} & 0_{2\times 2} \\ 0_{2\times 2} & \tilde{q}^y C_k & 0_{2\times 2} \\ 0_{2\times 2} & 0_{2\times 2} & \tilde{q}^z C_k \end{bmatrix} \quad \text{where } C_k = \begin{bmatrix} \frac{\delta_k^3}{3} & \frac{\delta_k^2}{2} \\ \frac{\delta_k^2}{2} & \delta_k \end{bmatrix} \tag{59}$$

One approach for filter design is to set $\sqrt{\tilde{q}\delta_k}$ approximately equal to the maximum acceleration of the target under track.

EKF for Radar Measurements

The measurement equation is given by

$$Z_k = h(X_k) + W_k \tag{60}$$

where

$$\begin{aligned} Z_k &= \text{measurement vector at time } t_k \\ X_k &= \text{target state vector at time } t_k \\ W_k &= \text{white measurement error with } W_k \sim \mathcal{N}(0, R_k) \end{aligned} \tag{61}$$

EKF for Radar Measurements

$$Z_k = \begin{bmatrix} r_k \\ b_k \\ e_k \\ \dot{r}_k \end{bmatrix} = h(X_k) + W_k = \begin{bmatrix} h_r(X_k) \\ h_b(X_k) \\ h_e(X_k) \\ h_D(X_k) \end{bmatrix} + \begin{bmatrix} w_{rk} \\ w_{bk} \\ w_{ek} \\ w_{Dk} \end{bmatrix} \tag{62}$$

where

$$\begin{aligned} r_k &= \text{measured range at time } t_k \\ b_k &= \text{measured bearing at time } t_k \\ e_k &= \text{measured elevation at time } t_k \\ \dot{r}_k &= \text{Doppler-derived range rate at time } t_k \\ w_{rk} &= \text{error in range measurement with } w_{rk} \sim \mathcal{N}(0, \sigma_{rk}^2) \\ w_{bk} &= \text{error in bearing measurement with } w_{bk} \sim \mathcal{N}(0, \sigma_{bk}^2) \\ w_{ek} &= \text{error in elevation measurement with } w_{ek} \sim \mathcal{N}(0, \sigma_{ek}^2) \\ w_{Dk} &= \text{error in Doppler range rate measurement with } w_{Dk} \sim \mathcal{N}(0, \sigma_{Dk}^2) \end{aligned}$$

EKF for Radar Measurements

Also

$$h_r(X_k) = \sqrt{x_k^2 + y_k^2 + z_k^2} \tag{63}$$

$$h_b(X_k) = \begin{cases} \tan^{-1}\left(\frac{x_k}{y_k}\right), & |y_k| > |x_k| \\ \frac{\pi}{2} - \tan^{-1}\left(\frac{y_k}{x_k}\right), & |x_k| > |y_k| \end{cases} \tag{64}$$

$$h_e(X_k) = \begin{cases} \tan^{-1}\left(\frac{z_k}{\sqrt{x_k^2 + y_k^2}}\right), & |\sqrt{x_k^2 + y_k^2}| > |z_k| \\ \frac{\pi}{2} - \tan^{-1}\left(\frac{\sqrt{x_k^2 + y_k^2}}{z_k}\right), & |z_k| > |\sqrt{x_k^2 + y_k^2}| \end{cases} \tag{65}$$

$$h_D(X_k) = \frac{x_k\dot{x}_k + y_k\dot{y}_k + z_k\dot{z}_k}{\sqrt{x_k^2 + y_k^2 + z_k^2}} \tag{66}$$

EKF for Radar Measurements

The EKF for the target state estimation with nonlinear measurements is given by

State prediction:

$$X_{k|k-1} = F_{k-1}X_{k-1|k-1} \tag{67}$$

$$P_{k|k-1} = F_{k-1}P_{k-1|k-1}F_{k-1}^T + Q_{k-1} \tag{68}$$

State update with the measurement:

$$X_{k|k} = X_{k|k-1} + K_k\widetilde{Z}_k \tag{69}$$

$$P_{k|k} = [I - K_kH_k]P_{k|k-1} \tag{70}$$

$$\widetilde{Z}_k = Z_k - h(X_{k|k-1}) \tag{71}$$

$$K_k = P_{k|k-1}H_k^TS_k^{-1} \tag{72}$$

$$S_k = H_kP_{k|k-1}H_k^T + R_k \tag{73}$$

EKF for Radar Measurements

$X_{k|j}$ = state estimate at time t_k given measurements through t_j

$\tilde{Z}_k$ = filter residuals at time t_k

$P_{k|j}$ = error covariance at time t_k given measurements through t_j

$$H_k = \left[\begin{array}{c} \frac{\partial h_r(X_k)}{\partial X_k} \\ \frac{\partial h_b(X_k)}{\partial X_k} \\ \frac{\partial h_e(X_k)}{\partial X_k} \\ \frac{\partial h_D(X_k)}{\partial X_k} \end{array} \right]_{X_k = X_{k|k-1}} = \left[\begin{array}{c} H_{rk} \\ H_{bk} \\ H_{ek} \\ H_{Dk} \end{array} \right] \tag{74}$$

EKF for Radar Measurements

For

$$X_{k|k-1} = \left[\begin{array}{cccccc} x_{k|k-1} & \dot{x}_{k|k-1} & y_{k|k-1} & \dot{y}_{k|k-1} & z_{k|k-1} & \dot{z}_{k|k-1} \end{array} \right]^T \tag{75}$$

the rows of H_k are given by

$$H_{rk} = \left[\begin{array}{cccccc} \frac{x_{k|k-1}}{r_{k|k-1}} & 0 & \frac{y_{k|k-1}}{r_{k|k-1}} & 0 & \frac{z_{k|k-1}}{r_{k|k-1}} & 0 \end{array} \right] \tag{76}$$

$$H_{bk} = \left[\begin{array}{cccccc} \frac{y_{k|k-1}}{rh^2_{k|k-1}} & 0 & -\frac{x_{k|k-1}}{rh^2_{k|k-1}} & 0 & 0 & 0 \end{array} \right] \tag{77}$$

$$H_{ek} = \left[\begin{array}{cccccc} -\frac{x_{k|k-1}z_{k|k-1}}{r^2_{k|k-1}rh_{k|k-1}} & 0 & -\frac{y_{k|k-1}z_{k|k-1}}{r^2_{k|k-1}rh_{k|k-1}} & 0 & \frac{rh_{k|k-1}}{r^2_{k|k-1}} & 0 \end{array} \right] \tag{78}$$

$$H_{Dk} = \left[\begin{array}{cccccc} H_{Dk}(1) & \frac{x_{k|k-1}}{r_{k|k-1}} & H_{Dk}(3) & \frac{y_{k|k-1}}{r_{k|k-1}} & H_{Dk}(5) & \frac{z_{k|k-1}}{r_{k|k-1}} \end{array} \right] \tag{79}$$

EKF for Radar Measurements

$$H_{Dk}(1) = \frac{(y^2_{k|k-1} + z^2_{k|k-1})\dot{x}_{k|k-1} - (y_{k|k-1}\dot{y}_{k|k-1} + z_{k|k-1}\dot{z}_{k|k-1})x_{k|k-1}}{r^3_{k|k-1}} \tag{80}$$

$$H_{Dk}(3) = \frac{(x^2_{k|k-1} + z^2_{k|k-1})\dot{y}_{k|k-1} - (x_{k|k-1}\dot{x}_{k|k-1} + z_{k|k-1}\dot{z}_{k|k-1})y_{k|k-1}}{r^3_{k|k-1}} \tag{81}$$

$$H_{Dk}(5) = \frac{rh^2_{k|k-1}\dot{z}_{k|k-1} - (x_{k|k-1}\dot{x}_{k|k-1} + y_{k|k-1}\dot{y}_{k|k-1})z_{k|k-1}}{r^3_{k|k-1}} \tag{82}$$

$$r_{k|k-1} = \sqrt{x^2_{k|k-1} + y^2_{k|k-1} + z^2_{k|k-1}} \tag{83}$$

$$rh_{k|k-1} = \sqrt{x^2_{k|k-1} + y^2_{k|k-1}} \tag{84}$$

EKF for Radar Measurements

The covariance of the measurement errors in the platform reference frame is given by

$$\text{COV}\begin{bmatrix} w_{rk} \\ w_{bk} \\ w_{ek} \end{bmatrix} = \begin{bmatrix} H_{rk} \\ H_{bk} \\ H_{ek} \end{bmatrix} M_k^T Q E_k^{\mathcal{S}} \begin{bmatrix} \bar{\sigma}^2_{rk} & 0 & 0 \\ 0 & \bar{\sigma}^2_{bk} & 0 \\ 0 & 0 & \bar{\sigma}^2_{ek} \end{bmatrix} Q E_k^{\mathcal{S}})^T M_k \begin{bmatrix} H_{rk}^T & H_{bk}^T & H_{ek}^T \end{bmatrix} \tag{85}$$

where $\bar{\sigma}^2_{rk}$, $\bar{\sigma}^2_{bk}$ and $\bar{\sigma}^2_{ek}$ are the variances of the measurements in the sensor reference frame and

$$E_k^{\mathcal{S}} = E_k\Big|_{X_{k|k-1}=M_k X_{k|k-1}+L_k} \quad \text{with} \quad E_k = \begin{bmatrix} \frac{x_{k|k-1}}{r_{k|k-1}} & y_{k|k-1} & -\frac{x_{k|k-1}z_{k|k-1}}{rh_{k|k-1}} \\ \frac{y_{k|k-1}}{r_{k|k-1}} & -x_{k|k-1} & -\frac{y_{k|k-1}z_{k|k-1}}{rh_{k|k-1}} \\ \frac{z_{k|k-1}}{r_{k|k-1}} & 0 & rh_{k|k-1} \end{bmatrix} \tag{86}$$

$$Q^T = \begin{bmatrix} 1 & 0 & 0 & 0 & 0 & 0 \\ 0 & 0 & 1 & 0 & 0 & 0 \\ 0 & 0 & 0 & 0 & 1 & 0 \end{bmatrix} \tag{87}$$

EKF for Radar Measurements

When considering the measurements in the u-plane and the v-plane,

$$Z_k = \begin{bmatrix} h_r(X_k) \\ h_U(X_k) \\ h_V(X_k) \\ h_D(X_k) \end{bmatrix} + \begin{bmatrix} w_{rk} \\ w_{Uk} \\ w_{Vk} \\ w_{Dk} \end{bmatrix} \tag{88}$$

where

u_k = measured sine of the angle of the target in the u-plane at time t_k

v_k = measured sine of the angle of the target in the v-plane at time t_k

w_{uk} = error in the u_k measurement with $w_{uk} \sim \mathcal{N}(0, \sigma_{uk}^2)$

w_{vk} = error in the v_k measurement with $w_{vk} \sim \mathcal{N}(0, \sigma_{vk}^2)$

$$h_u(X_k) = \frac{x_k}{\sqrt{x_k^2 + y_k^2 + z_k^2}} \tag{89}$$

$$h_v(X_k) = \frac{y_k}{\sqrt{x_k^2 + y_k^2 + z_k^2}} \tag{90}$$

EKF for Radar Measurements

Covariance of the measurement errors in the platform reference frame is given by

$$\text{COV}\begin{bmatrix} w_{rk} \\ w_{bk} \\ w_{ek} \end{bmatrix} = \begin{bmatrix} H_{rk} \\ H_{bk} \\ H_{ek} \end{bmatrix} M_k^T Q U_k^S \begin{bmatrix} \bar{\sigma}_{rk}^2 & 0 & 0 \\ 0 & \sigma_{uk}^2 & 0 \\ 0 & 0 & \sigma_{vk}^2 \end{bmatrix} \times (QU_k^S)^T M_k \begin{bmatrix} H_{rk}^T & H_{bk}^T & H_{ek}^T \end{bmatrix} \tag{91}$$

where $\bar{\sigma}_{rk}^2$, σ_{uk}^2 and σ_{vk}^2 are variances of the measurements in the antenna aperture and

$$U_k^S = U_k\Big|_{X_{k|k-1} = M_k X_{k|k-1} + L_k} \tag{92}$$

$$U_k = \begin{bmatrix} \frac{x_{k|k-1}}{r_{k|k-1}} & r_{k|k-1} & 0 \\ \frac{y_{k|k-1}}{r_{k|k-1}} & 0 & r_{k|k-1} \\ \frac{z_{k|k-1}}{r_{k|k-1}} & -\frac{x_{k|k-1}}{z_{k|k-1}} r_{k|k-1} & -\frac{y_{k|k-1}}{z_{k|k-1}} r_{k|k-1} \end{bmatrix} \tag{93}$$

Processing Local Measurements

For local measurements on platform m, the dynamical motion and measurement equations are given by

$$X_k^m = M_{k|k-1}^{m|m} F_{k-1}^m X_{k-1}^m + L_{k|k-1}^{m|m} + V_{k-1}^m \quad (94)$$

$$Z_k^m = h^m(X_k^m + M_{k|k}^{m|\mathcal{D}m} L_{k|k}^{\mathcal{S}m|\mathcal{D}m}) + B_k^m + W_k^m \quad (95)$$

where

X_k^m = target state vector in ENU on platform m at time t_k

Z_k^m = measurement vector at time t_k on platform m

F_k^m = constraint on target dynamics at time t_k on platform m

$M_{k|k-1}^{m|m}$ = rotational from ENU on platform m at t_{k-1} to ENU on platform m at time t_k

$M_{k|k}^{m|\mathcal{D}m}$ = rotation from deck coordinates of platform m at $t_k$to ENU on platform m at t_k

$L_{k|k}^{m|m}$ = translation from ENU on platform m at time t_{k-1} to ENU on platform m at time t_k

$L_{k|k}^{\mathcal{S}m|\mathcal{D}m}$ = translation in deck coordinates from ENU on platform m at $t_k$to the sensor frame on platform m at t_k

V_{k-1}^m = error in the state process for platform m with $V_{k-1}^m \sim \mathcal{N}(0, Q_{k-1}^m)$

Processing Local Measurements

W_k^m = measurement errors for platform m with $W_k^m \sim \mathcal{N}(0, R_k^m)$

B_k^m = residual sensor bias for platform m with $B_k^m \sim \mathcal{N}(0, R_k^{Bm})$

Processing Local Measurements

$$M_{k|k-1}^{m|m} = P^T \begin{bmatrix} C_{k|k-1}^{m|m} & 0_{3\times 3} \\ 0_{3\times 3} & C_{k|k-1}^{m|m} \end{bmatrix} P \tag{96}$$

where $C_{k|j}^{m|n}$ denotes the rotation of (21) from ENU on platform n at time t_j to ENU on platform m at time t_k, and

$$P = \begin{bmatrix} 1 & 0 & 0 & 0 & 0 & 0 \\ 0 & 0 & 1 & 0 & 0 & 0 \\ 0 & 0 & 0 & 0 & 1 & 0 \\ 0 & 1 & 0 & 0 & 0 & 0 \\ 0 & 0 & 0 & 1 & 0 & 0 \\ 0 & 0 & 0 & 0 & 0 & 1 \end{bmatrix} \qquad L_{k|k-1}^{m|m} = \begin{bmatrix} D_{k|k-1}^{m|m}(1) \\ 0 \\ D_{k|k-1}^{m|m}(2) \\ 0 \\ D_{k|k-1}^{m|m}(3) \\ 0 \end{bmatrix} \tag{97}$$

where $D_{k|j}^{m|n}$ denotes the translation of (22) from ENU on platform n at time t_j to ENU on platform m at time t_k.

Processing Local Measurements

EKF for the target state estimation on platform m with nonlinear local measurements is given by

State prediction:

$$X_{k|k-1}^m = M_{k|k-1}^{m|m} F_{k-1}^m X_{k-1|k-1}^m + L_{k|k-1}^{m|m} \tag{98}$$

$$P_{k|k-1}^m = M_{k|k-1}^{m|m} F_{k-1}^m P_{k-1|k-1}^m (M_{k|k-1}^{m|m} F_{k-1}^m)^T + Q_{k-1}^m \tag{99}$$

State update with the measurement:

$$X_{k|k}^m = X_{k|k-1}^m + K_k^m \tilde{Z}_k^m \tag{100}$$

$$\tilde{Z}_k^m = Z_k^m - h^m(X_{k|k-1}^m + M_{k|k}^{m|\mathcal{D}m} L_{k|k}^{\mathcal{S}m|\mathcal{D}m}) \tag{101}$$

$$P_{k|k}^m = [I - K_k^m H_k^m] P_{k|k-1}^m \tag{102}$$

$$K_k^m = P_{k|k-1}^m (H_k^m)^T [S_k^m]^{-1} \tag{103}$$

$$S_k^m = H_k^m P_{k|k-1}^m (H_k^m)^T + R_k^{Bm} + R_k^m \tag{104}$$

$$\tilde{Z}_k^m = \text{filter residuals on platform } m \text{ at } t_k$$

$$H_k^m = \left. \frac{\partial h^m(X_k)}{\partial X_k} \right|_{X_k = X_{k|k-1}^m + M_{k|k}^{m|\mathcal{D}m} L_{k|k}^{\mathcal{S}m|\mathcal{D}m}} \tag{105}$$

Processing Local Measurements in Deck Frame

For local measurements in deck coordinates on platform m, the measurement equation becomes

$$Z_k^{\mathcal{D}m} = h^m(M_{k|k}^{\mathcal{D}m|m} X_k^m + L_{k|k}^{\mathcal{S}m|\mathcal{D}m}) + B_k^m + W_k^m \tag{106}$$

where

$M_{k|k}^{\mathcal{D}m|m}$ = rotational from ENU on platform m at t_k to deck coordinates on platform m at t_k

For processing the measurements in deck coordinates, the measurement update is given by

$$X_{k|k}^m = X_{k|k-1}^m + K_k^{\mathcal{D}m} \tilde{Z}_k^{\mathcal{D}m} \tag{107}$$

$$\tilde{Z}_k^{\mathcal{D}m} = Z_k^{\mathcal{D}m} - h^m(M_{k|k}^{\mathcal{D}m|m} X_{k|k-1}^m + L_{k|k}^{\mathcal{S}m|\mathcal{D}m}) \tag{108}$$

$$P_{k|k}^m = [I - K_k^{\mathcal{D}m} H_k^{\mathcal{D}m|m} M_{k|k}^{\mathcal{D}m|m}] P_{k|k-1}^m \tag{109}$$

$$K_k^{\mathcal{D}m} = P_{k|k-1}^m (H_k^{\mathcal{D}m|m} M_{k|k}^{\mathcal{D}m|m})^T [S_k^{\mathcal{D}m|m}]^{-1} \tag{110}$$

$$S_k^{\mathcal{D}m|m} = H_k^{\mathcal{D}m|m} M_{k|k}^{\mathcal{D}m|m} P_{k|k-1}^m (H_k^{\mathcal{D}m|m} M_{k|k}^{\mathcal{D}m|m})^T + R_k^{Bm} + R_k^m \tag{111}$$

where

$$H_k^{\mathcal{D}m|m} = \left. \frac{\partial h^m(X_k)}{\partial X_k} \right|_{X_k = M_{k|k}^{\mathcal{D}m|m} X_{k|k-1}^m + L_{k|k}^{\mathcal{S}m|\mathcal{D}m}} \tag{112}$$

Processing Local Measurements

The covariance of the measurement errors in ENU for platform m is given by

$$\mathrm{COV} \begin{bmatrix} w_{rk}^m \\ w_{bk}^m \\ w_{ek}^m \end{bmatrix} = \begin{bmatrix} H_{rk}^m \\ H_{bk}^m \\ H_{ek}^m \end{bmatrix} (M_{k|k}^{\mathcal{S}m|m})^T Q E_k^{\mathcal{S}m|m} \begin{bmatrix} \bar{\sigma}_{rk}^2 & 0 & 0 \\ 0 & \bar{\sigma}_{bk}^2 & 0 \\ 0 & 0 & \bar{\sigma}_{ek}^2 \end{bmatrix}$$
$$\times (Q E_k^{\mathcal{S}m|m})^T M_{k|k}^{\mathcal{S}m|m} \begin{bmatrix} (H_{rk}^m)^T & (H_{bk}^m)^T & (H_{ek}^m)^T \end{bmatrix} \tag{113}$$

where $\bar{\sigma}_{rk}^2$, $\bar{\sigma}_{bk}^2$, and $\bar{\sigma}_{ek}^2$ are variances of the measurements in the sensor reference frame and

$$E_k^{\mathcal{S}m|m} = \left. E_k \right|_{X_{k|k-1} = M_{k|k}^{\mathcal{S}m|m} X_{k|k-1}^m + L_{k|k}^{\mathcal{S}m|\mathcal{D}m}} \tag{114}$$

with E_k defined by (86) and Q defined by (87).

Processing Local Measurements

For angular measurements in terms of u and v as in (88), the measurement covariance matrix for range, bearing, and elevation in ENU is given by

$$\text{COV}\begin{bmatrix} w_{rk}^m \\ w_{bk}^m \\ w_{ek}^m \end{bmatrix} = \begin{bmatrix} H_{rk}^m \\ H_{bk}^m \\ H_{ek}^m \end{bmatrix} (M_{k|k}^{\mathcal{S}m|m})^T Q U_k^{\mathcal{S}m|m} \begin{bmatrix} \bar{\sigma}_{rk}^2 & 0 & 0 \\ 0 & \sigma_{uk}^2 & 0 \\ 0 & 0 & \sigma_{vk}^2 \end{bmatrix}$$
$$\times (QU_k^{\mathcal{S}m|m})^T M_{k|k}^{\mathcal{S}m|m} \begin{bmatrix} (H_{rk}^m)^T & (H_{bk}^m)^T & (H_{ek}^m)^T \end{bmatrix} \tag{115}$$

where $\bar{\sigma}_{rk}^2$, σ_{uk}^2, and σ_{vk}^2 are variances of the measurements in the sensor reference frame and

$$U_k^{\mathcal{S}m|m} = U_k\Big|_{X_{k|k-1}=M_{k|k}^{\mathcal{S}m|m} X_{k|k-1}^m + L_{k|k}^{\mathcal{S}m|\mathcal{D}m}} \tag{116}$$

with U_k defined by (93)

Processing Remote Measurements

For processing remote measurements from ENU on platform n in ENU on platform m, the dynamical motion and measurement equations are given by

$$X_k^m = M_{k|k-1}^{m|m} F_{k-1}^m X_{k-1}^m + L_{k|k-1}^{m|m} + V_{k-1}^m \tag{117}$$

$$Z_k^n = h^n[M_{k|k}^{n|m} X_k^m + L_{k|k}^{n|m} + M_{k|k}^{n|\mathcal{D}n} L_{k|k}^{\mathcal{S}n|\mathcal{D}n}] + G_k^{n|m} + B_k^n + W_k^n \tag{118}$$

where

$G_k^{n|m}$ = residual gridlock bias for ENU on platform n relative to ENU on platform m with $G_k^{n|m} \sim \mathcal{N}(0, R_k^{Gn|m})$

The exact form of $G_k^{n|m}$ and $R_k^{Gn|m}$ depends on the method of gridlock (e.g., relative or absolute).

Processing Remote Measurements

EKF for target state estimation in ENU on platform m with with nonlinear remote measurements in ENU on platform n is given by

State prediction:

$$X^m_{k|k-1} = M^{m|m}_{k|k-1} F^m_{k-1} X^m_{k-1|k-1} + L^{m|m}_{k|k-1} \tag{119}$$

$$P^m_{k|k-1} = M^{m|m}_{k|k-1} F^m_{k-1} P^m_{k-1|k-1} (M^{m|m}_{k|k-1} F^m_{k-1})^T + Q^m_{k-1} \tag{120}$$

State update with the measurement:

$$X^m_{k|k} = X^m_{k|k-1} + K^{n|m}_k \widetilde{Z}^{n|m}_k \tag{121}$$

$$\widetilde{Z}^{n|m}_k = Z^n_k - h^n(M^{n|m}_{k|k} X^m_{k|k-1} + L^{n|m}_{k|k} + M^{n|\mathcal{D}n}_{k|k} L^{\mathcal{S}n|\mathcal{D}n}_{k|k}) \tag{122}$$

$$P^m_{k|k} = [I - K^{n|m}_k H^{n|m}_k M^{n|m}_{k|k}] P^m_{k|k-1} \tag{123}$$

$$K^{n|m}_k = P^m_{k|k-1} (H^{n|m}_k M^{n|m}_{k|k})^T [S^{n|m}_k]^{-1} \tag{124}$$

$$S^{n|m}_k = H^{n|m}_k M^{n|m}_{k|k} P^m_{k|k-1} (H^{n|m}_k M^{n|m}_{k|k})^T + R^{Bn}_k + R^{Gn|m}_k + R^n_k \tag{125}$$

$$H^{n|m}_k = \left. \frac{\partial h^n(X_k)}{\partial X_k} \right|_{X_k = M^{n|m}_{k|k} X^m_{k|k-1} + L^{n|m}_{k|k} + M^{n|\mathcal{D}n}_{k|k} L^{\mathcal{S}n|\mathcal{D}n}_{k|k}} \tag{126}$$

Processing Remote Measurements in Deck Frame

For remote measurements in deck coordinates on platform n, the measurement equation becomes

$$Z^{\mathcal{D}n}_k = h^n(M^{\mathcal{D}n|m}_{k|k} X^m_k + M^{\mathcal{D}n|n}_{k|k} L^{n|m}_{k|k} + L^{\mathcal{S}n|\mathcal{D}n}_{k|k}) + B^n_k + M^{\mathcal{D}n|n}_{k|k} G^{n|m}_k + W^n_k \tag{127}$$

$$M^{\mathcal{D}n|m}_{k|k} = M^{\mathcal{D}n|n}_{k|k} M^{n|m}_{k|k} \tag{128}$$

For processing measurements in deck coordinates on platform n, the measurement update is given by

$$X^m_{k|k} = X^m_{k|k-1} + K^{\mathcal{D}n|m}_k \widetilde{Z}^{\mathcal{D}n|m}_k \tag{129}$$

$$\widetilde{Z}^{\mathcal{D}n|m}_k = Z^{\mathcal{D}n}_k - h^n(M^{\mathcal{D}n|m}_{k|k} X^m_{k|k-1} + M^{\mathcal{D}n|n}_{k|k} L^{n|m}_{k|k} + L^{\mathcal{S}n|\mathcal{D}n}_{k|k}) \tag{130}$$

$$P^m_{k|k} = [I - K^{\mathcal{D}n|m}_k H^{\mathcal{D}n|m}_k M^{\mathcal{D}n|m}_{k|k}] P^m_{k|k-1} \tag{131}$$

$$K^{\mathcal{D}n|m}_k = P^m_{k|k-1} (H^{\mathcal{D}n|m}_k M^{\mathcal{D}n|m}_{k|k})^T [S^{\mathcal{D}n|m}_k]^{-1} \tag{132}$$

$$S^{\mathcal{D}n|m}_k = H^{\mathcal{D}n|m}_k M^{\mathcal{D}n|m}_{k|k} P^m_{k|k-1} (H^{\mathcal{D}n|m}_k M^{\mathcal{D}n|m}_{k|k})^T + R^{Bn}_k M^{\mathcal{D}n|n}_{k|k} R^{Gn|m}_k (M^{\mathcal{D}n|n}_{k|k})^T + R^n_k \tag{133}$$

$$H^{\mathcal{D}n|m}_k = \left. \frac{\partial h^n(X_k)}{\partial X_k} \right|_{X_k = M^{\mathcal{D}n|m}_{k|k} X^m_{k|k-1} + M^{\mathcal{D}n|n}_{k|k} L^{n|m}_{k|k} + L^{\mathcal{S}n|\mathcal{D}n}_{k|k}} \tag{134}$$

Processing Time-Delayed, Out-of-Sequence Measurements

Processing the time-delayed, out-of-sequence measurement Z_{k-1} is given by

State update with the measurement:

$$X_{k|k} = X_{k|k|k-1} + K_{k-1}[Z_{k-1} - h(F_k^{-1}(X_{k|k|k-1} - Q_k H_k^T S_k^{-1} \widetilde{Z}_k))] \quad (135)$$

$$P_{k|k} = [I - K_{k-1}H_{k-1}F_k^{-1}]P_{k|k|k-1} + K_{k-1}H_{k-1}F_k^{-1}Q_k(I - K_k H_k)^T \quad (136)$$

$$K_{k-1} = [P_{k|k|k-1} - (I - K_k H_k)Q_k](H_{k-1}F_k^{-1})^T S_{k-1}^{-1} \quad (137)$$

$$S_{k-1} = H_{k-1}F_k^{-1}[P_{k|k|k-1} - (I - K_k H_k)Q_k - Q_k(I - K_k H_k)^T + Q_k - Q_k H_k^T S_k^{-1} H_k Q_k](H_{k-1}F_k^{-1})^T + R_{k-1} \quad (138)$$

where

K_k = Kalman gain at t_k

$\widetilde{Z}_k$ = filter residuals at t_k

S_k = covariance of the residuals at t_k

H_k = linearized output matrix at t_k

H_{k-1} = linearized output matrix at t_{k-1}

Note that $\delta_k = t_k - t_{k-1}$ is positive in the definition of F_k and Q_k as specified by (58) and (59).

Interacting Multiple Model (IMM) Estimator

The dynamical motion and measurement equations for system with Markovian switching coefficients and nonlinear measurements are given by

$$X_{k+1} = F_k(\theta_{k+1})X_k + V_k(\theta_{k+1}) \quad (139)$$

$$Z_k = h(\theta_k, X_k) + W_k \quad (140)$$

where θ_k is a finite-state Markov chain taking values in $\{1, \ldots, N\}$ according to the transition probabilities p_{ij} of switching from mode i to mode j, and
$E[V_k(\theta_{k+1} = i)V_k^T(\theta_{k+1} = i)] = Q_k(\theta_{k+1} = i)$.

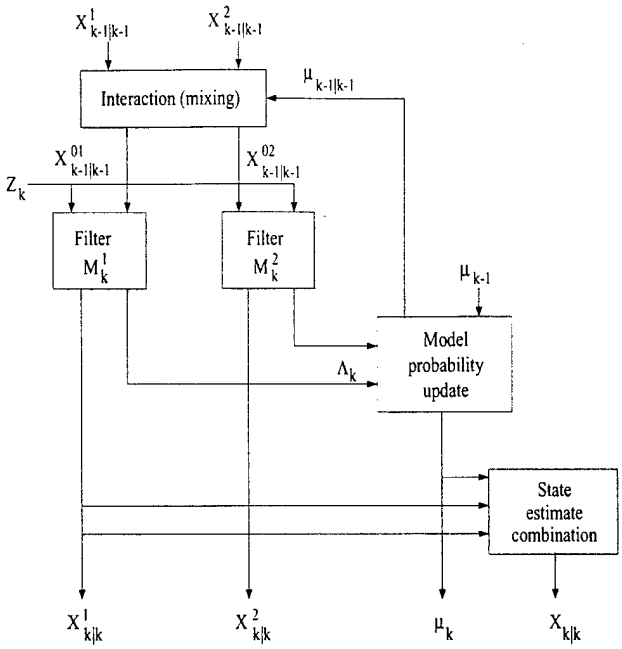

Figure 11: IMM estimator with two modes

Concluding Remarks

- Multiplatform-Multisensor Data Association
- Track Management
  - Track Number Management
  - Split or Diveraging Tracks
  - Track Swaps
  - Track Deletion
  - Deleting Redundant Tracks
- Multisensor Resource Allocation

REPORT DOCUMENTATION PAGE

Form Approved
OMB No. 0704-0188

1. AGENCY USE ONLY (*Leave blank*)	2. REPORT DATE	3. REPORT TYPE AND DATES COVERED
	October 12, 2000	Annual Report, Oct. 1999 – Sept. 2000

4. TITLE AND SUBTITLE
Information-Based Multisensor Detection:
Progress Report for October 1998 through September 1999

5. FUNDING NUMBERS
Grant
N00014-99-1-0084

6. AUTHOR(S)
William Dale Blair

7. PERFORMING ORGANIZATION NAME(S) AND ADDRESS(ES)
Georgia Institute of Technology
Georgia Tech Research Institute
Atlanta, GA 30332-0800

8. PERFORMING ORGANIZATION REPORT NUMBER
Annual Report
GTRI A-5858 (2)

9. SPONSORING/MONITORING AGENCY NAME(S) AND ADDRESS(ES)
Office of Naval Research
800 North Quincy Street
Arlington, Virginia 22217-5660

10. SPONSORING/MONITORING AGENCY REPORT NUMBER

11. SUPPLEMENTARY NOTES

12a. DISTRIBUTION/AVAILABILITY STATEMENT
Approved for Public Release

12b. DISTRIBUTION CODE

13. ABSTRACT (*Maximum 200 words*)

This program addresses the Navy need for extended firm track range for low altitude cruise missiles through the integration of multiple sensors. Track-Before-Declare (TBD) techniques that utilize signal features are proposed for the synergistic integration of an Electronically Scanned Array (ESA) radar with other sensors for the detection of weak targets. The computer simulation models of the sensors will include the effects of many issues such as finite sensor resolution, limitations on the sensor resources, atmospheric refraction, sensor pointing errors, sea-surface induced multipath, nonhomogeneous clutter, sea clutter, etc. that are omitted in most of the legacy simulations. The two primary accomplishments for the first year of this program were the development of a phased array radar model with search and track management functions for multiple targets as well as the development of a sea-clutter model with moving target indictor (MTI) waveform designs.

14. SUBJECT TERMS
Target Tracking, Radar Systems, Modeling and Simulation,
Sea Clutter Modeling, Multisensor Integration

15. NUMBER OF PAGES
97

16. PRICE CODE

17. SECURITY CLASSIFICATION OF REPORT	18. SECURITY CLASSIFICATION OF THIS PAGE	19. SECURITY CLASSIFICATION OF ABSTRACT	20. LIMITATION OF ABSTRACT
Unclassified	Unclassified	Unclassified	UL